Cartesian Elastodynamics Modelling of Parallel-kinematics Machines Under High-frequency, Small-amplitude Manoeuvres

Qi Sun

Department of Mechanical Engineering
McGill University
Montreal, Canada

July 18, 2023

A thesis submitted to McGill University in partial fulfillment of the requirements for the degree of Doctorate of Philosophy in Mechanical Engineering.

Abstract

A novel class of three-limb, full-mobility parellel-kinematics machines (PKMs), dubbed the SDelta, is proposed as a promising alternative to the traditional six-limb Stewart-Gough platforms. This simple architecture, with fewer moving components, leads to a lower inertia load, which extends its applications domain, the SDelta being deemed fit for generating *high-frequency, small-amplitude* (HFSA) motions, which are needed, e.g., in the inertia-parameter identification of rigid bodies.

Prior work conducted by the applicant on three-limb, full-mobility PKMs includes architecture design plus kinematics, singularity and dexterity analyses. This work was conducted upon modelling the PKM as a multi-rigid-body system. However, for HFSA applications, where *high speeds* are required, the inherent flexibility of the light limb rods should be taken into account. Thus, the PKM should be modeled as a *multibody system with rigid and flexible links.* In this vein, a *concise lumped-parameter elastodynamics linear model* is essential, since it includes the system stiffness and vibration characteristics in a swift, effective way.

Instead of a detailed n-degree-of-freedom(n-dof) generalized model considering flexibility and inertia of all system links, this thesis focuses on the six-dof simplified model in Cartesian space. This model is deemed suitable for flexible mechanical systems whose operation link is much stiffer and heavier than its counterparts coupling it to the rigid base. In this case, the system *elastodynamics model* can be simplified into a rigid moving platform (MP) *mounted on a massless, linearly elastic suspension.* Under this assumption, the system inertia is lumped into the rigid MP, while the system stiffness is lumped into a *Cartesian spring.* The whole system is thus simplified into a *Cartesian mass-spring* model. This model is not only a natural extension of its one-dof mass-spring counterpart, but also a pertinent simplification of the n-dof generalized model. Our model is deemed to be a convenient and useful tool in the preliminary-design stages, in which *the detailed di-*

mensions of the mechanical system are not yet determined. Moreover, the Cartesian space is more intuitive and visualizable than its $n(>6)$-dof counterpart. With the help of *screw theory*, geared to Cartesian models, engineers can gain insight into the elastodynamics behavior of the mechanical system under design.

In the Cartesian mass-spring model, the system elastodynamics behaviour is governed by a second-order differential equation in the time-domain, in terms of the six-dof small-amplitude displacement screw of the MP. The stiffness is represented by means of Lončarić's 6×6 *Cartesian stiffness matrix* (CSM) of the *Cartesian spring*, the inertia by what von Mises termed the *inertia dyad*, i.e., the 6×6 Cartesian mass matrix (CMM) of the rigid MP. The stiffness system modelling is based on the *virtual joint method*, whereby each flexible link is replaced by a rigid link and a *virtual joint*. The PKM with flexible links is thus transformed into a *multi-rigid-body system*. Then, with the help of knowledge on the multi-rigid-body system, the CSM is put forward. By means of the modified eigenproblem of the CSM, three types of elastostatic performance indices are defined. These concepts are used to evaluate, respectively, the overall stiffness, the translational stiffness and the torsional stiffness of the PKM. Different types of elastostatic performance indices allow us to choose the most appropriate one to optimize the dimensions of the robot so as to making it insensitive to frequencies affecting its higher modes. Furthermore, the Cartesian frequency matrix (CFM) is defined as a *congruent transformation* of its stiffness counterpart, the transformation matrix being the inverse of *the square root of the positive-definite CMM*. The CFM thus defined is *dimensionally-homogenous*, *symmetric* and at least *positive-semidefinite*. Upon the eigenvalue decomposition of the same matrix, the natural frequencies and the corresponding natural modes, i.e., the eigenscrews of the system, are obtained, to evaluate the system elasodynamics performance. The physical meaning of the CFM, together with that of its eigenvalues and eigenscrews, are given due interpretation in the thesis, within the context of screw theory.

RÉSUMÉ

L'auteur epropose une nouvelle classe de machines à cinématique parallèle, à trois membres, et à mobilité complète (abrégée PKM dans la theśe), le *SDelta*, qui offre une alternative prometteuse aux plateformes traditionnelles dites *Stewart-Gough* à six membres. Cette architecture, plus simple, à un nombre reduit de composants mobiles, offre une charge inertielle plus faible, ce qui étend son domaine d'application. Le SDelta s'avère capable de générer des mouvements à haute fréquence et de faible amplitude (HFFA), qui peuvent être utilisés, par exemple, pour l'identification des paramètres d'inertie des corps rigides.

Les travaux antérieurs sur les PKM à trois membres et à mobilité complète portent sur la conception de l'architecture et sur l'analyse de cinématique, de singularité et de dextérité. Ces travaux out été effectué en modélisant le PKM comme un système à plusieurs corps rigides. Cependant, pour les applications HFFA, où des vitesses élevées sont requises, la flexibilité inhérente des tiges de membres légèrs doit être prise en compte. Ainsi, le PKM doit être modélisée comme un système multicorps portant des membrures rigides et flexibles. Dans cette optique, un modèle linéaire élastodynamique à multiples paramètres discrets est essentiel, car il comporte la rigidité du système et les caractéristiques de vibration de manière exhaustive.

Au lieu d'un modèle généralisé détaillé à n degrés de liberté considérant la flexibilité et l'inertie de tous les liens du système, l'auteur propose un modèle simplifié à six degrés de liberté du système dans l'espace cartésien. Ce modèle convient particulièrement aux systèmes mécaniques à membrures flexibles dont la plateforme d'opération est beaucoup plus rigide et plus lourde que ses homologues la couplant à la base rigide. Dans ce cas, le modèle du système se réduit à une plateforme mobile (PM) *rigide* montée sur *une suspension linéairement élastique à masse négligeable*. Selon cette hypothèse, l'inertie du système est regroupée dans la plateforme mobile rigide, tandis que la raideur du système

s'exprime à l'aide d'un ressort cartésien. L'ensemble du système se reduit à un modèle cartésien masse-ressort. Ce modèle s'avère non seulement une extension naturelle de son homologue masse-ressort à un degré de liberté, mais aussi une simplification pertinente du modèle généralisé à n degrés de liberté. Notre modèle est considéré comme un outil pratique et utile dans le cadre des phases de *conception préliminaires*, dans lesquelles les dimensions détaillées du système mécanique ne sont pas encore déterminées. En outre, l'espace cartésien est plus intuitif et plus facile à visualiser que son homologue à $n(> 6)$ degrés de liberté. À l'aide de la théorie des vis, adaptée aux modèles cartésiens, l'ingénieur peu visualiser le comportement élastodynamique du système mécanique en question.

Dans le modèle masse-ressort cartésien, le comportement élastodynamique du système est gouverné par une équation différentielle du deuxième ordre dans le domaine temporel, en termes de la vis de déplacement de faible amplitude à six degrés de liberté de la PM. La raideur se modèle au moyen de la matrice cartésienne de raideur (MCR) 6×6 de Lončarić, du ressort cartésien, et l'inertie par ce que von Mises a appelé la *dyade d'inertie*, c'est-à-dire la matrice cartésienne 6×6 de masse (MCM) de la PM rigide. La modélisation de la raideur du système se base sur la méthode de l'articulation virtuelle, où chaque lien flexible est remplacé par *un lien rigide et une articulation virtuelle.* Le système mécanique portant des liens rigides et flexibles se transforme ainsi en un système à plusieurs corps rigides, dit *multicorps.* Ensuite, à l'aide des connaissances sur les systèmes multicorps, l'auteur propose, la MCR. Au moyen du problème à valeurs propres modifié de la MCR l'auteur définit trois types d'indices de performance élastostatique. Ces concepts sont ensuite utilisés pour évaluer la raideur globale, la raideur de translation et la raideur de torsion de la PKM. Différents types d'indices de performance élastostatique nous permettent de choisir la raideur la mieux adaptèe à l'optimisation des dimensions du robot de manière à le rendre insensible aux fréquences affectant ses modes supérieurs. En outre, la matrice cartésienne de fréquence (MCF) se définit comme transformation congruente de sa contrepartie de raideur, la matrice de transformation étant l'inverse de la racine carrée de la matrice définie positive de MCM. La MCF ainsi définie est dimensionnellement homogène, symétrique et au moins semi-définie positive. Après analyse de valeurs propres de cette matrice, on obtient les fréquences naturelles et les modes naturels correspondants, c'est-à-dire les *vis propres* du système, qui servent à évaluer la performance élastodynamique du système. La thèse se termine par l'interpretation physique de la MCF au moyen de ses valeurs et vecteurs propres.

Acknowledgements

Firstly, I would like to express my most sincere gratitude to my supervisors, Profs. Jorge Angeles and James Forbes. Starting as a student with little research experience, I faced numerous challenges during my PhD studies, which I could never have overcome without their unreserved guidance and encouragement. I would like to thank them for introducing me to the exciting world of scientific research, which led to my determination of embarking on this path. Moreover, I would like to express my gratitude to Profs. Meyer Nahon and Arun K. Misra, for both serving in my Ph.D. Committee and their valuable comments. Furthermore, I acknowledge the financial support from the *McGill Engineering Doctoral Award* and the *Chinese Scholarship Council*.

Finally, I would like to thank Jon Arsenault for his kind help on the French abstract. Moreover, I would like to express my gratitude to Drs. Wei Li, Ting Zou and Bruno Belzile, former members of of the *Robotic Mechanical Systems Laboratory* (RMSL), who provided me not only with plenty of help in my research, but also with many good memories of our work together. Most importantly, I would like to thank my parents, Hong Wang and Feiwei Sun, besides my best friends, Yiwen Li and Yuning Liu, for their endless support.

Contents

List of Figures

List of Tables

List of Acronyms

w.r.t.	with respect to
c.o.m.	centre of mass
dof	degree of freedom
C, P, S, H	cylindrical, prismatic, spherical, helical joints
MSMG	McGill Schönflies Motion Generator
FEA	finite element analysis
VJM	virtual-joint method
MSA	matrix structural analysis
PKM	parallel-kinematic machines
GEM	generalized elastodynamics model
CEM	Cartesian elastodynamics model
MP	moving platform
BP	base platform
SAD	small-amplitude displacement
GSM	generalized stiffness matrix
CMM	Cartesian mass matrix
CSM	Cartesian stiffness matrix
CCM	Cartesian compliance matrix
CFM	Cartesian frequency matrix

CDM	Cartesian dynamic matrix
PGA	perturbed generalized-coordinate array
SPD	symmetric and positive-definite
HFSA	high-frequency, small-amplitude application
VJM	virtual joint method

List of Symbols

$\mathbf{q}$	n-dimensional generalized-coordinate array
$\delta\mathbf{q}$	n-dimensional perturbed generalized-coordinate array
$\mathbf{M}_E$	$n \times n$ generalized mass matrix at the equilibrium state $\mathbf{q} = \mathbf{q}_E$
$\mathbf{K}_E$	$n \times n$ generalized stiffness matrix at the equilibrium state $\mathbf{q} = \mathbf{q}_E$
$\delta\mathbf{x}$	six-dimensional small-amplitude displacement (SAD) screw of the moving platform (MP)
$\mathbf{M}$	6×6 Cartesian mass matrix
$\mathbf{K}$	6×6 Cartesian stiffness matrix
$\mathbf{w}$	external wrench applied onto the MP centre of mass (c.o.m.)
V	system elastic potential energy
$\mathbf{t}$	MP twist
$\mathbf{K}_q$	generalized stiffness matrix
μ_i	ith eigenstiffness
$\mathbf{p}_i$	ith eigenpitches
$\mathbf{k}_i$	ith eigenscrew
κ	elastostatic performance index representing the overall PKM stiffness
κ_t	elastostatic performance index representing the translational stiffness
κ_r	elastostatic performance index representing the torsional stiffness
$\mathbf{D}$	6×6 Cartesian dynamic matrix

$\boldsymbol{\Omega}$	6×6 Cartesian frequency matrix
ω_i	ith natural frequency
$\mathbf{h}_i$	ith natural modes, a six-dimensional vector array

Chapter 1

Introduction

1.1 Motivation and Background

A parallel-kinematic machine (PKM) is defined as a closed-loop mechanism whose moving platform (MP) is linked to the base platform via at least two kinematic chains [1]. The PKMs allow for a better performance in terms of *accuracy*, *rigidity* and *load-carrying capacity* over their serial counterparts. Therefore, they have great potential in various applications, such as flight simulators, pick-and-place machines and surgical robots, as illustrated in Fig. 1.1. The *Stewart-Gough platform* [2, 3], consisting of one MP and one BP connected via six limbs, as shown in Fig. 1.2, is the foremost and most widely used full-mobility PKM in industry. However, its large number of components in the closed-loop structure brings about significant drawbacks, namely, severe limb-interference, complex kinematics and limited workspace, which leads to complex modelling, analysis and control [4, 5].

In order to improve their performance, extensive research on the design of six-dof PKMs with simpler architectures has been conducted. Among them, the three-limb, six-dof symmetric PKMs are deemed to be promising alternatives to the traditional *Stewart-Gough platforms* [6, 7]. Li and Angeles [8] proposed a novel class of three-limb, full-

(a) CAE 7000 series flight simulator

(b) Adept Quattro pick-and-place machine

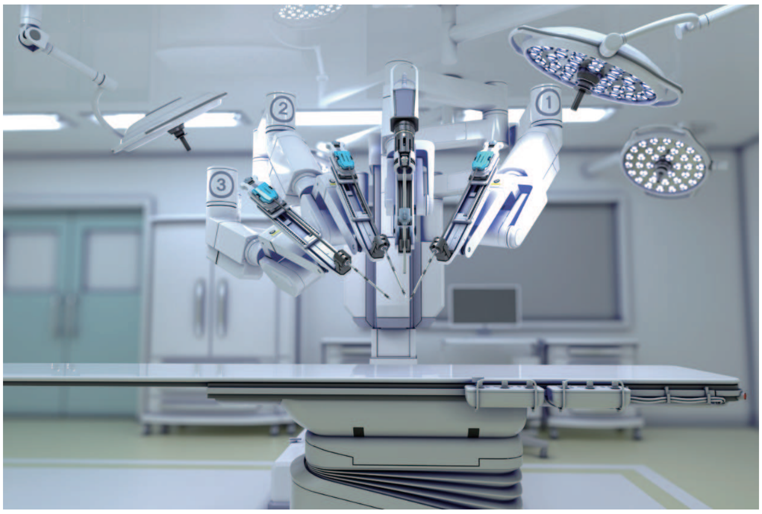

(c) Da Vinci surgical robot

Fig. 1.1 Various application of the PKMs

mobility parallel robots with a $3\underline{\mathsf{C}}\mathsf{PS}$[1] topology, dubbed SDelta, as shown in Fig. 1.3. The reduction of the number of limbs from six to three is realized by virtue of the two-dof cylindrical actuator, the C-drive [9], capable of driving the T-shaped tube with a cylindrical motion: rotation around an axis and translation in a direction parallel to the same axis. The simple architecture of the SDelta with only three limbs, reduces limb-interference, thereby offering a larger workspace. More importantly, compared with most alternative designs of three-limb, six-dof PKMs with some motors mounted on the

[1] C, P and S stand for *cylindrical*, *prismatic* and *spherical* joints, respectively, the *actuated* joint being underlined.

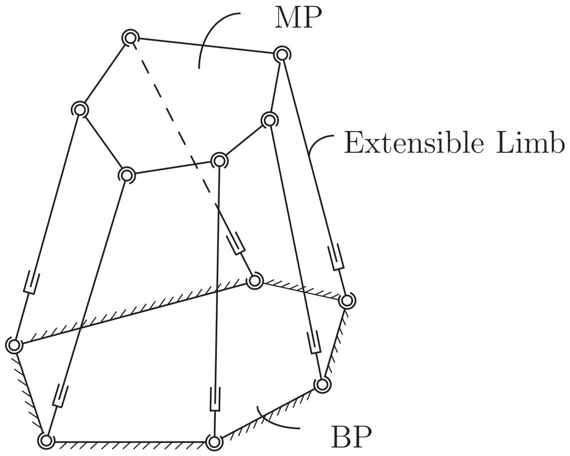

Fig. 1.2 The Stewart-Gough platform

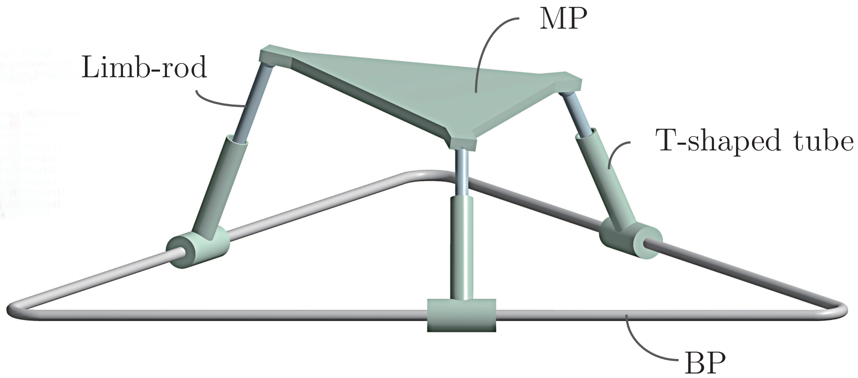

Fig. 1.3 The SDelta Robot

moving links [10, 11, 12], or designs with all the motors on the base but with a complex actuation system [13, 14], the C-drive allows all motors of the SDelta to be mounted on the base, thereby calling for fewer components. The lower inertia load extends its applications domain, making the SDelta suitable for generating *high-frequency, small-amplitude* (HFSA) motions, which can be used, for example, for the *inertia-parameter identification* of rigid bodies.

The identification of the 10 inertia parameters—the mass, the position vector of the centre of mass (c.o.m.) and the inertia tensor—of a rigid body is crucial since the rigid-body dynamic behaviour is significantly governed by these parameters [15]. A test specimen is attached to the MP of a full-mobility PKM and is excited by prescribed spatial trajectories. Meanwhile, the motion (acceleration and velocity) of the specimen and the wrench exerted onto it are recorded in the time domain. Then, the inertia parameters can be estimated via the PKM dynamics model. A key issue for the identification process is the exciting trajectory. Compared with the large-amplitude motion at a relatively low frequency, the HFSM exciting trajectory is advantageous. On the one hand, the system dynamics model is safely assumed to be constant along the whole exciting trajectory under small-amplitude conditions. On the other hand, high-frequency excitation increases the system signal-to-noise ratio, which allows for a better identification accuracy.

Prior work on the SDelta includes topology design, kinematics, singularity and dexterity analyses [8, 16]. These were conducted under the modelling of the PKM as a multi-rigid-body system. However, when applying the PKM for HFSA manoeuvres, where high speeds are required, the inherent flexibility of the light links should be taken into its modelling and analysis.

In practice, a PKM with flexible links is usually modelled as a n-dof system, where n, a finite integer usually in the tens, hundreds, or even higher orders, is the number of generalized deformation coordinates that define the *finite* configuration of the deformed system. However, a detailed n-dof model with high accuracy, considering flexibility and inertia of all the system links, is not possible at the early design stages and, to some extent, not even necessary. Then, a *concise lumped-parameter elastic linear model* is essential, since it provides the *system stiffness* and *vibration characteristics* in a swift, effective way. These features are the basis for the optimum design and real-time control of the PKM for HFSA applications.

1.2 Thesis Objectives

The thesis aims to establish a concise lumped-parameter linearly elastic model of the PKM with flexible links, intended for HFSA applications, in Cartesian space. Based on the Cartesian model, *elastostatics*, which accounts for the system *stiffness*, and *elastodynamics*, i.e., the dynamic response of the system to external and inertial loads, are studied and evaluated.

The objectives of the thesis follow:

- Simplification of a PKM with flexible links into a *Cartesian mass-spring model*.
- Formulation of the *Cartesian elastostatic model* for the Cartesian mass-spring system and identification of *performance indices* to be used to evaluate the system stiffness characteristics.
- Establishing the *Cartesian elastodynamics model* for the Cartesian mass-spring system and hence formulate performance indices to evaluate the system vibration response.
- To validate the Cartesian mass-spring model of a novel three-limb, full-mobility PKM, the SDelta robot.

1.3 Literature Survey

1.3.1 Cartesian Mass-Spring Model

The one-dof mass-spring system consists of a block of mass m suspended from the ceiling by a linear[2] spring of stiffness k. In this system, the mass is known to respond to a perturbation from its *equilibrium state* with *small-amplitude* harmonic oscillations about

[2]Linearity refers here to the spring *constitutive relation* between the *force* acting at its ends and its *deformation*, extension or compression.

its *equilibrium state*, with a frequency $\omega = \sqrt{k/m}$, termed the mass-spring system *natural frequency*. This concept can be ported directly into a multi-dof purely rotational or purely translational system, even in the presence of n degrees of freedom. However, a *systematic* investigation on the generalization of the one-dof case to its six-dof counterpart in *Cartesian space*, with rotation and translation coupled, is still lacking in the literature.

Compared with the one-dof mass-spring system, the point mass and the simple spring in the *Cartesian mass-spring model* are replaced with the *rigid body* and the *Cartesian spring*, respectively. The *Cartesian spring* is a *fundamental generalization* [17] of the single translational or torsional spring to the six-dof *Cartesian space*. Thereafter, the scalar quantities, i.e., the mass, the spring stiffness and the displacement, are extended to their 6×6 counterparts: the *Cartesian mass matrix*, i.e., the *von Mises inertia dyad* [18] of the *rigid body*; the 6×6 *Cartesian stiffness matrix* (CSM) [19, 20, 21, 22, 23, 24] of the *Cartesian spring*; and the 6-dimensional rigid-body displacement screw [25]. Next, upon bringing together the three foregoing concepts, the elastodynamics model of *the Cartesian mass-spring system* is formulated.

This model is deemed a pertinent simplification for systems whose operation platform is much stiffer than its light-weight structural components coupling it to a rigid base. Such systems occur in compliant mechanisms, microelectromechanical systems and fast robots. One important application targeted by this model is as a tool at the early stages of design, in which the detailed dimensions of the mechanical system in question are not yet determined. All the designer has at her/his disposal is the payload, the task trajectory, and *knowledge of structural mechanics*. With this knowledge, it is possible to plausibly assume the properties of a 6×6 stiffness matrix that encompasses the elastostatic properties of the mechanical system playing the role of a *Cartesian suspension*. The latter is a massless, linearly elastic body capable of *following* the *rigid body* attached to it through its six-dimensional motion space.

1.3.2 Elastostatics and Performance Evaluation

Compliant displacements of the PKM introduce negative effects on the accuracy, dynamic stability and wear resistance [26]. Therefore, *elastostatics*, which studies the response of a structurally elastic mechanical system to the applied load under static equilibrium, is crucial in the design and control of a PKM intended for HFSA applications. The elastostatic behaviour is taken into account by means of a 6×6 CSM, which maps the six-dimensional small-amplitude displacement (SAD) screw of the operation link into the applied wrench.

Generally speaking, three approaches can be adopted for elastostatic analysis: *finite element analysis (FEA)*, *virtual-joint method (VJM)* and *matrix structural analysis (M-SA)*.

In FEA, every component is modelled with its true dimensions and shape, which guarantees a high accuracy and reliability of the stiffness analysis. However, the *re-meshing* in FEA may lead to a high computational cost, which limits the applications of FEA to the final stage of the design [27]. Corradini et al. [28] evaluated the stiffness of a four-dof PKM, dubbed H4, by means of FEA, then extracted design rules in terms of static behaviour from the analysis results for further improvement. Moreover, due to its high accuracy, FEA is widely applied for validation and comparison with the results from other elastostatic analysis tools [26, 29, 30].

VJM, which is also known as *lumped modelling*, is drawn from Gosselin's work [31]. In VJM, the stiffness of the elastic components is analyzed by adding virtual compliant joints to their original rigid models. Upon simplification of the relations in the stiffness analysis, VJM achieves a short computation time with acceptable accuracy, which makes it suitable at the preliminary design stage [32]. Majou et al. [33] applied the VJM to conduct the parametric stiffness analysis of the *Orthoglide* robot, from which the stiffest workspace region was determined. A VJM model was also used by Caro et al. [30] to approximate the stiffness of a six-dof haptic interface device throughout the regular workspace at the pre-design stage. However, in the VJM, the coupling between the rotational and the translational deflections is neglected because of the use of one-dimensional virtual springs in the model.

Compared to FEA, in MSA, each component of the robot is modelled as a simple structural element, such as a beam, a cable or a rod, instead of a large number of elements. This kind of approximation in MSA is *simpler* but *realistic*, which reduces the computational cost while maintaining the accuracy of more elaborate models [34]. Furthermore, by means of MSA, the stiffness matrix can be obtained in parametric form, which allows for optimum design, whereby the overall stiffness of the robot needs to be maximized. The MSA was employed by Deblaise et al. [29] and Gonçalves and Carvalho [26] to conduct the stiffness analysis of the Delta robot and the 6-$\underline{\text{R}}$SS PKM, respectively. Kefer et al. [35] applied MSA to model the stiffness of articulated industrial robots and verified the method by FEA. The high accuracy and real-time computation potential of VJM achieved by Kefer et al. [35] showed the importance of VJM in the applications of mechanical design and real-time control of the PKMs.

Moreover, novel methods have been proposed based on the basic approaches cited above. A new systematic method for computing the stiffness matrix of overconstrained PKMs was reported by Pashkevich et al. [34]. This method is based on a multidimensional lumped-parameter model, in which the flexible components are replaced by six-dof *virtual springs*. Both the rotational/translational deflections and their coupling are well described. Taghvaeipour et al. [36] proposed a novel method for the elastostatic analysis of PKMs based on the concept of *generalized spring*. Specifically, each flexible component was replaced with a six-dimensional linearly elastic spring, whose stiffness parameters were obtained by means of FEA. This method followed the MSA, but developed the MSA by using a novel formulation to model the six *lower kinematic pairs*. Thereafter, by means of stiffness matrices computed off-line, parametrically or numerically, the CSM of the robot at any posture was available. This method was successfully applied to the elastostatic analysis of the *McGill Schönflies Motion Generator* (MSMG), which is composed of four Π-joints [37].

After deriving the CSM, *frame-invariant* scalar indices are to be defined from this matrix to assess the *robot stiffness*. The said matrix CSM is defined in the realm of *screw theory* [38, 39], representing not only the translational and rotational stiffness properties of the PKM, but also their *coupling*. In the literature, some indices have been defined independent of the physical meaning of the CSM. For example, Bhattacharya et al. [40] first multiplied the CSM by its transpose[3], then defined the determinant of the product as the *performance index*. One major problem here lies in that the product—in the case of a *symmetric* matrix, the said product is, in fact, the matrix-squared—i.e., the square of the stiffness matrix, is *physically meaningless*, as it involves *additions of quantities with disparate units*. Because of its *dimensional incompatibility*, the product of the CSM by its transpose, or its square, for that matter, has no physical meaning. Xu et al. [41] defined the stiffness index directly, as the minimum eigenvalue of the CSM. This index also poses some challenges. Unlike the 3×3 purely translational stiffness matrix, the eigenvalues and eigenvectors of the 6×6 CSM are not *preserved* under a change of frame. To cope with the foregoing problems, Griffis and Duffy [42] and Patterson and Lipkin [19] considered the eigenvalue decomposition of the CSM in a generalized form, with the help of a *swapping matrix*. Thereafter, *frame-invariant* eigenscrews and their corresponding eigenstiffnesses were derived to represent the properties of the CSM. Moreover, *wrench-compliant* and *twist-complaint* axes [20, 43], together with their corresponding eigenvalues, were used to reflect the robot stiffness.

[3] This step in fact, is not needed because this matrix is not only *symmetric*, but also, at least, *positive-semidefinite*.

1.3.3 Elastodynamics and Performance Evaluation

If the PKM is intended for HFSA applications, the inherent flexibility of the light-weight limbs may lead to unwanted vibration [44]; thus, not only the elastostatics, but also the elastodynamics, which studies the dynamic response of flexible multi-body systems to external and inertial loads, should be taken into consideration in the PKM design and control. Elastodynamic analysis, pertaining to vibration analysis, starts from the elastodynamics modelling. Considering the inertia wrench due to the mass and moment of inertia of the PKM, and neglecting damping, the linearized dynamics model of PKMs becomes a simple system of second-order ordinary differential equations in the SAD of the MP [45]. The coefficient of the SAD term is the posture-dependent CSM, while the coefficient of the second-derivative of the SAD term is the posture-dependent CMM of the whole system. Thereafter, the natural frequencies are calculated as the eigenvalues of the *dynamic matrix* [46, 47, 48, 49, 50], which is defined as the product of the inverse of the system mass matrix times the system stiffness matrix. The determination of the natural frequencies of PKMs is needed for both design and control purposes, since they determine a poor region of operation frequencies, where unwanted resonant vibrations are likely to occur [51, 50]. Therefore, for the envisioned applications, PKMs should be designed with a frequency spectrum outside of the range of the operation frequencies, which means that the lowest natural frequency of PKMs should be placed above the expected *spectrum of the operation frequencies*.

The calculation of the natural frequencies relies on the CSM and the CMM. The CSM can be computed by the FEA, the VJM, the MSA or an ad-hoc method based on them, which were reviewed in the foregoing paragraphs. Regarding the mass matrix, this is generally obtained based on the system kinetic energy [52]. The mass matrix of the robot is calculated as the Hessian matrix of the system kinetic energy with respect to the generalized velocities [53]. With this method, Codourey [54] obtained the mass matrix of PKMs. Based on the same method, Taghvaeipour et al. [55] computed the mass matrix of the MSMG at certain postures. With the Cartesian stiffness matrix computed by the modified MSA, the natural frequencies over the test trajectory were calculated, which provided important indices to evaluate the performance of the MSMG from the elastodynamic point of view at the design stage.

1.4 Claim of Originality

To the knowledge of the author, the main contributions proposed in this thesis, as listed below, are original:

- The six-dof Cartesian mass-spring model proposed as a simplification of the n-dof generalized model to represent a PKM with flexible links.
- The Cartesian elastostatic model of the PKM with flexible links, considering different types of stiffness.
- Frame-invariant performance indices, defined based on the Cartesian stiffness matrix, to evaluate the overall, the translational and the rotational stiffness of the PKM with flexible links.
- The Cartesian elastostatics model of the PKM with flexible links, based on the Cartesian mass-spring model.
- The Cartesian frequency matrix, defined based on the Cartesian stiffness matrix and the Cartesian mass matrix, as an extension of the natural frequency of the one-dof mass-spring system to the six-dof Cartesian mass-spring system, to evaluate the vibration characteristics of the PKM with flexible links.

1.5 Thesis Organization

An outline of the thesis follows:

In Chapter 2, the six-degree-of-freedom (six-dof) Cartesian mass-spring model is introduced as a simplification of the n-dof generalized elastodynamics model for particular types of PKMs with flexible links. Then, the relation and comparison between the generalized model and the Cartesian model are explained. The significance of the Cartesian mass-spring model is emphasized: it is *concise* and *intuitive*, which provides the engineer not only with insight into the behaviour of the flexible mechanical system, but also with guidance towards their design at the preliminary stage.

In Chapter 3, the Cartesian elastostatics model is established and studied on a novel PKM with flexible links, intended for HFSA operations. Each flexible link is modelled as a rigid link with a virtual joint. The CSM, representing the robot stiffness, is formulated from the stiffness values of the flexible links via the pertinent kinetostatic relations. Within the formulation, a means to compare two different kinds of stiffness, namely, the *torsional* and the *translational* stiffness of the different links, is proposed. Thereafter, frame-invariant indices are defined based on the CSM to evaluate the *overall stiffness*, the *translational stiffness* and the *torsional stiffness* of the PKM. Different elastostatic performance indices allow us to choose the most appropriate one to optimize the geometry of the robot so as to make it insensitive to frequencies affecting its higher modes. Finally, the foregoing methods are applied on a desktop-scale PKM, dubbed the *SDelta robot*. By comparison of the results with FEA simulation, the elastotatics model is validated.

In Chapter 4, the Cartesian elastostatics model is established and studied on a novel PKM with flexible links, intended for HFSA operations. In particular, the main novelty is the CFM definition: an *analytic function* of both the CMM and the CSM in a symmetric expression, its properties being discussed. Then, the natural frequencies and the modal screws calculated from the CFM are chosen to evaluate the elasodynamics performance of the system. Finally, numerical examples obtained at two postures of the SDelta are included, to better understand the concept of CFM and the physical meaning of the corresponding performance indices.

Finally, Chapter 5 includes conclusions and recommendations for future work.

Chapter 2

Cartesian Mass-spring Model of PKMs with Flexible Links

2.1 Overview

A *concise* lumped-parameter elastodynamics model is essential for the analysis of mechanical systems with flexible links to evaluate their elastic properties. However, a detailed n-dof *generalized elastic model* with high accuracy, considering flexibility and inertia of all the system bodies, is not possible at the *early design stages* and, to some extent, not even necessary. In this chapter, the six-dof *Cartesian mass-spring model* is introduced as a *simplification* the n-dof *generalized elastodynamics model* for particular types of flexible mechanical systems, namely, PKMs with flexible links intended for high-frequency operations. Moreover, relations and comparison between the generalized and Cartesian e-lasotdynamics models are provided. Finally, the significance of the *Cartesian mass-spring model* is emphasized.

2.2 Generalized Elastodynamics Model

The elastodynamics response of a mechanical system with flexible links is usually described by n (≥ 6) generalized coordinates. Here, n equals the number of independent deformation coordinates that define the *system deformed configuration*; its elastodynamics behaviour in the generalized space is governed by the model [56, 57]:

$$\mathbf{M}(\mathbf{q})\ddot{\mathbf{q}} + \mathbf{h}(\mathbf{q}, \dot{\mathbf{q}}) = \boldsymbol{\phi} \tag{2.1}$$

where $\mathbf{q}$ is the n-dimensional generalized-coordinate array, whose entry q_i, $i = 1, \cdots, n$, denotes the ith generalized coordinate, i.e., the deformation displacement of the corresponding flexible link *along* sliding joints (P) or *about* turning joints (R) the ith deformation axis, as the case may be. Furthermore, $\mathbf{M}(\mathbf{q})$ is the $n \times n$ posture-dependent *generalized mass matrix*, $\boldsymbol{\phi}$ the n-dimensional *generalized-force array* of the system. Moreover, the term $\mathbf{h}(\mathbf{q}, \dot{\mathbf{q}})$ is *nonlinear* in $\mathbf{q}$ and quadratic[1] in $\dot{\mathbf{q}}$. Under a *small-amplitude* deformation, eq. (2.1) is *linearized* around an equilibrium state, which yields

$$\mathbf{M}_E\delta\ddot{\mathbf{q}} + \mathbf{C}_E\delta\dot{\mathbf{q}} + \mathbf{K}_E\delta\mathbf{q} = \delta\boldsymbol{\phi} \tag{2.2}$$

with $\delta\mathbf{q}$ and $\delta\boldsymbol{\phi}$ denoting the *perturbed* generalized-coordinate array and the *perturbed* generalized-force array, respectively, while $\mathbf{M}_E$, $\mathbf{C}_E$ and $\mathbf{K}_E$ denote the *constant* generalized *mass*, *damping* and *stiffness* matrices evaluated at the *equilibrium state* $\mathbf{q} = \mathbf{q}_E$, respectively. As well, since the damping term has usually little effect on the natural frequencies and natural modes of the system [58], it is usually neglected in eq. (2.2). Then,

[1] While quadratic terms are also nonlinear, these terms have properties that are not present in arbitrary nonlinear terms which are exploited in their analysis.

the *generalized elastodynamics model* (GEM) of the system becomes:

$$\mathbf{M}_E \delta\ddot{\mathbf{q}} + \mathbf{K}_E \delta\mathbf{q} = \delta\boldsymbol{\phi} \tag{2.3}$$

2.3 Cartesian Mass-spring Model

The n *deformation coordinates* of all the flexible links, defined as the *generalized co-ordinates*, provide a suitable means of describing the system *elastodynamics behaviour*. However, the n-dof model can be cumbersome when n is large—in the 10s or 100s. For most mechanical systems with flexible links, particularly for the high-frequency PKMs of interest in this thesis, the operation link—the link at which the given task is described—is designed to be much stiffer and heavier than the limb-links connecting it to the base, as shown in Fig. 2.1(a). Under this condition, the operation link, as well as the BP, is assumed to be rigid, while the balance links are assumed to be flexible and massless. Then, the system can be safely modelled as a rigid moving platform (MP) mounted on the base platform (BP) via a *massless*, *linearly elastic suspension*, as illustrated in Fig. 2.1(b)[2]. In this model, the inertia of the system is lumped into that of the rigid MP, the stiffness of the system being lumped into that of the linearly elastic suspension, as a *Cartesian spring*.

When all motors are locked, the MP, under an external-wrench disturbance, will undergo *small-amplitude* motion with respect to (w.r.t.) the BP, mainly by virtue of the compliance of the limb-links. The motion of the MP, involving both *rotation* and *translation*, is described by a *six-dimensional screw* defined in the three-dimensional *special Euclidian group* SE(3) [59]. The suspension between the MP and the base is correspongdingly modelled as a *Cartesian spring*, a.k.a. a six-dof *generalized spring* [17] in *Cartesian space*. The

[2]Note that the notation $\boldsymbol{\theta}$ in Fig. 2.1(b) is purely illustrative, as rotations in 3D space are defined by 3×3 rotation matrices.

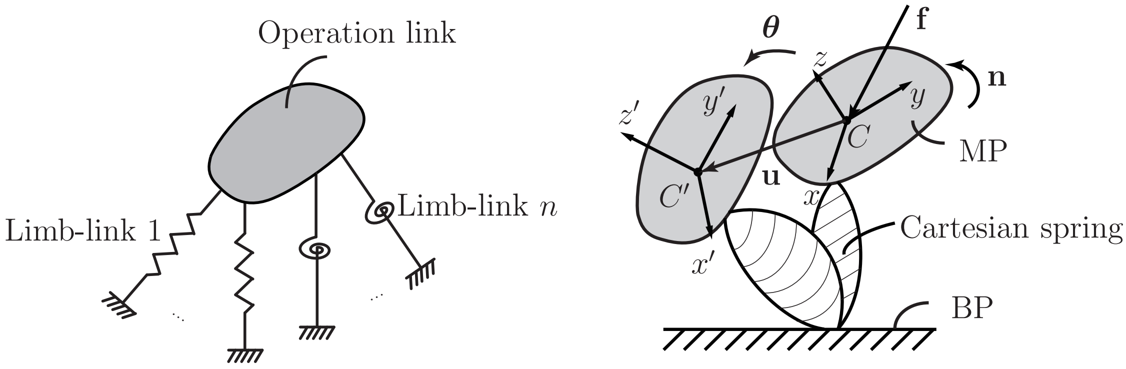

(a) Conceptual representation

(b) Cartesian mass-spring model, with $\boldsymbol{\theta}$ denoting a 3D rotation

Fig. 2.1 A Cartesian elastodynamic system

system is then simplified into the *Cartesian mass-spring model* depicted in Fig. 2.1(b).

Under a *Cartesian mass-spring model*, the system stiffness is visualized as a lump of massless, linearly elastic material supported at the BP by a *fixed rigid plate*. This lump carries, on another region of its boundary, a rigid MP fixedly attached to it. The *Cartesian spring* is capable of deforming under a *small-amplitude* displacement of the MP on top of it. This displacement is suitably represented by a *small-amplitude displacement* (SAD) screw, namely, a rigid-body *screw* displacement [25, 60], involving concurrently a "small" rotation[3] *about* a given axis and a "small" translation—small *w.r.t.* the pertinent longitudinal dimensions of the lump and the *rigid body* at stake—in the direction of the foregoing axis. The SAD screw can be readily visualized if it is regarded as the product of a *twist* [61] times a "small" time-increment—small enough to allow for a rotation through a "small" angle that differs from its sine by a *negligible* amount.

The elastodynamics response of the *Cartesian mass-spring system* is thus governed by

$$\mathbf{M}\delta\ddot{\mathbf{x}} + \mathbf{K}\delta\mathbf{x} = \mathbf{w} \tag{2.4}$$

[3]Under the small-amplitude assumption, a rigid-body rotation admits a vector representation.

where $\mathbf{w}$ is the six-dimensional external wrench applied onto the c.o.m. of the MP, while $\delta\mathbf{x}$ is the six-dimensional SAD screw of the MP at its c.o.m. C. That is, $\delta\mathbf{x}$ is the *perturbed* pose of the MP, equivalent, in this case, to the *perturbed* displacement array of the Cartesian mass-spring system, in response to the external wrench. Furthermore, $\mathbf{M}$ and $\mathbf{K}$ denote the 6×6 *Cartesian mass and stiffness matrices* that represent the corresponding properties of the system. Equation (2.4) is thus the *Cartesian elastodynamics model* (CEM) of the system.

For the sake of simplicity, henceforth, matrices and screws are represented w.r.t. the system c.o.m., displacement screw and wrench being defined as

$$\delta\mathbf{x} = \begin{bmatrix} \boldsymbol{\theta} \\ \mathbf{u} \end{bmatrix} \in \mathbb{R}^6, \quad \mathbf{w} = \begin{bmatrix} \mathbf{n} \\ \mathbf{f} \end{bmatrix} \in \mathbb{R}^6 \tag{2.5}$$

with $\boldsymbol{\theta} = \theta\mathbf{e}$ denoting the *rotation vector* of the body-fixed frame $Cxyz$ through a "small" angle[4] θ around the axis of rotation parallel to vector $\mathbf{e}$; as well, $\mathbf{u}$ is the *small-amplitude translation* of C. Moreover, $\mathbf{n}$ and $\mathbf{f}$ denote the moment about and the force applied at C. Furthermore, the SAD screw is defined in *ray-coordinates*, while the wrench in *axis-coordinates* [62]. The purpose of this difference in representations is to enable the definition of the work developed by a wrench $\mathbf{w}$ on a *rigid body* moving with a displacement screw $\mathbf{s}$ as an *inner product* of the pertinent vector arrays[5], i.e., as $\mathbf{w}^T\delta\mathbf{x}$. When $\mathbf{w} = \mathbf{0}$, eq. (2.4) becomes

$$\mathbf{M}\delta\ddot{\mathbf{x}} + \mathbf{K}\delta\mathbf{x} = \mathbf{0} \tag{2.6}$$

which represents the *free-vibration Cartesian model* of the system.

The *Cartesian mass matrix* (CMM) $\mathbf{M}$ encapsulates all the inertia properties of the

[4]It is known that, while a rotation through a finite angle is represented by a 3×3 proper orthogonal matrix, rotations through "small" angles are isomorphic to three-dimensional vectors.

[5]Else, the *reciprocal product* of screws makes the presentation a bit cumbersome.

system. The inertia of the operation link and the light-weight limb-links are integrated into the MP of the *Cartesian mass-spring model* in Fig. 2.1(b). In our case, this is the *von Mises inertia dyad* of the MP. Given the mass m of the MP and the moment of inertia $\mathbf{I}$ about its c.o.m., $\mathbf{M}$ takes the form [18]:

$$\mathbf{M} = \begin{bmatrix} \mathbf{I} & \mathbf{O} \\ \mathbf{O} & m\mathbf{1} \end{bmatrix} \tag{2.7}$$

with $\mathbf{1}$ denoting the 3×3 identity matrix. The CMM is *dimensionally inhomogeneous*, its upper and lower diagonal blocks bearing units of kg·m^2 and kg, respectively. Moreover, the CMM (i) is *symmetric* and positive-definite and (ii) takes a block-diagonal form when it is represented at the body c.o.m. When represented at any other point, whether inside or outside of the physical boundary of the body, the matrix is full [61].

The *Cartesian stiffness matrix* (CSM) $\mathbf{K}$ represents the stiffness properties of the system. This is a 6×6 matrix, describing the stiffness of the *Cartesian spring*, its block-form being

$$\mathbf{K} = \begin{bmatrix} \mathbf{K}_{11} & \mathbf{K}_{12} \\ \mathbf{K}_{12}^T & \mathbf{K}_{22} \end{bmatrix} \tag{2.8}$$

with $\mathbf{K}_{11}$ denoting the 3×3 rotational stiffness, carrying the pertinent units of N·m; $\mathbf{K}_{22}$ is its translational counterpart, bearing units of N/m; and $\mathbf{K}_{12}$ the 3×3 block of *coupled* rotational-and-translational stiffness, with units of N. The CSM is *symmetric* and at least *positive semi-definite*.

In summary, in the *Cartesian mass-spring model*, the inertia of the system is concentrated at the MP, while the system stiffness is lumped into a six-dof *generalized spring*, i.e., a *Cartesian spring*. Then, the elastodynamics response of the system is represented by the *small-amplitude* motion of the MP in *Cartesian space*. The model of eq. (2.4) is thus based on the well-known concept of the CSM, its companion, the CMM, and the two six-dimensional screws, the SAD screw and the wrench. The foregoing screws are attributes pertaining to the mechanics of a *rigid body*, in our case, the MP.

2.4 Relation Between the Generalized and the Cartesian Models

The kinematic relation between the SAD screw $\delta\mathbf{x}$ of the MP and the generalized-coordinate array $\delta\mathbf{q}$ is represented as

$$\mathbf{A}\delta\mathbf{x} = \mathbf{B}\delta\mathbf{q} \tag{2.9}$$

where $\mathbf{A} \in \mathbb{R}^{6\times 6}$ and $\mathbf{B} \in \mathbb{R}^{6\times n}$ are the *forward* and *inverse* Jacobian matrices of the mechanical system under analysis. Further, both $\mathbf{A}$ and $\mathbf{B}$ are assumed to have full rank. Hence, given a certain $\delta\mathbf{q}$, $\delta\mathbf{s}$ is unique, i.e.,

$$\delta\mathbf{x} = \mathbf{A}^{-1}\mathbf{B}\delta\mathbf{q} \tag{2.10}$$

However, since $n \geq 6$, for a given $\delta\mathbf{x}$, $\delta\mathbf{q}$ *need not be unique*, which means that different sets of generalized coordinates may lead to the same SAD screw of the MP. Here, the *minimum-energy solution* is taken,[6] of eq. (2.9) to express $\delta\mathbf{q}$ as

$$\delta\mathbf{q} = \mathbf{G}\delta\mathbf{x}, \quad \mathbf{G} = \mathbf{K}_E^{-1}\mathbf{B}^T(\mathbf{B}\mathbf{K}_E^{-1}\mathbf{B}^T)^{-1}\mathbf{A} \in \mathbb{R}^{n\times 6} \tag{2.11}$$

The above $\delta\mathbf{q}$ is *the most likely to occur*, since it *minimizes* the total elastic potential energy of the system. With the aid of eq. (2.11), the GEM is transformed into the CEM.

The mass matrix is the *Hessian* of the system kinetic energy w.r.t. the velocity array,

[6]The *minimum-energy solution* refers to the unique solution $\mathbf{q}$ of the eq. (2.9), that minimizes the system elastic potential energy, $K = (1/2)\delta\mathbf{q}^T\mathbf{K}_E\delta\mathbf{q}$.

while the stiffness matrix is the *Hessian* of the system elastic potential energy w.r.t. the displacement array. Moreover, the system kinetic energy is expressed as

$$K = \frac{1}{2}\delta\dot{\mathbf{q}}^T\mathbf{M}_E\delta\dot{\mathbf{q}} = \frac{1}{2}(\mathbf{Gt})^T\mathbf{M}_E(\mathbf{Gt}) = \frac{1}{2}\mathbf{t}^T\mathbf{Mt} \tag{2.12}$$

where, for a *small time increment* Δt, the time-rate of change of the *perturbed* displacement vector $\delta\mathbf{q}$ can be expressed as

$$\delta\dot{\mathbf{q}} = \frac{\delta\mathbf{q}}{\Delta t}, \quad \mathbf{t} = \frac{\delta\mathbf{x}}{\Delta t} \equiv \begin{bmatrix} \boldsymbol{\omega} \\ \dot{\mathbf{u}} \end{bmatrix} \tag{2.13}$$

where $\mathbf{t}$ is the six-dimensional *twist* of the MP, $\boldsymbol{\omega}$ the three-dimensional angular velocity array of the MP. The system elastic potential energy is expressed, in turn, as

$$V = \frac{1}{2}\delta\mathbf{q}^T\mathbf{K}_E\delta\mathbf{q}^T = \frac{1}{2}(\mathbf{G}\delta\mathbf{x})^T\mathbf{K}_E(\mathbf{G}\delta\mathbf{x}) = \frac{1}{2}\delta\mathbf{x}^T\mathbf{K}\delta\mathbf{x} \tag{2.14}$$

which leads to the relations sought:

$$\mathbf{M} = \mathbf{G}^T\mathbf{M}_E\mathbf{G}, \quad \mathbf{K} = \mathbf{G}^T\mathbf{K}_E\mathbf{G} \tag{2.15}$$

By means of eqs. (2.10) and (2.15), the n-dof generalized model is reduced to a six-dof *Cartesian model*.

Both the GEM and the CEM are *abstract* mathematical representations of the same physical mechanical system with flexible links. The GEM is based on the model established in the *generalized space*[7], considering all n independent deformations of the flexible links. By contrast, the CEM is based on the model established in *Cartesian space*, considering only the six degrees of freedom of a rigid-body motion, namely, the three

[7] i.e., the space described by the *generalized coordinates*.

small-amplitude translations and the three *small-amplitude* rotations of the operation link in *Cartesian space*. The GEM is more accurate but more complex, while the CEM is a six-dof simplification of the GEM, in *Cartesian space*.

Next, the difference and the relation between the generalized and the Cartesian models are discussed, from an *algebraic viewpoint*. The QR decomposition [63] of a full column-rank rectangular matrix $\mathbf{G} \in \mathbb{R}^{n\times 6}$, with $n > 6$, is expressed as

$$\mathbf{G} = \mathbf{Q}\begin{bmatrix} \mathbf{R} \\ \mathbf{O} \end{bmatrix}, \quad \mathbf{Q}^T\mathbf{Q} = \mathbf{1}_n \tag{2.16}$$

where: $\mathbf{1}_n$ represents the $n \times n$ identity matrix; $\mathbf{O}$, the $(n-6)\times 6$ zero matrix; $\mathbf{Q}$,a $n \times n$ orthogonal matrix, while $\mathbf{R}$ is a 6×6 *upper triangular* matrix.

Upon substitution of eq. (2.16) into eq. (2.10), the change of variables is expressed as

$$\delta\mathbf{x} = \begin{bmatrix} \mathbf{R}^{-1} & \mathbf{O}^T \end{bmatrix}\mathbf{Q}^T\delta\mathbf{q} \tag{2.17}$$

From eq. (2.17), it is apparent that the transformation from the *generalized-coordinate array* $\delta\mathbf{q}$ to the *Cartesian array* $\delta\mathbf{x}$, takes place in two steps:

(i) rotate the coordinate system in 12-dimensional space by means of a rotation matrix $\mathbf{Q}^T$;

(ii) reduce the dimension from n to six: the linear transformation, represented by $\mathbf{R}^{-1}$, of the first six components of the 12-dimensional generalized array $\mathbf{Q}^T\delta\mathbf{q}$, becomes the Cartesian array $\mathbf{s}$.

Furthermore, upon substitution of eq. (2.16) into eq. (2.15), the transformation from the generalized mass and stiffness matrices into their Cartesian counterparts is readily obtained:

$$\mathbf{M} = \begin{bmatrix} \mathbf{R}^T & \mathbf{O}^T \end{bmatrix} \mathbf{Q}^T \mathbf{M}_E \mathbf{Q} \begin{bmatrix} \mathbf{R} \\ \mathbf{O} \end{bmatrix} \tag{2.18a}$$

and (2.18b)

$$\mathbf{K} = \begin{bmatrix} \mathbf{R}^T & \mathbf{O}^T \end{bmatrix} \mathbf{Q}^T \mathbf{K}_E \mathbf{Q} \begin{bmatrix} \mathbf{R} \\ \mathbf{O} \end{bmatrix} \tag{2.18c}$$

Based on eqs. (2.18), the transformation of the *Cartesian matrices* undergoes two steps as well:

(i) rotate the coordinate system in 12-dimensional space by means of $\mathbf{Q}$;

(ii) reduce the dimension of the system thus resulting from n to six: the CMM is the linear transformation, represented by $\mathbf{R}$, of the the first 6×6 diagonal block of the 12×12 transformed matrix $\mathbf{Q}$ in (i).

When $n = 6$, both the forward and inverse Jacobian matrices are square. In this case, $\mathbf{G} = \mathbf{B}^{-1}\mathbf{A}$, $\mathbf{B}$ denoting a 6×6 nonsingular matrix. The GEM and the CEM thus have the same degree of freedom. The CEM is a *similarity transformation* of the GEM. Therefore, the two systems are equivalent, as they share the same sets of natural modes and natural frequencies. When $n > 6$, the degree of freedom of the GEM is larger than that of the CEM. After the transformation in eqs. (2.17) and (2.18), the dimension of the system reduces from n to six. According to eqs. (2.18), due to the zero block, information in the 12-dimensional matrices, $\mathbf{Q}^T\mathbf{M}_E\mathbf{Q}$ and $\mathbf{Q}^T\mathbf{K}_E\mathbf{Q}$, is partly lost.

In conclusion, the generalized model and the Cartesian model are usually established in spaces with different dimensions, *the transformation between them thus not being a similarity transformation involving simply a change of coordinates*. The Cartesian model is thus a *simplification* of the n-dof generalized model. That is, the Cartesian model does not contain all the n-dimensional dynamics information of the system. The sets of the Cartesian natural frequencies and natural modes do not identically equal the sets of the first six generalized natural frequencies and natural modes.

2.5 Significance of the Cartesian Mass-spring Model

The value of the *Cartesian mass-spring model* lies in two aspects. On the one hand, the *Cartesian mass-spring system* is a generalization of the one-dof mass-spring system

$$m\ddot{s} + ks = 0 \tag{2.19}$$

to its six-dimensional spatial counterpart. The CMM $\mathbf{M}$, the CSM $\mathbf{K}$ and the SAD screw $\mathbf{s}$ are the counterparts of the mass m of the particle, the stiffness k and the deformation s of the one-dof *linear*[8] *spring*, respectively. The elastodynamics model of a particle suspended by a simple spring is thus extended to the elastodynamics model of a *rigid body* suspended by means of a *Cartesian spring*.

On the other hand, the *Cartesian mass-spring model* is a six-dof simplification of the n-dof generalized model. The advantages of the *Cartesian mass-spring model* are:

(i) The *Cartesian mass-spring model* bears a concise expression, which makes it a useful tool in the *preliminary-design stages*, where the detailed dimensions of the mechanical system are not yet determined. All the designer has at her/his disposal is the payload, the task trajectory and knowledge of structural mechanics. With this knowledge, the properties of the Cartesian mass and stiffness matrices of the system can be assumed appropriately. The CEM can be established swiftly, while providing guidance towards the design of the system at stake.

(ii) The *Cartesian space* is more intuitive and visualizable than the n-dof generalized

[8] *Linearity* is understood here in the *algebraic sense*.

space. The elastodynamics response is usually represented by the rigid-body motion of the operation link. This kind of motion is described by the six-dimensional displacement screw of the MP in the *Cartesian space*. With the help of *screw theory*, engineers can thus gain insight into the elastodynamics behaviour of the mechanical system *under design*.

2.6 Summary

Cartesian mass-spring models represent not only a generalization of the one-dof mass-spring model, but also a practical simplification of the n-dof generalized elastodynamics model for particular flexible mechanical systems, such as PKMs with flexible links intended for *high-frequency operations*. In light of its concise expression, the *Cartesian mass-spring model* provides a guidance to the design engineer on the *spectrum* of the elastodynamics response of the system *under design*. This model is deemed to be valuable in: (i) the stiffness and vibration evaluation of the system; (ii) the *preliminary stages* of design; and (iii) the *task-space real-time feedback control of flexible mechanical systems*.

Chapter 3

Elastostatics: Cartesian Stiffness Modelling and Evaluation

3.1 Overview

Elastostatics is the study of *linearly elastic systems* under equilibrium conditions. In this chapter, the Cartesian elstostatics of a novel parallel-kinematics machine (PKM) with flexible links, intended for *high-frequency, small-amplitude* operations, is studied. The PKM is modelled as a rigid body elastically attached to the base platform via a six-dof *Cartesian spring*. Neglecting the inertia force in eq. (2.4), the elastostatics model of the *Cartesian mass-spring system* takes the form:

$$\mathbf{K}\delta\mathbf{x} = \mathbf{w} \tag{3.1}$$

The objective in this chapter is to establish the *Cartesian stiffness matrix* **K**, while defining *stiffness performance indices* capable of guiding the structural design of the robots of interest.

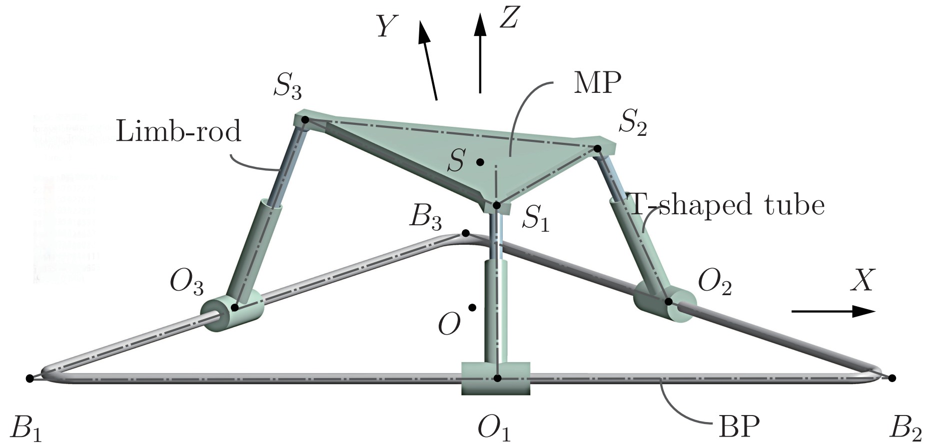

Fig. 3.1 Notations of the SDelta Robot

3.2 Assumptions and Stiffness Modelling of Flexible Links

The PKM of interest is the *SDelta robot*, shown in Fig. 3.1, which bears a *symmetric architecture*. The MP and the BP, illustrated as *equilateral triangles*, are connected via three identical limbs. Each limb is a $\underline{\mathsf{C}}\mathsf{PS}$ serial chain. The axes of the C joints define corresponding sides of an equilateral triangle of vertices $\{B_j\}_1^3$ and centre O. The MP is also represented by an equilateral triangle, this one of vertices $\{S_j\}_1^3$, and c.o.m. S, which is the *centroid* of the triangle $S_1S_2S_3$. Moreover, the intersection of each limb-axis with the axis of the corresponding C-joint is denoted $\{O_j\}_1^3$, $j = 1, 2, 3$. Each C joint is actuated by a *C-drive* [64], capable of driving the (inverted) T-shaped element in Fig. 3.1, henceforth referred to as the *tube*, with a *cylindrical motion*. Details of an implementation of the C-joint are illustrated in Fig. 3.2 [9]. This motion includes both a *rotation* through an angle ϕ around axis $\mathcal{A}$, and a *translation* r in a direction parallel to the same axis. The *C-drive* bears a $\underline{\mathsf{R}}\mathsf{HH}\underline{\mathsf{R}}$[1] topology. The *SDelta* works based on the synchronized rotation of two nuts, driven by two parallel screws, one *right-hand*, one *left-hand*, with pitches of identical absolute values, as depicted in Fig. 3.2. Details on the design and operation of these drives are available [9].

[1] H and R stand for *helical* and *revolute* joints, respectively, underlines indicating *actuated* joints.

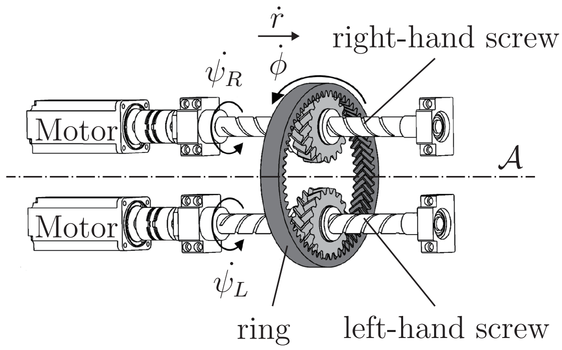

Fig. 3.2 C-drive Schematic

Some assumptions are made in order to study the elastostatics of the *SDelta Robot*:

- Joint friction is negligible.
- The six motor-shafts, together with their corresponding couplings, connecting each motor with its corresponding screw, are modelled as identical linearly elastic *torsional springs*.
- The three limb-rods, connecting the tubes with the MP via S joints, are modelled as identical linearly elastic beams of circular cross-section.
- The balance links, namely the MP, the BP, the tubes, the *left-* and *right-hand* screws of the *C-drives*, are modelled as rigid bodies[2].

3.2.1 Modelling of the Motor Stiffness

The motor shaft, transmitting torque from one motor to its screw, only bears torque around its axis. The shaft does not bend because of its mounting on a highly stiff base, supported by a stiff frame. The shaft is thus modelled as a massless, linearly elastic *torsional spring*, of stiffness k_1, given by

$$k_1 = \frac{GJ}{l_s} \ (\text{N}\cdot\text{m}), \quad J = \frac{\pi d_s^4}{32} \ (\text{m}^4) \tag{3.2}$$

[2] Screws are designed to withstand the design loads without significant deformation, which would jam them.

where G, J, l_s and d_s are, correspondingly: the *shear modulus*; the *torsional constant* for a shaft with a circular cross-section; the *shaft length*; and the *shaft diameter*. Moreover, the coupling between the motor shaft and its corresponding screw is assumed to exert torque only around the shaft axis; this coupling is thus modelled as a linearly elastic *torsional spring*, of stiffness k_2. As a result, the six motor shafts, together with their corresponding couplings in the three *C-drives*, are modelled as six identical linearly elastic *torsional springs*. The elastic deformation allowed by the motor shaft and its coupling is represented by a *small-amplitude* torsional displacement around the shaft axis. The total torsional stiffness of the *C-drive* is thus calculated using the expression for a series array of *torsional springs*, which yields

$$k_s = \frac{k_1 k_2}{k_1 + k_2} \ (\text{N}\cdot\text{m}) \tag{3.3}$$

3.2.2 Modelling of the Link Stiffness

The limb-rod, connecting each *C-drive* tube to the MP in each limb, is light and slender. Hence, in HFSA applications, its compliance should be taken into consideration. The objective of this subsection is the modelling of the stiffness of the limb-rod.

The upper end of the limb-rod, shown in Fig. 3.4, is connected to the MP via a S joint, while its lower end is attached to the piston, which slides freely w.r.t. the tube. Friction between piston and tube is neglected, the rod thus being assumed to be free of any axial force, by virtue of a lubricant whose viscosity is neglected in our *elastostatic analysis*. When an external wrench is applied onto the MP, given that the S joint can only transmit force, the rod is subjected to both one bending force, normal to the limb-axis at its upper end, and one axial force along the same axis. Notice that, in the absence of friction, the axial force transmitted to the limb vanishes. The bending force is decomposed into two mutually orthogonal components, denoted $\mathbf{f}_{lj}$ and $\mathbf{f}_{nj}$, that lie in

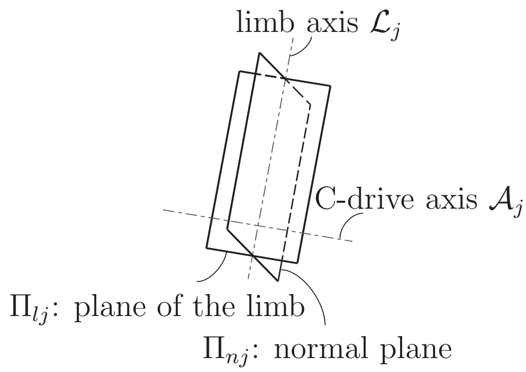

Fig. 3.3 Bending Planes of the jth Limb

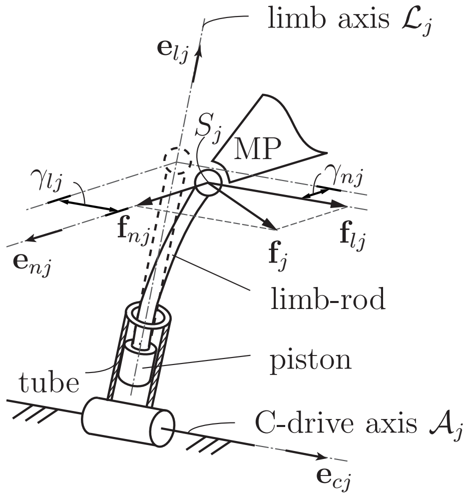

Fig. 3.4 Bending of the jth limb-rod

planes Π_{lj} and Π_{nj}, respectively, as depicted in Figs. 3.3 and 3.4. Plane Π_{lj} is spanned by the jth limb axis $\mathcal{L}_j$ and the jth *C-drive* axis $\mathcal{A}_j$, while plane Π_{nj} is normal to plane Π_{lj}, passing through $\mathcal{L}_j$. Thus, on the rod lower end, two reacting forces and two moments are applied, transmitted by the tube, to balance the effect of the two pairs of forces. In this case, bending occurs in the rod, i.e., neglecting longitudinal deformation, the rod deforms in a direction perpendicular to its axis along the intersection of planes Π_{lj} and Π_{nj}. The maximum deflection γ_{max} occurs at its upper end. Then, the deflection γ_{max} is decomposed into two mutually orthogonal components, γ_{lj} and γ_{nj}, lying in planes Π_{lj} and Π_{nj}, respectively.

As a result, the three limb-rods connecting the tubes with the MP are modelled as three identical linearly elastic beams, the elastic deformation of the jth rod being represented by its maximum deflection γ_{max} at the upper end. The calculation of the beam deflection and the beam potential energy are described below.

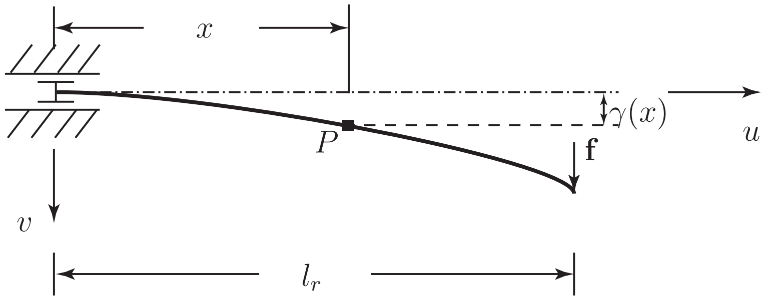

Fig. 3.5 Free Body Diagram of the Beam

Deflection

For modelling purposes, the limb-rods are simplified as identical clamped-free beams of uniform circular cross-section. Shown in Fig. 3.5 is the free-body diagram of a limb-rod of length l_r, modulus of elasticity E, and cross-section area moment of inertia I. The u-axis denotes the limb axis before bending, while the v-axis is normal to the limb axis. The intersection of the u- and v-axes is the lower end of the limb-rod. An external force $\mathbf{f}$ of magnitude F is applied in the direction of the v-axis at the upper end of the limb-rod.

Let $x \geq 0$ denote the u-coordinate of an arbitrary point P on the *elastica* of the limb-rod and $\gamma(x)$ the bending deflection of the rod along the v-axis at P. The boundary conditions associated with the limb-rod are

$$\gamma(0) = 0, \quad \left.\frac{\mathrm{d}\gamma(x)}{\mathrm{d}x}\right|_{x=0} = 0 \tag{3.4}$$

the *rod elastica* thus being given by

$$\gamma(x) = \frac{Fl_r}{2EI}x^2 - \frac{F}{6EI}x^3, \quad 0 \leq x \leq l_r \tag{3.5}$$

The maximum deflection of the jth limb-rod at its upper end is, therefore,

$$\gamma_{max} = \sqrt{\gamma_{lj}^2 + \gamma_{nj}^2} = \gamma(l_r) = \frac{Fl_r^3}{3EI} \tag{3.6}$$

Potential Energy

The strain energy of the beam, i.e., its *potential energy*, is given by [65]

$$V = \int_0^l \frac{EI}{2} \left[\frac{\mathrm{d}^2 \gamma(x)}{\mathrm{d}x^2} \right]^2 \mathrm{d}x = \frac{F^2 l_r^3}{6EI} = \frac{1}{2} \frac{3EI}{l_r^3} \gamma_{max}^2 \tag{3.7}$$

The potential energy of the limb-rod is thus quadratic in the maximum deflection γ_{max}, the rod stiffness being readily found as

$$k_r = \frac{3EI}{l_r^3} \ (\mathrm{N/m}), \quad I = \frac{\pi d_r^4}{64} \ (\mathrm{m}^4) \tag{3.8}$$

where d_r is the rod diameter.

Since the jth limb-rod bends in planes Π_{lj} and Π_{nj}, its total potential energy is

$$V_j = \frac{1}{2} k_r \gamma_{max}^2 = \frac{1}{2} k_r (\gamma_{lj}^2 + \gamma_{nj}^2) \tag{3.9}$$

3.3 Cartesian Elastostatic Modelling

Within the *elastostatic analysis*, all the motors are assumed to be locked, thereby locking the PKM at a reference *posture*[3]. When an external wrench is applied onto the MP, the PKM posture undergoes a perturbation due to the flexibility of the limb-rods and motor shafts. Thereafter, the MP will undergo a *small-amplitude displacement* (SAD) screw w.r.t. the *reference* MP pose in response to the applied wrench.

The relation between the MP SAD screw $\delta\mathbf{x}$ of a rigid body and the wrench $\mathbf{w}$ applied

[3]Posture pertains to a multi-body system. The emphasized term is used to describe the *pose* of all the individual *coupled* bodies constituting the system.

onto it is modelled as

$$\mathbf{w} = \mathbf{K}\delta\mathbf{x}, \quad \mathbf{K} = \begin{bmatrix} \mathbf{K}_{11} & \mathbf{K}_{12} \\ \mathbf{K}_{12}^T & \mathbf{K}_{22} \end{bmatrix} \in \mathbb{R}^{6\times 6} \tag{3.10}$$

In general, the directions of the two *screw vectors*, $\delta\mathbf{x}$ and $\mathbf{w}$, are different; so are their pitches. Therefore, the mapping from $\delta\mathbf{x}$ into $\mathbf{w}$ is represented by a 6×6 matrix $\mathbf{K}$, *rather than by a scalar*. Matrix $\mathbf{K}$ is termed the *Cartesian stiffness matrix* [66], characterizing the stiffness of the PKM. This matrix is *symmetric* and *positive-(semi-)definite*, carrying four 3×3 blocks. Its diagonal blocks, $\mathbf{K}_{11}$ and $\mathbf{K}_{22}$, bear units of Nm and N/m, respectively, its off-diagonal blocks carrying units of N.

The stiffness model of the PKM is now obtained based on the virtual-joint method (VJM) [31, 67]. In this context, the stiffness of every flexible part is lumped into a *virtual* spring. Then, all *virtual* springs are replaced with the *virtual* joints located at the distal end of each link. The translational spring is regarded as a *virtual* P joint, the *torsional spring* as a *virtual* R joint. The deformation axis of a flexible link is the axis of its corresponding *virtual* joint. By means of the VJM, the multibody system with rigid and flexible links is transformed into a multi-rigid-body system with *virtual* joints. Thereafter, the Cartesian stiffness of the PKM can be modelled via its kinematic relations and the *principle of virtual work*.

The CSM, key to elastostatics, is calculated as the *Hessian* [4] of the total *elastic potential energy* stored in the PKM w.r.t. the SAD screw of the MP [68]. The steps to derive the CSM are listed below:

(1) Lock all the motors at a *reference* posture of the PKM and assume that an external wrench is applied onto the MP.

[4] i.e., the $n \times n$ matrix of second-order partial derivatives of potential energy of a linearly elastic body w.r.t. the n independent variables occurring in the pertinent expression.

(2) Select a set of generalized coordinates to represent a perturbed PKM posture w.r.t. the *reference* one.

(3) Derive the relation between the MP SAD screw and the array representing the perturbed PKM posture.

(4) Calculate the total *elastic potential energy* and express the energy as a quadratic form of the MP SAD screw.

(5) Derive the CSM as the *Hessian* matrix of the *elastic potential energy* w.r.t. the MP SAD screw.

3.3.1 Virtual-joint Model of the PKM

Based on the virtual-joint model, the flexible limb-rod of Fig. 3.4 is replaced with a rigid rod carrying a *virtual* P joint located at its upper end. The direction of the P joint is parallel to the deflection direction of the limb-rod, its joint variable being the deflection of the rod at the upper end. Moreover, the flexible motor shaft is replaced with a *virtual* R joint. The joint axis is the shaft axis, while the joint variable is the torsional deformation of the shaft. An *abstract* virtual-joint model of the *C-drive* is illustrated in Fig. 3.6, using the notation introduced in Table 3.1. By virtue of the "small" deformation of the motor shafts, the tube rotates about and slides along a direction parallel to the *C-drive* axis by "small" amounts. Notice that tube rotation and sliding amount to a *cylindrical motion*, coupled by the screw pitch values. The *C-drive* is thus replaced with a *virtual* C joint.

By means of the VJM, the PKM with flexible links is modelled as a multi-rigid-body system coupled by both *virtual* and *physical* joints. An *abstract* virtual-joint model of the PKM is shown in Fig. 3.7; for visualization purposes, the icons of its components are listed in Table 3.1.

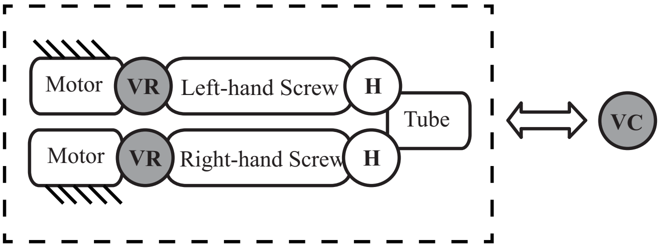

Fig. 3.6 Virtual-joint model of the C-drive

Table 3.1 Abstract representations of the components of a VJ model

Components	Geometrical Representations
Physical P, S, H joints	P S H
Virtual P, R, C joints	VP VR VC
Rigid link	Link
Rigid MP	MP
Rigid BP	Base

3.3.2 Kinematic Relations of the Virtual-joint Model

When all the motors are locked, the response of the *SDelta* under static load is fully determined by the elastic deformation of each of its flexible parts. Therefore, the deflections of the three limb-rods at their upper ends and the *small-amplitude torsional deformations* of the six motor shafts are selected as the generalized coordinates to define the *perturbed* posture of the PKM under the applied wrench. These coordinates are stored in a 12-dimensional array $\delta\mathbf{q}$, termed *the perturbed generalized-coordinate array* (PGA) of

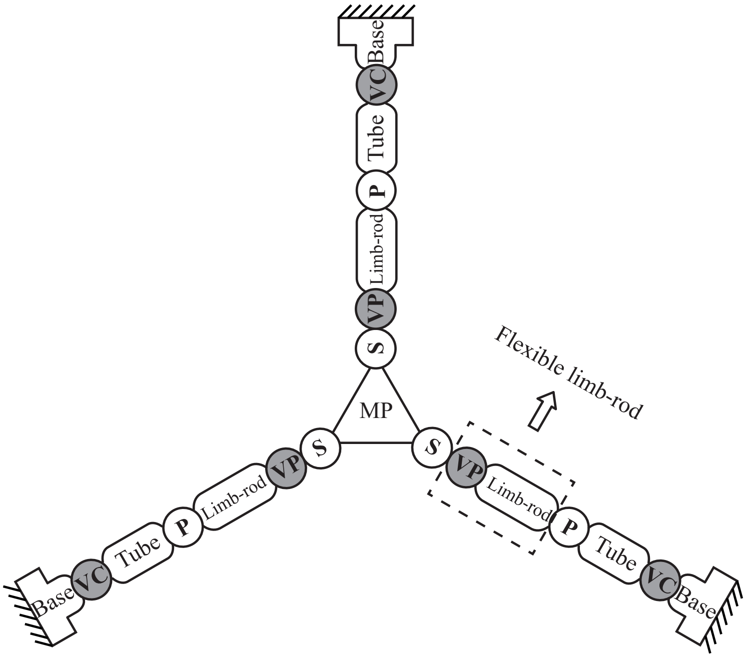

Fig. 3.7 Virtual-joint model of the SDelta

the PKM, namely,

$$\delta\mathbf{q} = \begin{bmatrix} \boldsymbol{\psi}^T & \boldsymbol{\gamma}^T \end{bmatrix}^T, \ \boldsymbol{\psi} \in \mathbb{R}^6, \ \boldsymbol{\gamma} \in \mathbb{R}^6 \tag{3.11a}$$

with $\boldsymbol{\psi}$ representing the torsional-deformation array of the six motor shafts, $\boldsymbol{\gamma}_r$ the bending-deflection array of the three limb-rods, i.e.,

$$\boldsymbol{\psi} = \begin{bmatrix} \boldsymbol{\psi}_1 \\ \boldsymbol{\psi}_2 \\ \boldsymbol{\psi}_3 \end{bmatrix}, \quad \boldsymbol{\psi}_j = \begin{bmatrix} \psi_{Lj} \\ \psi_{Rj} \end{bmatrix} \quad j = 1, 2, 3 \tag{3.11b}$$

$$\boldsymbol{\gamma} = \begin{bmatrix} \boldsymbol{\gamma}_1 \\ \boldsymbol{\gamma}_2 \\ \boldsymbol{\gamma}_3 \end{bmatrix}, \quad \boldsymbol{\gamma}_j = \begin{bmatrix} \gamma_{lj} \\ \gamma_{nj} \end{bmatrix} \quad j = 1, 2, 3 \tag{3.11c}$$

ψ_{Lj} and ψ_{Rj} representing the torsional deformation of the motor shafts associated, respectively, with the *left-* and the *right-hand* screws in the jth limb, γ_{lj} and γ_{nj} the *maximum bending deflections* of the jth limb-rod in planes Π_{lj} and Π_{nj}, respectively.

In Fig. 3.7, the *virtual* C and P joints, which represent the *motor-shaft flexibility* and the *limb-rod flexibility*, respectively, are regarded as the active joints of the system, the physical P and S joints as passive joints. Therefore, each limb is a serial $\underline{\text{C}}\text{P}\underline{\text{P}}\text{S}$ chain. At the upper end of the limb-rod, the kinematic subchain composed of a *virtual* P joint and a S joint becomes a sliding S joint[5]. The PGA $\delta\mathbf{q}$ is also the active-joint array of the virtual-joint model of the PKM.

An expression for the MP SAD screw $\delta\mathbf{x}$ in terms of the PGA is derived via the kinematic relations of the virtual-joint model, while regarding the *perturbed* MP pose $\delta\mathbf{x}$ as $\mathbf{t}\Delta t$, where $\mathbf{t} = [\boldsymbol{\omega}^T,\ \dot{\mathbf{u}}^T]^T$ is the (six-dimensional) twist of the MP, Δt a "small" time-increment[6], as expressed in eq. (2.13). Moreover, $\boldsymbol{\omega}$ and $\dot{\mathbf{c}}$ represent the MP angular velocity and the velocity of its c.o.m. Then, the relation between $\delta\mathbf{x}$ and $\delta\mathbf{q}$ can be transformed into the corresponding relation at the velocity level, i.e., the relation between MP twist $\mathbf{t}$ and active joint-rate array $\delta\dot{\mathbf{q}}$ of the virtual-joint model.

For the jth limb, the relations between the MP twist and the limb joint-rate array are described by

$$\mathbf{t} = \mathbf{J}_j\dot{\boldsymbol{\vartheta}}_j \tag{3.12a}$$

[5] In our case, at the upper end of the jth limb-rod, the sliding S joint allows five degrees of freedom, i.e., one translation along each of the $\mathbf{e}_j$ and $\mathbf{f}_j$ directions, plus three independent rotations.

[6] "Small" here means w.r.t. the reciprocal of the highest *design frequency*, 10 Hz in our case.

with

$$\mathbf{J}_j = \begin{bmatrix} \mathbf{e}_{cj} & \mathbf{0} & \mathbf{0} & \mathbf{0} & \mathbf{0} & \mathbf{e}_{cj} & \mathbf{e}_{lj} & \mathbf{e}_{nj} \\ \mathbf{e}_{cj} \times \mathbf{p}_{1j} & \mathbf{e}_{cj} & \mathbf{e}_{lj} & \mathbf{e}_{cj} & \mathbf{e}_{nj} & \mathbf{p}_j \times \mathbf{e}_{cj} & \mathbf{p}_j \times \mathbf{e}_{lj} & \mathbf{p}_j \times \mathbf{e}_{nj} \end{bmatrix} \tag{3.12b}$$

$$\dot{\boldsymbol{\vartheta}}_j = \begin{bmatrix} \dot{u}_j & \dot{\phi}_j & \dot{b}_j & \dot{\gamma}_{lj} & \dot{\gamma}_{nj} & \dot{\theta}_{1j} & \dot{\theta}_{2j} & \dot{\theta}_{3j} \end{bmatrix}^T, \quad j = 1, 2, 3 \tag{3.12c}$$

where $\dot{\boldsymbol{\vartheta}}_{\boldsymbol{j}}$ is the array of the jth-limb rates, consisting of the passive joint rates and the deformation rates, while $\mathbf{J}_j$ is the 6×8 Jacobian that maps the jth limb-rate array into the MP twist. The unit vector $\mathbf{e}_{cj}$ is parallel to the *C-drive* axis, the unit vector $\mathbf{e}_{lj}$ parallel to the limb axis, and $\mathbf{e}_{nj} \equiv \mathbf{e}_{cj} \times \mathbf{e}_{lj}$, as depicted in Fig. 3.4. Moreover, u_j and ϕ_i are the *small-amplitude* sliding and rotational displacement of the *virtual* R joint; b_j the *small-amplitude* translational displacement of the passive P joint; γ_{lj} and γ_{nj} the *small-amplitude* translational displacement of the *virtual* P joint along the $\mathbf{e}_{cj}$ and $\mathbf{e}_{nj}$ directions, respectively. Besides, θ_{1j}, θ_{2j} and θ_{3j} are the *small-amplitude* rotational displacements, as allowed by the jth S joint. Furthermore, $\mathbf{0}$ is the three-dimensional zero vector, $\mathbf{p}_{1j}$ the vector stemming from O_j and ending at the MP c.o.m. S; finally, $\mathbf{p}_j$ is the vector stemming from the MP c.o.m. and ending at the centre of the jth S joint.

As shown in Fig. 3.6, the *virtual* C joint bears a 2-H$\underline{\text{R}}$ structure. The output displacements, i.e., the *small-amplitude* sliding u_j and rotational ϕ_j displacements of the tube, are determined by the torsional displacements ψ_{Li} and ψ_{Rj} of the *virtual* R joints. The relation between the foregoing variables is expressed by the *Jacobian matrix* of the *C-drive*, as described below [9]:

$$\dot{\boldsymbol{\phi}}_j = \mathbf{J}_C \dot{\boldsymbol{\psi}}_j, \quad j = 1, 2, 3 \tag{3.13a}$$

with

$$\mathbf{J}_C = \begin{bmatrix} p/4\pi & -p/4\pi \\ 1/2\iota & 1/2\iota \end{bmatrix}, \quad \boldsymbol{\phi}_j = \begin{bmatrix} \dot{u}_j \\ \dot{\phi}_j \end{bmatrix} \tag{3.13b}$$

where p is the pitch of the screws in the *C-drive*[7] and ι[8] the total gear-reduction ratio due to the planetary gear transmissions.

The next step is the *elimination of the passive joint rates*. The unit screws $\mathbf{s}_{1j}$ and $\mathbf{s}_{2j}$, representing the Plücker arrays [69] of the lines passing through the centre of the jth S joint and parallel to $\mathbf{e}_{cj}$ and $\mathbf{e}_{nj}$, respectively, are introduced below. These screws are *reciprocal*[9] to the third and the last three columns of $\mathbf{J}_j$, the *small-amplitude relative translation* allowed by the piston and the *small-amplitude relative rotations* allowed by the S_j joint thus being eliminated. Therefore,

$$\mathbf{s}_{1j} = \begin{bmatrix} \mathbf{e}_j \\ \mathbf{e}_j \times \mathbf{p}_j \end{bmatrix}, \quad \mathbf{s}_{1j}^T \boldsymbol{\Gamma} \mathbf{J}_j \dot{\boldsymbol{\vartheta}}_j = \dot{u}_j + \dot{w_{lj}} \tag{3.14a}$$

$$\mathbf{s}_{2j} = \begin{bmatrix} \mathbf{g}_j \\ \mathbf{g}_j \times \mathbf{p}_j \end{bmatrix}, \quad \mathbf{s}_{2j}^T \boldsymbol{\Gamma} \mathbf{J}_j \dot{\boldsymbol{\vartheta}}_j = l_j \dot{\phi}_j + \dot{w_{nj}} \tag{3.14b}$$

with $\boldsymbol{\Gamma}$ defined below:

$$\boldsymbol{\Gamma} = \begin{bmatrix} \mathbf{O} & \mathbf{1}_3 \\ \mathbf{1}_3 & \mathbf{O} \end{bmatrix} = \boldsymbol{\Gamma}^{-1} \;\Rightarrow\; \boldsymbol{\Gamma}^2 = \mathbf{1}_6 \tag{3.15}$$

which is termed a *swapping matrix*. Indeed, matrix $\boldsymbol{\Gamma}$ *swaps* the order of the two three-dimensional vectors of a screw array, hence the moniker. Moreover, $\mathbf{O}$ is the 3×3 zero matrix and $\mathbf{1}_k$ the $k \times k$ identity matrix, l_j denoting the distance between O_j and the centre of the jth S joint, i.e., a variable.

[7]One positive, one negative.
[8]Greek letter "iota".
[9]Two screws $\mathbf{s}_1$ and $\mathbf{s}_2$ are said to be reciprocal if $\mathbf{s}_1^T \boldsymbol{\Gamma} \mathbf{s}_2 = 0$, with $\boldsymbol{\Gamma}$ defined in eq. (3.15).

According to eqs. (3.12)–(3.15), the relation between MP twist $\mathbf{t}$ and active joint-rate array $\delta\dot{\mathbf{q}}$ is given by

$$\mathbf{N}\mathbf{t} = \mathbf{D}\mathbf{J}\delta\dot{\mathbf{q}} \tag{3.16}$$

where

$$\mathbf{N} = \begin{bmatrix} \mathbf{s}_{11}^T\mathbf{\Gamma} \\ \mathbf{s}_{21}^T\mathbf{\Gamma} \\ \mathbf{s}_{12}^T\mathbf{\Gamma} \\ \mathbf{s}_{22}^T\mathbf{\Gamma} \\ \mathbf{s}_{13}^T\mathbf{\Gamma} \\ \mathbf{s}_{23}^T\mathbf{\Gamma} \end{bmatrix} = \begin{bmatrix} (\mathbf{e}_{c1}\times\mathbf{p}_1)^T & \mathbf{e}_{c1}^T \\ (\mathbf{e}_{n1}\times\mathbf{p}_1)^T & \mathbf{e}_{n1}^T \\ (\mathbf{e}_{c2}\times\mathbf{p}_2)^T & \mathbf{e}_{c2}^T \\ (\mathbf{e}_{n2}\times\mathbf{p}_2)^T & \mathbf{e}_{n2}^T \\ (\mathbf{e}_{c3}\times\mathbf{p}_3)^T & \mathbf{e}_{c3}^T \\ (\mathbf{e}_{n3}\times\mathbf{p}_3)^T & \mathbf{e}_{n3}^T \end{bmatrix} \tag{3.17a}$$

$$\mathbf{D}_L = \begin{bmatrix} \mathbf{L} & \mathbf{1}_6 \end{bmatrix} \in \mathbb{R}^{6\times 12}, \quad \mathbf{L} = \mathrm{diag}(1,\, l_1,\, 1,\, l_2,\, 1,\, l_3) \tag{3.17b}$$

$$\mathbf{J} = \mathrm{diag}(\mathbf{J}_L, \mathbf{1}_6) \in \mathbb{R}^{12\times 12}, \quad \mathbf{J}_L = \mathrm{diag}(\mathbf{J}_C, \mathbf{J}_C, \mathbf{J}_C) \in \mathbb{R}^{6\times 6} \tag{3.17c}$$

with the Jacobian $\mathbf{J}_C$ of the *C-drive* defined in eq. (3.13b).

Under the small-amplitude assumption, the SAD screw of the MP, namely, the *perturbed* MP *pose* $\delta\mathbf{x}$, is regarded as $\delta\mathbf{x} \equiv \mathbf{t}\Delta t$, where Δt is a small time-increment, the *perturbed* PKM *posture* $\delta\mathbf{q}$ being regarded as $\delta\mathbf{q} \equiv \dot{\mathbf{q}}\Delta t$. Thus, the relation between $\delta\mathbf{x}$ and $\delta\mathbf{q}$ is

$$\mathbf{N}\delta\mathbf{x} = \mathbf{D}_J\delta\mathbf{q}, \quad \mathbf{D}_J \equiv \mathbf{D}_L\mathbf{J} \tag{3.18}$$

where $\mathbf{D}_L \in \mathbb{R}^{6\times 12}$ is a full-rank rectangular matrix, $\mathbf{J}$ a nonsingular 12×12 matrix.

3.3.3 Calculation of the Elastic Potential Energy

The CSM is calculated as the *Hessian* of the *elastic potential energy*, as stated in the preamble to this section. In turn, the *elastic potential energy* is determined by the deformation of the flexible parts, i.e., by the values of the generalized coordinates. The total *elastic potential energy* is the sum of the *elastic potential energy* of motor shafts and limb-rods, the *elastic potential energy* of the whole system thus taking the form

$$\begin{aligned} V &= \sum_{j=1}^{3}\left[\frac{1}{2}k_s(\psi_{Lj}^2+\psi_{Rj}^2)+\frac{1}{2}k_r(\gamma_{lj}^2+\gamma_{nj}^2)\right] \\ &= \frac{1}{2}\boldsymbol{\psi}^T\mathbf{K}_s\boldsymbol{\psi}+\frac{1}{2}\boldsymbol{\gamma}^T\mathbf{K}_r\boldsymbol{\gamma}=\frac{1}{2}\delta\mathbf{q}^T\mathbf{K}_q\delta\mathbf{q} \end{aligned} \tag{3.19}$$

with

$$\mathbf{K}_s = k_s\mathbf{1}_6, \quad \mathbf{K}_r = k_r\mathbf{1}_6 \in \mathbb{R}^{6\times 6}, \quad \mathbf{K}_q = \mathrm{diag}(\mathbf{K}_s, \mathbf{K}_r) \in \mathbb{R}^{12\times 12} \tag{3.20}$$

and $\mathbf{K}_q$ denoting the generalized stiffness matrix (GSM), namely, the *Hessian* of the system *elastic potential energy* w.r.t. the PGA $\delta\mathbf{q}$.

To obtain the *elastic potential energy* in terms of the MP SAD screw, the mapping from the SAD screw $\delta\mathbf{x}$ of the MP into the PGA $\delta\mathbf{q}$ is crucial. However, vectors $\delta\mathbf{q}$ and $\delta\mathbf{x}$ carry different dimensions. That is, given $\delta\mathbf{x}$, vector $\delta\mathbf{q}$ is *underdetermined*, which means that nine different sets of *perturbed* coordinates may lead to the same MP SAD screw. There is, however, one particular $\delta\mathbf{q}^*$ array that *minimizes* the total *elastic potential energy* of the system, displayed in eq. (3.19). This array, termed the *minimum-energy* solution of eq. (3.18), is expressed as

$$\delta\mathbf{q}^* = \mathbf{F}\delta\mathbf{x} \tag{3.21}$$

with

$$\mathbf{F} = \mathbf{K}_q^{-1}\mathbf{D}_J^T\mathbf{H}^{-1}\mathbf{N}, \quad \mathbf{H} \equiv \mathbf{D}_J\mathbf{K}_q^{-1}\mathbf{D}_J^T \tag{3.22}$$

$\mathbf{H}^{-1}$ being available, as $\mathbf{H}$ is *nosingular*, besides being *dimensionally homogeneous*[10]. The total *elastic potential energy* of the robot associated with the foregoing $\delta\mathbf{q}^*$ is the smallest among all possible solutions of eq. (3.18), and hence, *the most likely* to occur. Therefore, the *elastic potential energy* associated with $\delta\mathbf{q}^*$ and the corresponding CSM are selected to represent the overall stiffness of the robot for a given $\delta\mathbf{x}$.

Under the above conditions, the *elastic potential energy* of the whole robot is then rearranged into a quadratic form in terms of the MP SAD screw $\delta\mathbf{x}$:

$$V^* = \frac{1}{2}\delta\mathbf{q}^{*T}\mathbf{K}_q\delta\mathbf{q}^* = \frac{1}{2}(\mathbf{F}\delta\mathbf{x})^T\mathbf{K}_q(\mathbf{F}\delta\mathbf{x}) = \frac{1}{2}\delta\mathbf{x}^T(\mathbf{F}^T\mathbf{K}_q\mathbf{F})\delta\mathbf{x} \tag{3.23}$$

3.3.4 Derivation of the Cartesian Stiffness Matrix

Given that the CSM $\mathbf{K}$ is calculated as the *Hessian* of the *elastic potential energy* w.r.t. the MP SAD screw, eq. (3.23) leads to

$$\mathbf{K} = \mathbf{F}^T\mathbf{K}_q\mathbf{F} \tag{3.24}$$

The CSM is thus a *congruent transformation* [70] of the GSM $\mathbf{K}_q$ via matrix $\mathbf{F}$, representing the mapping of the MP SAD screw $\delta\mathbf{x}$ into the PGA $\delta\mathbf{q}^*$ that leads to the *minimum potential energy*.

[10] All the entries of $\mathbf{H}$ bear the same physical units.

Substitution of eqs. (3.21) and (3.22) into eq. (3.24) leads to

$$\begin{aligned}
\mathbf{K} &= \mathbf{N}^T\mathbf{H}^{-T}\mathbf{D}_J\mathbf{K}_q^{-T}\mathbf{K}_q\mathbf{K}_q^{-1}\mathbf{D}_J^T\mathbf{H}^{-1}\mathbf{N} \\
&= \mathbf{N}^T\mathbf{H}^{-T}\mathbf{D}_J\mathbf{K}_q^{-T}(\mathbf{K}_q\mathbf{K}_q^{-1})\mathbf{D}_J^T\mathbf{H}^{-1}\mathbf{N} \\
&= \mathbf{N}^T\mathbf{H}^{-T}(\mathbf{D}_J\mathbf{K}_q^{-T}\mathbf{D}_J^T)\mathbf{H}^{-1}\mathbf{N} \\
&= \mathbf{N}^T(\mathbf{H}^{-T}\mathbf{H}^T)\mathbf{H}^{-1}\mathbf{N} \\
&= \mathbf{N}^T\mathbf{H}^{-1}\mathbf{N}
\end{aligned} \tag{3.25}$$

Matrix $\mathbf{H}$ in the above equation turns out to be *block-diagonal*, namely,

$$\mathbf{H} = \mathrm{diag}(\mathbf{H}_1, \mathbf{H}_2, \mathbf{H}_3) \in \mathbb{R}^{6\times 6} \tag{3.26a}$$

its jth diagonal block being

$$\mathbf{H}_j = \frac{1}{k_s}\mathbf{D}_{Lj}\mathbf{J}_C\mathbf{J}_C^T\mathbf{D}_{Lj}^T + \frac{1}{k_r}\mathbf{1}_2 = \begin{bmatrix} \dfrac{1}{k_s'} + \dfrac{1}{k_r} & 0 \\ 0 & \dfrac{1}{k_{sj}''} + \dfrac{1}{k_r} \end{bmatrix} \ (\mathrm{m/N}) \tag{3.26b}$$

with the definitions below:

$$k_s' = 2\left(\frac{2\pi}{p}\right)^2 k_s, \quad k_{sj}'' = 2\left(\frac{\iota}{l_j}\right)^2 k_s, \quad j = 1, 2, 3 \tag{3.26c}$$

and k_s introduced in eq. (3.3).

Generally speaking, due to their different physical units, the stiffness k_s of the motor shaft and the stiffness k_r of the limb-rod cannot be compared directly. However, eqs. (3.26c) transform the torsional stiffness k_s into its translational counterparts, k_s' and k_{sj}''. Upon comparing the magnitudes of the latter with the magnitude of k_r, how the stiffness of the motor shaft and that of the limb-rod contribute to the overall stiffness of the robot can be assessed.

Next, upon defining $\mathbf{K}_D \equiv \mathbf{H}^{-1}$, the CSM $\mathbf{K}$ takes the form

$$\mathbf{K} = \mathbf{N}^T \mathbf{K}_D \mathbf{N} \tag{3.27}$$

with

$$\mathbf{K}_D = \mathrm{diag}(\mathbf{K}_{D1}, \mathbf{K}_{D2}, \mathbf{K}_{D3}) \tag{3.28}$$

its (diagonal) blocks being

$$\mathbf{K}_{Dj} = \mathbf{H}_j^{-1} = \begin{bmatrix} \dfrac{k'_s k_r}{k'_s + k_r} & 0 \\ 0 & \dfrac{k''_{sj} k_r}{k''_{sj} + k_r} \end{bmatrix} \text{(N/m)}, \quad j = 1, 2, 3 \tag{3.29}$$

The CSM $\mathbf{K}$ is thus a *congruent transformation* [70] of the matrix $\mathbf{K}_D$ via matrix $\mathbf{N}$. Moreover, $\mathbf{K}_D$ is determined by the stiffnesses of the flexible parts, i.e., the torsional stiffness of the motor shaft and the translational stiffness of the limb-rod. This matrix is diagonal and *dimensionally homogeneous*. Stiffness values of different units are then transformed into the same units for comparison purposes. Moreover, each of the entries of $\mathbf{K}_D$ can be treated as the total stiffness of a series array of two springs whose stiffness values are the transformed motor-shaft stiffness k'_s (or k'_{sj}, as the case maybe) and the limb-rod stiffness k_r. Therefore, the overall robot stiffness will be smaller than the stiffness of any of its flexible parts, given that the ensemble forms a *serial array* of springs. Matrix $\mathbf{N}$ is posture-dependent, besides depending on the dimensions of the robot. As a result, the CSM is not only related to the stiffness of the flexible parts, but also to the robot posture and its geometry. On the other hand, the GSM $\mathbf{K}_q$ is *dimensionally inhomogeneous*, and depends only on the stiffness of the flexible parts, not on the robot posture. Therefore, the CSM can fully capture the stiffness properties of the robot, thus representing the *overall robot stiffness*.

3.4 Elastostatic Performance Indices

For elastostatic analysis, the *SDelta* is modelled as a rigid MP elastically suspended on a six-dof linear generalized spring, whose stiffness is characterized by a 6×6 *symmetric* and *positive-definite* (SPD) CSM $\mathbf{K}$. Because of its dimensional inhomogeneity, this matrix cannot represent the whole PKM stiffness. Therefore, scalar *performance indices* need to be defined to gain a clearer physical insight into the elastostatic response of the PKM.

To characterize the stiffness properties of the PKM, any *performance index* must be independent of the coordinate frame used to represent the CSM. In this section, the change of frame in *screw theory* is first recalled. Then, a *modified eigen-decomposition* of the CSM is introduced, to define the elastostatic *performance indices*.

3.4.1 Cartesian-frame Transformation

In the realm of *screw theory* [38, 39], a change of frame calls for an *affine transformation*, involving both the *rotation of the frame* and the *translation of the frame origin* [71]. The *affine transformation* between two frames is referred to as a *Cartesian frame transformation*, represented by a 6×6 matrix $\mathbf{S}$ [66, 72]:

$$\mathbf{S} = \begin{bmatrix} \mathbf{Q} & \mathbf{O} \\ \boldsymbol{\Delta}\mathbf{Q} & \mathbf{Q} \end{bmatrix}, \quad \boldsymbol{\Delta} = \mathrm{CPM}(\boldsymbol{\delta}) \equiv \frac{\partial(\boldsymbol{\delta} \times \mathbf{v})}{\partial \mathbf{v}}, \ \forall \mathbf{v} \in \mathbb{R}^3 \tag{3.30}$$

$\mathbf{Q}$ denoting, in turn, a 3×3 proper orthogonal matrix, representing the rotation of the frame axes, $\boldsymbol{\Delta}$ a 3×3 *skew-symmetric matrix* representing the *cross-product matrix* of the *shift* $\boldsymbol{\delta}$ of the frame origin.

The Cartesian-frame transformation $\mathbf{S}$ is *invertible*, but, in general, not orthogonal[11], namely,

$$\mathbf{S}^{-1} = \begin{bmatrix} \mathbf{Q}^T & \mathbf{O} \\ -\mathbf{Q}^T\boldsymbol{\Delta} & \mathbf{Q}^T \end{bmatrix}, \quad \mathbf{S}^T = \begin{bmatrix} \mathbf{Q}^T & -\mathbf{Q}^T\boldsymbol{\Delta} \\ \mathbf{O} & \mathbf{Q}^T \end{bmatrix} \tag{3.31}$$

$$\mathbf{S}^T = \boldsymbol{\Gamma}\mathbf{S}^{-1}\boldsymbol{\Gamma} \tag{3.32}$$

Under the foregoing change of frame, the CSM transforms into:

$$\mathbf{K}' = \boldsymbol{\Gamma}\mathbf{S}^{-1}\boldsymbol{\Gamma}\mathbf{K}\mathbf{S} = \mathbf{S}^T\mathbf{K}\mathbf{S} \tag{3.33}$$

The transformed CSM $\mathbf{K}'$ is thus a *congruent transformation* of $\mathbf{K}$ via $\mathbf{S}$, *symmetry* and *positive-definiteness* of the stiffness matrix thus being *preserved*. However, since the transformation matrix $\mathbf{S}$ is not orthogonal, $\mathbf{K}'$ is *not a similarity transformation* of $\mathbf{K}$. The eigenvalues and eigenvectors of the CSM are thus *not preserved* under the foregoing transformation. Therefore, *the conventional eigen-decomposition of the CSM can not be relied on to define any* frame-invariant *stiffness index*. Alternatives are introduced below.

3.4.2 Eigenstiffness and Eigenscrew

Upon pre-multiplying both sides of eq. (3.33) by $\boldsymbol{\Gamma}$, the Cartesian frame transformation is obtained:

$$\boldsymbol{\Gamma}\mathbf{K}' = \mathbf{S}^{-1}(\boldsymbol{\Gamma}\mathbf{K})\mathbf{S} \tag{3.34}$$

which represents a *similarity transformation* between $\boldsymbol{\Gamma}\mathbf{K}$ and $\boldsymbol{\Gamma}\mathbf{K}'$, the eigenvalues and eigenvectors of the product $\boldsymbol{\Gamma}\mathbf{K}$ thus being *preserved* [12].

[11] $\mathbf{S}$ need not be orthogonal because, in general, it carries one block with units of length.

[12] Eigenvalues, being scalars, are *immutable* under a similarity transformation; an eigenvector $\mathbf{e}$ changes, under such a transformation $\mathbf{S}$, to $\mathbf{S}\mathbf{e}$.

The eigenproblem of the CSM $\mathbf{K}$ is then modified into that of $\mathbf{\Gamma K}$:

$$\mathbf{\Gamma K k}_i = \mu_i \mathbf{k}_i, \quad i = 1, \cdots, 6 \tag{3.35}$$

Since $\mathbf{K}$ is a matrix with multiple units, as shown in eq. (3.10), the eigenvalue μ_i carries units of N, the corresponding eigenvector $\mathbf{k}_i$ being a *unit screw*, namely,

$$\mathbf{k}_i \equiv \begin{bmatrix} \mathbf{e}_i \\ \mathbf{p}_i \times \mathbf{e}_i + p_i \mathbf{e}_i \end{bmatrix}, \quad \|\mathbf{e}_i\| = 1, \quad i = 1, \cdots, 6 \tag{3.36}$$

$\mathbf{e}_i$ representing the direction of the ith screw axis, $\mathbf{p}_i$ the position vector of one point of this axis, and p_i the screw pitch, carrying units of length.

Then, the CSM $\mathbf{K}$ can be uniquely decomposed into a linear combination of rank-1 matrices, namely,

$$\mathbf{K} = \sum_{i=1}^{6} \frac{\mu_i}{2p_i} \mathbf{k}_i \mathbf{k}_i^T \tag{3.37}$$

This decomposition shows that $\mathbf{K}$ is fully determined by the *frame-invariant* μ_i, p_i and $\mathbf{k}_i$. The eigenvalues μ_i, for $i = 1, \cdots, 6$, are termed the *eigenstiffnesses*, p_i the *eigenpitches* of $\mathbf{K}$, and $\mathbf{k}_i$ the *eigenscrews*.

For a SPD CSM, its eigenstiffnesses, eigenpiches and eigenscrews have the properties [19, 66, 73]:

1. A SPD CSM has three negative and three positive eigenstiffnesses. They occur in real, *symmetric* pairs.

2. A SPD CSM has a full set of eigenscrews. All the eigenscrews have non-zero, finite pitches. The eigenscrews are *mutually reciprocal*.

3. Every eigenstiffness and its corresponding eigenpitch bear the same sign[13].

[13]If the sign of the eigenstiffness is positive, the direction of the wrench axis is the same as that of the

The eigenscrew decomposition in eq. (3.35) provides a means to interpret the PKM stiffness. Along the eigenscrew axis, the PKM behaves as a screw spring[14]. Then, under these conditions, the stiffness matrix $\mathbf{K}$ can be described by scalars $\{\mu_i\}_1^6$. The eigenstiffness μ_i reflects the PKM stiffness along the corresponding eigenscrew. Then, the rms value $\mu_{\rm rms}$ of the set of eigenstiffness values is adopted as the *elastostatic performance index κ to evaluate the overall PKM stiffness*, namely,

$$\kappa \equiv \mu_{\rm rms} = \sqrt{\frac{1}{6}\sum_{i=1}^{6}\mu_i^2} \quad \text{(N)} \tag{3.38}$$

In practice, an *eigensolver* is used to solve the eigenproblem of any square matrix. Any eigensolver treats $\mathbf{\Gamma K}$ as a *dimensionally homogeneous* matrix, then returns *dimensionally homogeneous* eigenvalues λ_i and the corresponding *unit, dimensionless eigenvectors* $\boldsymbol{\lambda}_i$, namely,

$$\mathbf{\Gamma K}\boldsymbol{\lambda}_i = \lambda_i\boldsymbol{\lambda}_i, \quad \|\boldsymbol{\lambda}_i\| = 1, \quad i = 1, 2, \cdots, 6 \tag{3.39}$$

with $\boldsymbol{\lambda}_i$ expressed block-wise as

$$\boldsymbol{\lambda}_i \equiv \begin{bmatrix} \boldsymbol{\eta}_i \\ \boldsymbol{\varsigma}_i \end{bmatrix} \in \mathbb{R}^6, \quad i = 1, \cdots, 6 \tag{3.40}$$

Upon looking at eqs. (3.36) and (3.37), in light of eqs. (3.39) and (3.40), the eigenstiffnesses and eigenscrews $\{\mu_i, \mathbf{k}_i\}_1^6$ of the CSM $\mathbf{K}$ are derived from the results $\{\lambda_i, \boldsymbol{\lambda}_i\}_1^6$

screw displacement axis. Otherwise, these two directions are opposite. If the sign of the eigenpitch is positive, the eigenscrew is right-handed. Otherwise, the eigenscrew is *left-handed*.

[14]Screw springs belong to a type of elastic devices, which provide *coupling* between a *translational spring* and a *torsional spring*. A screw spring allows a screw deformation, given by the vector array $\mathbf{x}_s$, containing a translational deformation *along* and a torsional deformation *around* the same axis. Moreover, the behaviour of a screw spring is characterized by $\mathbf{\Gamma w}_s = k_s\mathbf{x}_s$; that is, the screw deformation $\mathbf{x}_s$ only produces a wrench $\mathbf{w}_s$ along the same direction of $\mathbf{x}_s$[74].

returned by the *eigensolver*, i.e.,

$$\mu_i = \lambda_i, \quad p_i = \frac{\boldsymbol{\eta}_i^T \boldsymbol{\varsigma}_i}{\|\boldsymbol{\eta}_i\|^2}, \quad \mathbf{e}_i = \frac{\boldsymbol{\eta}_i}{\|\boldsymbol{\eta}_i\|}, \quad \mathbf{p}_i = \frac{\boldsymbol{\eta}_i \times \boldsymbol{\varsigma}_i}{\|\boldsymbol{\eta}_i\|^2} \tag{3.41}$$

3.4.3 Translational Stiffness and Wrench-compliant Axis

Although the eigenscrew decomposition reduces the matrix nature of the Cartesian stiffness to a scalar index, μ_i in our case, the eigenscrew $\mathbf{k}_i$ still represents a decoupling between translation and rotation. In the subsections below, the concepts of *wrench-compliant* axes and *twist-compliant* axes are introduced. Along these axes, translation and rotation are partially decoupled [19].

A wrench applied onto the *wrench-compliant* axis produces a pure translational deformation parallel to the same axis, i.e.,

$$\begin{bmatrix} \mathbf{K}_{11} & \mathbf{K}_{12} \\ \mathbf{K}_{12}^T & \mathbf{K}_{22} \end{bmatrix} \begin{bmatrix} \mathbf{0} \\ \mathbf{e}_{wi} \end{bmatrix} = \alpha_i \boldsymbol{\Gamma} \underbrace{\begin{bmatrix} \mathbf{e}_{wi} \\ \mathbf{g}_{wi} \end{bmatrix}}_{\mathbf{w}_{ci}}, \quad i = 1, 2, 3 \tag{3.42}$$

where the *wrench-compliant* axis is given by $\mathbf{w}_{ci} = [\mathbf{e}_{wi}^T, \mathbf{g}_{wi}^T]^T$, the unit vector $\mathbf{e}_{wi}$ representing the direction of the axis, while α_i is a translational stiffness, carry units of N/m. The set $\{\alpha_i, \mathbf{e}_{wi}\}_1^6$ is calculated from the eigenvalues and the corresponding eigenvectors of the SPD block $\mathbf{K}_{22}$, the set thus being *frame-invariant*[15].

In summary, a SPD CSM has three *wrench-compliant* axes, whose direction vectors are mutually orthogonal. Along the $\mathbf{w}_{ci}$ axis, the PKM behaves as a *quasi-translational spring*. The wrench applied onto the *wrench-compliant axis* $\mathbf{w}_{ci}$ can only produce a *pure translational deformation* parallel to the direction $\mathbf{t}_{wi}$ of $\mathbf{e}_{wi}$. Moreover, the eigenvalue α_i of $\mathbf{K}_{22}$ reflects the PKM translational stiffness along the corresponding *wrench-compliant*

[15] Based on eq. (3.33), $\mathbf{K}'_{22} = \mathbf{Q}^T \mathbf{K}_{22} \mathbf{Q}$, where $\mathbf{Q}$ denotes an orthogonal 3×3 rotation matrix, which indicates that the eigenvalues of $\mathbf{K}_{22}$ are *preserved* under a change of frame.

axis. Then, the elastostatic *performance index* κ_t to evaluate the translational stiffness of the PKM is defined as the rms value α_{rms} of α_i, for $i = 1, 2, 3$, namely,

$$\kappa_t = \alpha_{\text{rms}} = \sqrt{\frac{1}{3}\sum_{i=1}^{3}\alpha_i^2} \quad (\text{N/m}) \tag{3.43}$$

3.4.4 Torsional Stiffness and Twist-compliant Axis

The elastostatics of the PKM can be also modelled as

$$\delta\mathbf{x} = \mathbf{C}\mathbf{w} \tag{3.44a}$$

with

$$\mathbf{C} \equiv \mathbf{K}^{-1} = \begin{bmatrix} \mathbf{C}_{11} & \mathbf{C}_{12} \\ \mathbf{C}_{12}^T & \mathbf{C}_{22} \end{bmatrix} \tag{3.44b}$$

denoting the *Cartesian compliance matrix* (CCM) of the PKM.

The *twist-compliant* axis is the *dual* of the *wrench-compliant* axis. A screw deformation along an axis produces a pure moment around the same axis, i.e.,

$$\begin{bmatrix} \mathbf{C}_{11} & \mathbf{C}_{12} \\ \mathbf{C}_{12}^T & \mathbf{C}_{22} \end{bmatrix} \begin{bmatrix} \beta_i \mathbf{e}_{ti} \\ \mathbf{0} \end{bmatrix} = \underbrace{\begin{bmatrix} \mathbf{e}_{ti} \\ \mathbf{g}_{ti} \end{bmatrix}}_{\mathbf{t}_{ci}}, \quad i = 1, 2, 3 \tag{3.45}$$

where the *twist-compliant* axis, $\mathbf{t}_{ci} \equiv \left[\mathbf{e}_{ti}^T,\ \mathbf{g}_{ti}^T\right]^T$, with the unit vector $\mathbf{e}_{ti}$ representing the direction of the said axis, β_i a torsional stiffness, carrying units of N·m. The set $\{\beta_i,\ \mathbf{e}_{ti}\}_1^6$ is calculated from the inverse of the eigenvalues and the corresponding eigenvectors of the SPD block $\mathbf{C}_{11}$, the set thus being *frame-invariant*[16].

[16]Under a change of frame $\mathbf{S}$, the Cartesian compliant matrix $\mathbf{C}$ is transformed into $\mathbf{C}' = \mathbf{S}^{-1}\mathbf{C}\mathbf{S}^{-T}$. Then, $\mathbf{C}'_{11} = \mathbf{Q}^T\mathbf{C}_{11}\mathbf{Q}$, which denotes a *similarity transformation* of $\mathbf{C}_{11}$, given that $\mathbf{Q}$ is orthogonal. Hence, the eigenvalues of $\mathbf{C}_{11}$ are *preserved* under a change of frame.

In summary, a SPD CSM has three *twist-compliant* axes, whose direction vectors are mutually orthogonal. Along the *twist-compliant* axis $\mathbf{t}_{ci}$, the PKM behaves as a *quasi-torsional spring*. The screw deformation along the *twist-compliant axis* $\mathbf{t}_{cj}$ can only produce a *pure moment* around the direction $\mathbf{e}_{ti}$ of $\mathbf{t}_{ci}$. Moreover, the inverse β_i of the corresponding eigenvalue of $\mathbf{C}_{11}$ reflects the PKM torsional stiffness along the *twist-compliant* axis. Then, the elastostatic *performance index* κ_r is defined as the rms value β_{rms} of β_i, for $i = 1, 2, 3$, to evaluate the torsional stiffness of the PKM, namely,

$$\kappa_r = \beta_{\mathrm{rms}} = \sqrt{\frac{1}{3}\sum_{i=1}^{3}\beta_i^2} \quad (\mathrm{N{\cdot}m}) \tag{3.46}$$

In this subsection, under the modified eigenvalue-decomposition, three types of alternative indices, namely, the eigenstiffness based on the eigenscrews, the translational stiffness based on the wrench-compliant axes and the torsional stiffness based on the twist-compliant axes, are defined from the CSM to evaluate the PKM stiffness; this allows us to choose the most appropriate one for specific applications. For optimum design to achieve better rigidity performance, the higher the stiffness indices are, the stiffer the PKM is.

3.5 Numerical Example: Elastostatic Analysis of the SDelta Robot

3.5.1 Cartesian Stiffness Matrix

For the application of interest, the rigid-body inertia-parameter identification, the PKM is required to generate six-dof small-amplitude vibration around a equilibrium position at a high-frequency. The evaluation of the elastostatic performance throughout the whole workspace is cumbersome, and to some extent, not necessary for such application; it is thus desirable to calculate the foregoing elastostatic performance indices at a specific posture. This posture is the "symmetric" posture shown in Fig. 3.8. At this posture, the PKM is *most likely* to attain its maximum dexterity (minimum condition number of the forward Jacobian matrix) [16]. It is recalled, first, that both the MP and the BP bear shapes of equilateral triangles, the operation point being the c.o.m. O of the MP triangle. Moreover, the posture of choice satisfies the conditions below:

- The operation point S lies on the vertical (Z-axis of Fig. 3.1) of the centroid O of the BP.

- The plane of the MP triangle is parallel to that of its BP counterpart.

Here, a, b and h denote, respectively, the side length of the BP triangle, that of the MP triangle, and the Z-coordinate of the operation point O. For purposes of analysis, a frame XYZ is attached to the BP, as shown in Fig. 3.1, with its origin located at the centroid O of the BP triangle. The vertices of the latter are represented by $\{B_j\}_1^3$. Moreover, the X-axis points along the B_1B_2 direction; the Y-axis along the OB_3 direction; and the Z-axis, passing through O, is normal to X and Y, thereby completing a right-hand orthogonal frame.

Next, the parameters to calculate the stiffness are introduced. The dimensions below are intended for a desktop-scale prototype:

$$r = 150 \text{ (mm)}, \quad R = 450 \text{ (mm)}, \quad h = 150 \text{ (mm)} \tag{3.47}$$

where r denotes the *circumradius* of the MP plane and R that of the BP plane.

Moreover, Titanium is selected as the material of the limb-rod[17]. The *length* l_r and the diameter d_r of the limb-rods are

$$l_r = 115 \text{ (mm)}, \quad d_r = 11.5 \text{ (mm)} \tag{3.48}$$

[17]Titanium is ideal for this application because of its low density and high stiffness. Due to these properties, Titanium is an ideal material for the limbs of the PKM intended for HFSA applications.

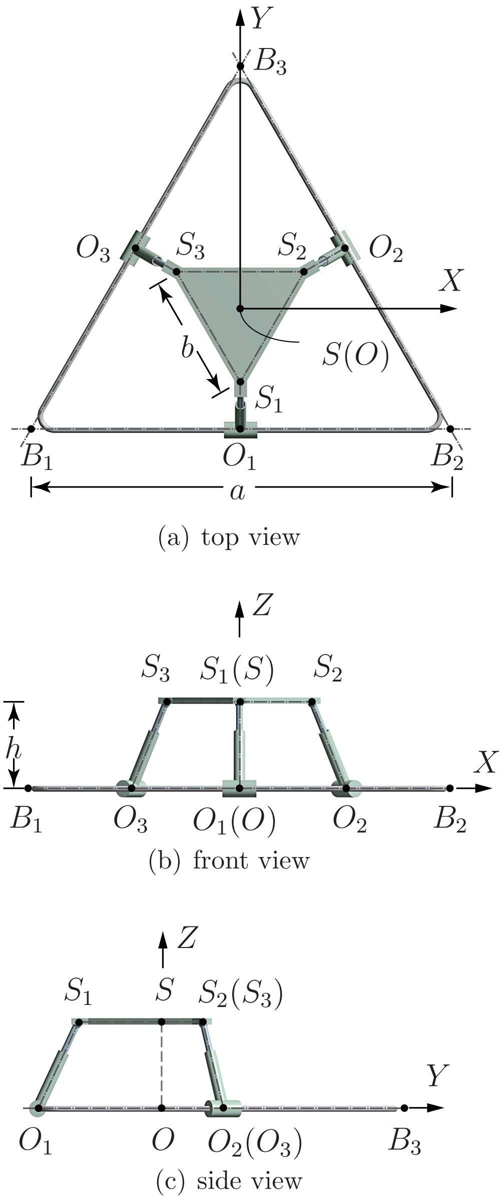

(a) top view

(b) front view

(c) side view

Fig. 3.8 Three views of the symmetric posture

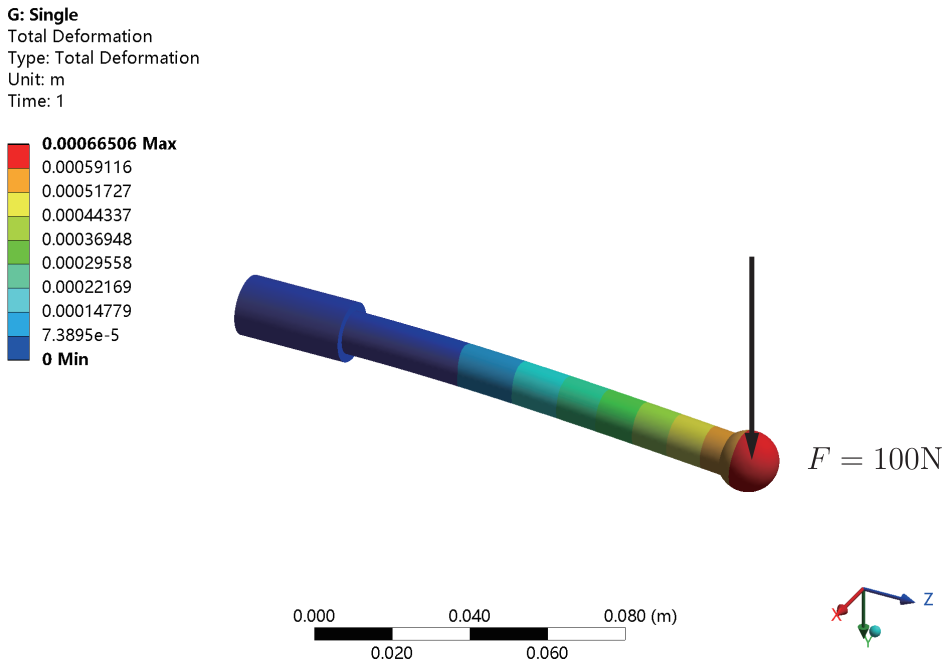

Fig. 3.9 Bending deflection of the limb-rod in ANSYS Workbench

The stiffness of the slender limb-rod is calculated by FEA. The CAD model of the rod is then ported into ANSYS. Its lower end is assumed to be fixed and an external force normal to its axis is applied onto its upper end, as shown in Fig. 3.9. According to the ANSYS results, when the magnitude of the external force is 100N, the bending deflection of the limb-rod at its upper end is 6.6506×10^{-4} m, the stiffness of the limb-rod thus being

$$k_r = \frac{100}{6.6506 \times 10^{-4}} = 1.5036 \times 10^5 \text{ N/m} \tag{3.49}$$

The *C-drive* is actuated by two identical Yaskawa[18] AC servomotors [75]. The length l_s, the diameter d_s and the *shear modulus* of the motor shaft are

$$l_s = 40 \text{ (mm)}, \quad d_s = 16 \text{ (mm)}, \quad G = 75 \text{ (GPa)} \tag{3.50}$$

[18] SGMAH08AAF4C

Thus, the stiffness k_1 of the motor shaft is

$$k_1 = 1.2064 \times 10^4 \text{ (N·m/rad)} \tag{3.51}$$

The coupling between the motor shaft and its corresponding screw is Disc Coupling[19] MCSLCWK-50, whose torsional stiffness is

$$k_2 = 3400 \text{ (N·m/rad)} \tag{3.52}$$

Therefore, the equivalent torsional stiffness of the motor shaft, together with the coupling, is

$$k_s = 2.6524 \times 10^3 \text{ (N·m/rad)} \tag{3.53}$$

Moreover, the speed-reduction ratio ι of the *C-drive* is[20]

$$\iota = 6 \tag{3.54}$$

Based on eq. (3.26c), when $\iota = 6$, the torsional stiffness k_s is transformed into its translational counterparts, namely,

$$k_s' = 5.8175 \times 10^7 \text{ (N/m)} \approx 387 k_r, \quad k_s'' = 6.7903 \times 10^6 \text{ (N/m)} \approx 45 k_r \tag{3.55}$$

Upon comparing the values of k_s' and k_s'' with that of k_r, the stiffness of the motor shaft, together with its coupling, is shown to be much higher than that of the limb-rod. Although the motor shaft and its coupling are more flexible when compared with other parts of the *C-drive*, they are much stiffer than the limb-rod.

[19]The MCSLCWK is a disc coupling for servo motors provided by MiSUMi. Details of this coupling are available at https://us.misumi-ec.com/vona2/detail/110300120520/?Tab=codeList.

[20]Greek letter ι.

Based on the above dimensions, and taking both the *C-drive* and the limb-rod flexibility into account, the 3×3 blocks of the *SDelta* CSM at the foregoing "symmetric posture" are[21]

$$\mathbf{K}_{11} = \begin{bmatrix} 0.0993 & 0 & 0 \\ 0 & 0.0993 & 0 \\ 0 & 0 & 1.0123 \end{bmatrix} \times 10^4 \text{ (N·m)} \tag{3.56a}$$

$$\mathbf{K}_{12} = \begin{bmatrix} 0 & 1.3239 & 0 \\ -1.3239 & 0 & 0 \\ 0 & 0 & 0 \end{bmatrix} \times 10^4 \text{ (N)} \tag{3.56b}$$

$$\mathbf{K}_{22} = \begin{bmatrix} 4.0149 & 0 & 0 \\ 0 & 4.0149 & 0 \\ 0 & 0 & 0.8826 \end{bmatrix} \times 10^5 \text{ (N/m)} \tag{3.56c}$$

3.5.2 Stiffness Performance Indices

Eigenstiffness

The six eigenforces are

$$\begin{aligned} \mu_1 = -\mu_2 &= -1.4946 \times 10^4 \text{ (N)} \\ \mu_3 = -\mu_4 &= -1.4946 \times 10^4 \text{ (N)} \\ \mu_5 = -\mu_6 &= -2.9892 \times 10^4 \text{ (N)} \end{aligned} \tag{3.57}$$

the eigenpitches of the corresponding eigenscrews being

$$\begin{aligned} p_1 = -p_2 &= -0.0372 \text{ (m)} \\ p_3 = -p_4 &= -0.0372 \text{ (m)} \\ p_5 = -p_6 &= -0.3387 \text{ (m)} \end{aligned} \tag{3.58}$$

[21] Notice that $\mathbf{K}_{11}$ and $\mathbf{K}_{22}$ are both *isotropic* in the X-Y plane because of both the symmetric design and the chosen posture.

Moreover, the position and direction vectors of the corresponding eigenscrews are, respectively,

$$\begin{aligned}
\mathbf{p}_1 = \mathbf{p}_2 &= [0,\ 0,\ -0.0330]^T \ \ (\mathrm{m}) \\
\mathbf{p}_3 = \mathbf{p}_4 &= [0,\ 0,\ -0.0330]^T \ \ (\mathrm{m}) \\
\mathbf{p}_5 = \mathbf{p}_6 &= \mathbf{0}
\end{aligned} \tag{3.59}$$

and

$$\begin{aligned}
\mathbf{e}_1 &= [-0.7485,\ 0.6631,\ 0]^T \\
\mathbf{e}_2 &= [-0.7485,\ -0.6631,\ 0]^T \\
\mathbf{e}_3 &= [0.7249,\ 0.6889,\ 0]^T \\
\mathbf{e}_4 &= [0.7083,\ -0.7059,\ 0]^T \\
\mathbf{e}_5 &= [0,\ 0,\ -1]^T \\
\mathbf{e}_6 &= [0,\ 0,\ -1]^T
\end{aligned} \tag{3.60}$$

The axes of the first four eigenscrews lie in a plane parallel to the X-Y plane and pass through the point P, of position vector $[0,\ 0,\ 0.0330]^T$ m. The first and the third eigenscrews are *left-handed*, the second and the fourth *right-handed*. The eigenpitches of the four eigenscrews are all 0.0372 m. Moreover, the stiffness of the PKM along the first four eigenscrews is 1.4946×10^4 N. The last two eigenscrews point in the Z-direction and pass through the origin. Moreover, the fifth eigenscrew is *left-handed*, the sixth right-handed. The eigenpitches of these two eigenscrews are both 0.3387 m. Furthermore, the stiffness of the PKM along the last two eigenscrews is 2.9892×10^4 N.

Thus, the elastostatic *performance index* κ that represents the overall stiffness of the PKM is the rms value of the eigenforces, i.e.,

$$\kappa = \sqrt{\frac{1}{6}\sum_{i=1}^{6} \mu_i^2} = 2.1137 \times 10^4 \ (\mathrm{N}) \tag{3.61}$$

Translational Stiffness

The translational stiffness values α_i are

$$\begin{aligned}\alpha_1 &= 4.0149 \times 10^5 \text{ (N/m)}\\ \alpha_2 &= 4.0149 \times 10^5 \text{ (N/m)}\\ \alpha_3 &= 0.8826 \times 10^5 \text{ (N/m)}\end{aligned} \tag{3.62}$$

The pitches p_{wi}, direction vectors $\mathbf{e}_{wi}$ and position vectors $\mathbf{p}_{wi}$ of the corresponding *wrench-compliant* axes are

$$\begin{aligned}p_{w1} &= 0, \quad \mathbf{e}_{w1} = [1,\ 0,\ 0]^T, \quad \mathbf{p}_{w1} = [0,\ 0,\ -0.0330]^T \text{ (m)}\\ p_{w2} &= 0, \quad \mathbf{e}_{w2} = [0,\ 1,\ 0]^T, \quad \mathbf{p}_{w2} = [0,\ 0,\ -0.0330]^T \text{ (m)}\\ p_{w3} &= 0, \quad \mathbf{e}_{w3} = [0,\ 0,\ 1]^T, \quad \mathbf{p}_{w3} = \mathbf{0}\end{aligned} \tag{3.63}$$

The first *wrench-compliant* axis is a line pointing in the X-direction, the second a line pointing in the Y-direction. These two axes pass through point P, of position vector $[0,\ 0,\ -0.0330]^T$ m. Moreover, the translational stiffness of the PKM along these two axes is 4.0149×10^5 N/m. The third *wrench-compliant* axis is a line pointing in the Z-direction and passing through the origin. The translational stiffness of the PKM along this axis is 8.826×10^4 N/m.

Then, the elastostatic *performance index* κ_t that represents the translational stiffness of the PKM, defined as the rms value of the three foregoing values, is

$$\kappa_t = \sqrt{\frac{1}{3}\sum_{i=1}^{3}\alpha_i^2} = 3.3175 \times 10^5 \text{ (N/m)} \tag{3.64}$$

Torsional Stiffness

The torsional stiffness values β_i are

$$\begin{aligned}\beta_1 &= 1/\lambda_{t1} = 0.5564 \times 10^3 \text{ (N·m)} \\ \beta_2 &= 1/\lambda_{t2} = 0.5564 \times 10^3 \text{ (N·m)} \\ \beta_3 &= 1/\lambda_{t3} = 1.0123 \times 10^4 \text{ (N·m)}\end{aligned} \tag{3.65}$$

The pitches p_{ti}, direction vectors $\mathbf{e}_{ti}$ and position vectors $\mathbf{p}_{ti}$ of the corresponding *twist-compliant* axes are, in turn,

$$\begin{aligned}&p_{t1} = 0, \quad \mathbf{e}_{t1} = [1,\ 0,\ 0]^T, \quad \mathbf{p}_{t1} = [0,\ 0,\ -0.0330]^T \text{ (m)} \\ &p_{t2} = 0, \quad \mathbf{e}_{t2} = [0,\ 1,\ 0]^T, \quad \mathbf{p}_{t2} = [0,\ 0,\ -0.0330]^T \text{ (m)} \\ &p_{t3} = 0, \quad \mathbf{e}_{t3} = [0,\ 0,\ 1]^T, \quad \mathbf{p}_{t3} = \mathbf{0}\end{aligned} \tag{3.66}$$

The first *twist-compliant* axis is thus a line pointing in the X-direction, the second a line pointing in the Y-direction. These two axes pass through point P, of position vector $[0,\ 0,\ -0.0330]^T$ (m). Moreover, the torsional stiffness of the PKM along these two axes is 0.556×10^3 (N·m). The third *twist-compliant* axis is a line pointing in the Z-direction and passing through the origin. The torsional stiffness of the PKM along this axis is 1.0123×10^4 (N·m).

Then, the elastostatic *performance index* κ_r that represents the torsional stiffness of the PKM is

$$\kappa_r = \sqrt{\frac{1}{3}\sum_{i=1}^{3}\beta_i^2} = 5.8623 \times 10^3 \text{ (N·m)} \tag{3.67}$$

3.5.3 Discussion and Comparison

According to eqs. (3.55), the motor shaft, together with its coupling, is much stiffer than the limb-rod. Therefore, under some conditions, for simplification, the compliance of the

C-drive can be neglected.

When taking only the limb-rod flexibility into account, the torsional stiffness k_s is assumed to be infinite. In this case, the CSM of the robot is expressed as

$$\mathbf{K}_0 = \mathbf{N}^T \mathbf{K}_r \mathbf{N}, \quad \mathbf{K}_r = k_r \mathbf{1}_6 \tag{3.68}$$

Here, "condition 1" indicates that only the limb-rod flexibility is taken into account, "condition 2" indicating that both the flexibility of the *C-drive* and that of the limb-rod are taken into account. Under "condition 2", the four blocks of the CSM at the "symmetric posture" are

$$\mathbf{K}_{11} = \begin{bmatrix} 0.1015 & 0 & 0 \\ 0 & 0.1015 & 0 \\ 0 & 0 & 1.0149 \end{bmatrix} \times 10^4 \text{ (N·m)} \tag{3.69a}$$

$$\mathbf{K}_{12} = \begin{bmatrix} 0 & 1.3533 & 0 \\ -1.3533 & 0 & 0 \\ 0 & 0 & 0 \end{bmatrix} \times 10^4 \text{ (N)} \tag{3.69b}$$

$$\mathbf{K}_{22} = \begin{bmatrix} 4.0598 & 0 & 0 \\ 0 & 4.0598 & 0 \\ 0 & 0 & 0.9022 \end{bmatrix} \times 10^5 \text{ (N/m)} \tag{3.69c}$$

The stiffness indices calculated from the CSMs under these two conditions are listed in Table 3.2.

Apparently, from Table 3.2, the overall stiffness of the PKM decreases by around 1.22% when the *C-drive* compliance is taken into account. Moreover, under the same conditions, the translational and torsional stiffnesses of the PKM decrease by around 1.13% and 0.27%, respectively. This indicates, again, that the *C-drive* is much stiffer

Table 3.2 Stiffness indices under two different conditions

Condition 1	Condition 2	Differences
$\mu_2 = -\mu_1 = 1.4946 \times 10^4$ $\mu_4 = -\mu_3 = 1.4946 \times 10^4$ $\mu_6 = -\mu_5 = 2.9892 \times 10^4$ $\kappa = 2.1137 \times 10^4$ (N)	$\mu_2 = -\mu_1 = 1.5130 \times 10^4$ $\mu_4 = -\mu_3 = 1.5130 \times 10^4$ $\mu_6 = -\mu_5 = 3.0260 \times 10^4$ $\kappa = 2.1397 \times 10^4$ (N)	1.22%
$\alpha_1 = 4.0149 \times 10^5$ $\alpha_2 = 4.0149 \times 10^5$ $\alpha_3 = 0.8826 \times 10^5$ $\kappa_t = 3.3175 \times 10^5$ (N/m)	$\alpha_1 = 4.0598 \times 10^5$ $\alpha_2 = 4.0598 \times 10^5$ $\alpha_3 = 0.9022 \times 10^5$ $\kappa_t = 3.3555 \times 10^5$ (N/m)	1.13%
$\beta_1 = 1/\lambda_{t1} = 0.5564 \times 10^3$ $\beta_2 = 1/\lambda_{t2} = 0.5564 \times 10^3$ $\beta_3 = 1/\lambda_{t3} = 1.0123 \times 10^4$ $\kappa_r = 5.8623 \times 10^3$ (N·m)	$\beta_1 = 0.5639 \times 10^3$ $\beta_2 = 0.5639 \times 10^3$ $\beta_3 = 1.0149 \times 10^4$ $\kappa_r = 5.8779 \times 10^3$ (N·m)	0.27%

than the limb-rods. Compared with the limb-rod flexibility, that of the *C-drive* barely influences the overall robot compliance. Therefore, under the dimensions adopted here, for simplification, the complance of the *C-drive* can be neglected when conducting the stiffness analysis of the robot.

3.6 Model Validation

3.6.1 Validation Method

The CAD model of the *SDelta Robot* is imported into a FEA environment. The three limb-rods are defined as flexible bodies and analyzed by FEA, all other parts of the *SDelta* being assumed rigid. During the simulation, at least six independent wrenches are applied onto the MP c.o.m. Upon collecting the corresponding SADs of at least three noncollinear *reference* points on the MP, the CCM of the *SDelta* can be estimated. The estimation is based on the relation

$$\delta \mathbf{x} = \mathbf{C}\mathbf{w} \tag{3.70}$$

with $\mathbf{C}$ denoting the CCM of the PKM.

At the *symmetric posture*, several entries of the CCM $\mathbf{C}$ vanish:

$$\mathbf{C} = \begin{bmatrix} c_{11} & 0 & 0 & 0 & c_{15} & 0 \\ 0 & c_{22} & 0 & c_{24} & 0 & 0 \\ 0 & 0 & c_{33} & 0 & 0 & 0 \\ 0 & c_{24} & 0 & c_{44} & 0 & 0 \\ c_{15} & 0 & 0 & 0 & c_{55} & 0 \\ 0 & 0 & 0 & 0 & 0 & c_{66} \end{bmatrix} \in \mathbb{R}^{6\times 6} \tag{3.71}$$

Therefore, only eight scalars—three rotational compliances (c_{11}, c_{22}, c_{33}), three translational compliances (c_{44}, c_{55}, c_{66}) and two coupling compliances (c_{15}, c_{24})—are to be estimated from measurements.

For simplicity, three independent moments and three independent forces along the X, Y and Z axes are applied at the MP c.o.m., respectively. These components determine six wrenches, arrayed columnwise in matrix $\mathbf{W}$, as displayed below:

$$\mathbf{W} = \begin{bmatrix} n_X & 0 & 0 & 0 & 0 & 0 \\ 0 & n_Y & 0 & 0 & 0 & 0 \\ 0 & 0 & n_Z & 0 & 0 & 0 \\ 0 & 0 & 0 & f_X & 0 & 0 \\ 0 & 0 & 0 & 0 & f_Y & 0 \\ 0 & 0 & 0 & 0 & 0 & f_Z \end{bmatrix} \tag{3.72}$$

whose first three diagonal entries denote moments, the last three forces.

Based on relation (3.70), the corresponding SAD screws of the MP evaluated at the c.o.m. C, arrayed columnwise in matrix $\mathbf{X}$, are

$$\mathbf{X} = \mathbf{CW} \tag{3.73}$$

i.e.,

$$\underbrace{\begin{bmatrix} \theta_{11} & 0 & 0 & 0 & \theta_{15} & 0 \\ 0 & \theta_{22} & 0 & \theta_{24} & 0 & 0 \\ 0 & 0 & \theta_{33} & 0 & 0 & 0 \\ 0 & u_{42} & 0 & u_{44} & 0 & 0 \\ u_{51} & 0 & 0 & 0 & u_{55} & 0 \\ 0 & 0 & 0 & 0 & 0 & u_{66} \end{bmatrix}}_{\mathbf{X}} = \underbrace{\begin{bmatrix} c_{11}n_Z & 0 & 0 & 0 & c_{15}f_Y & 0 \\ 0 & c_{22}n_Y & 0 & c_{24}f_X & 0 & 0 \\ 0 & 0 & c_{33}n_Z & 0 & 0 & 0 \\ 0 & c_{24}n_Y & 0 & c_{44}f_X & 0 & 0 \\ c_{15}n_X & 0 & 0 & 0 & c_{55}f_Y & 0 \\ 0 & 0 & 0 & 0 & 0 & c_{66}f_Z \end{bmatrix}}_{\mathbf{CW}} \tag{3.74}$$

where θ_{ij}, for $i = 1, 2, 3$, $j = 1, \ldots, 6$, represent the entries of the MP rotation under the jth wrench. Moreover, u_{ij}, for $i = 4, 5, 6$ and $j = 1, \ldots, 6$, represent the translation of the MP c.o.m., C, along the corresponding axis, under the jth wrench.

Furthermore, according to eq. (3.74), the *small-amplitude* translational/rotational entries in $\mathbf{X}$ are proportional to the corresponding force/moment entries given by $\mathbf{W}$, respectively:

$$\begin{cases} u_{44} = c_{44}f_X \\ u_{55} = c_{55}f_Y \\ u_{66} = c_{66}f_Z \end{cases}, \quad \begin{cases} u_{51} = c_{15}n_X \\ u_{42} = c_{24}n_Y \end{cases}, \quad \begin{cases} \theta_{11} = c_{11}n_X \\ \theta_{22} = c_{22}n_Y \\ \theta_{33} = c_{33}n_Z \end{cases} \tag{3.75}$$

The coefficients in the foregoing relations are the translational, the coupled and the rotational compliances under estimation.

The *small-amplitude* translational displacements of the *reference* points under given wrenches are computed directly by the simulation facility. Therefore, upon collecting the translational displacements, u_{44}, u_{55}, u_{66}, u_{15} and u_{24}, of the MP c.o.m. O under the forces applied along the X, Y and Z axes, along with the moments applied around the X and Y axes, the translational and coupled compliances are readily estimated via the linear relation in eq. (3.75). By contrast, the estimation of the rotational compliance is a bit more demanding, since the rotation of a rigid body is not provided directly, which needs to be calculated via the translation of *at least* three non-collinear points[22] on the body. In our case, the rotation of the MP is derived via the translational displacements of the MP c.o.m. O and the MP triangle vertices, S_1, S_2 and S_3. The SAD of S and the SAD of S_i are defined below:

$$\delta\mathbf{x}_S = \begin{bmatrix} \boldsymbol{\theta} \\ \delta\mathbf{s} \end{bmatrix}, \quad \delta\mathbf{x}_{S_i} = \begin{bmatrix} \boldsymbol{\theta} \\ \delta\mathbf{s}_i \end{bmatrix}, \quad i = 1, 2, 3 \tag{3.76}$$

with $\boldsymbol{\theta} = \theta\mathbf{e}$ denoting the *rotation vector*[23] of the MP through a "small" angle θ around the axis of rotation $\mathbf{e}$. Moreover, $\delta\mathbf{s}, \delta\mathbf{s}_i \in \mathbb{R}^3$ denote the *small-amplitude translation vector* of points S and S_i on the rigid MP under an external wrench. The translation vector $\delta\mathbf{s}_i$ can be derived from $\delta\mathbf{s}$ and $\boldsymbol{\theta}$:

$$\delta\mathbf{s}_i = \mathbf{s}' + \mathbf{p}_i' - \mathbf{s} - \mathbf{p} = (\mathbf{s}' - \mathbf{s}) + (\mathbf{Q}\mathbf{p}_i - \mathbf{p}_i) = \delta\mathbf{s} + (\mathbf{Q} - \mathbf{1})\mathbf{p}_i \tag{3.77}$$

$\mathbf{s}$ and $\mathbf{s}'$ denoting the position vector of S before and after the application of the external wrench, $\mathbf{p}_i$ and $\mathbf{p}_i'$ the vector stemming from S and ending at S_i. Furthermore, $\mathbf{Q}$ is the

[22] While the displacements of three non-collinear points of a rigid body *determine* the rotation of the body, unavoidable *noise measurements* call for a richer set of points when conducting experiments.

[23] While a rigid-body rotation bears a *tensor* nature, represented by a matrix, *small rotations* behave as vectors [76].

rotation matrix that takes the general form given below:

$$\mathbf{Q} = \mathbf{e}\mathbf{e}^T + \cos\theta(\mathbf{1} - \mathbf{e}\mathbf{e}^T) + \sin\theta\mathbf{E}, \quad \mathbf{E} \equiv \mathrm{CPM}(\mathbf{e}) \tag{3.78}$$

Upon collecting the translational displacements of points S and $\{S_i\}_1^3$, the rotation of the MP is derived via eqs. (3.77) and (3.78). Thereafter, the rotational compliance can be estimated based on the linear relation between the angles of rotation and the magnitudes of the moments in eq. (3.75).

3.6.2 Simulation Results

The translational displacements of the MP c.o.m. and the rotation of the MP under different moments and forces are calculated via both FEA simulation software, ANYSYS Workbench, and the mathematical model, with the results displayed in Figs. 3.10–3.12. According to the plots therein the simulation results match the computed results reasonably well. A numerical comparison is provided in Table 3.3.

Table 3.3 Stiffness indices under different conditions

	Mathematical Model	FEA Simulation	Units	Differences
c_{11}	1.7735×10^{-3}	1.7103×10^{-3}	$\mathrm{N}^{-1}\mathrm{m}^{-1}$	3.56%
c_{22}	1.7735×10^{-3}	1.8686×10^{-3}	$\mathrm{N}^{-1}\mathrm{m}^{-1}$	5.36%
c_{33}	0.9853×10^{-4}	0.8920×10^{-4}	$\mathrm{N}^{-1}\mathrm{m}^{-1}$	9.47%
c_{15}	-5.9116×10^{-5}	-6.2037×10^{-5}	N^{-1}	4.94%
c_{24}	5.9116×10^{-5}	6.6508×10^{-5}	N^{-1}	11.11%
c_{44}	4.4337×10^{-6}	4.8726×10^{-6}	$\mathrm{N}^{-1}\mathrm{m}$	9.90%
c_{55}	4.4337×10^{-6}	4.7917×10^{-6}	$\mathrm{N}^{-1}\mathrm{m}$	8.07%
c_{66}	1.1084×10^{-5}	1.0912×10^{-5}	$\mathrm{N}^{-1}\mathrm{m}$	1.55%

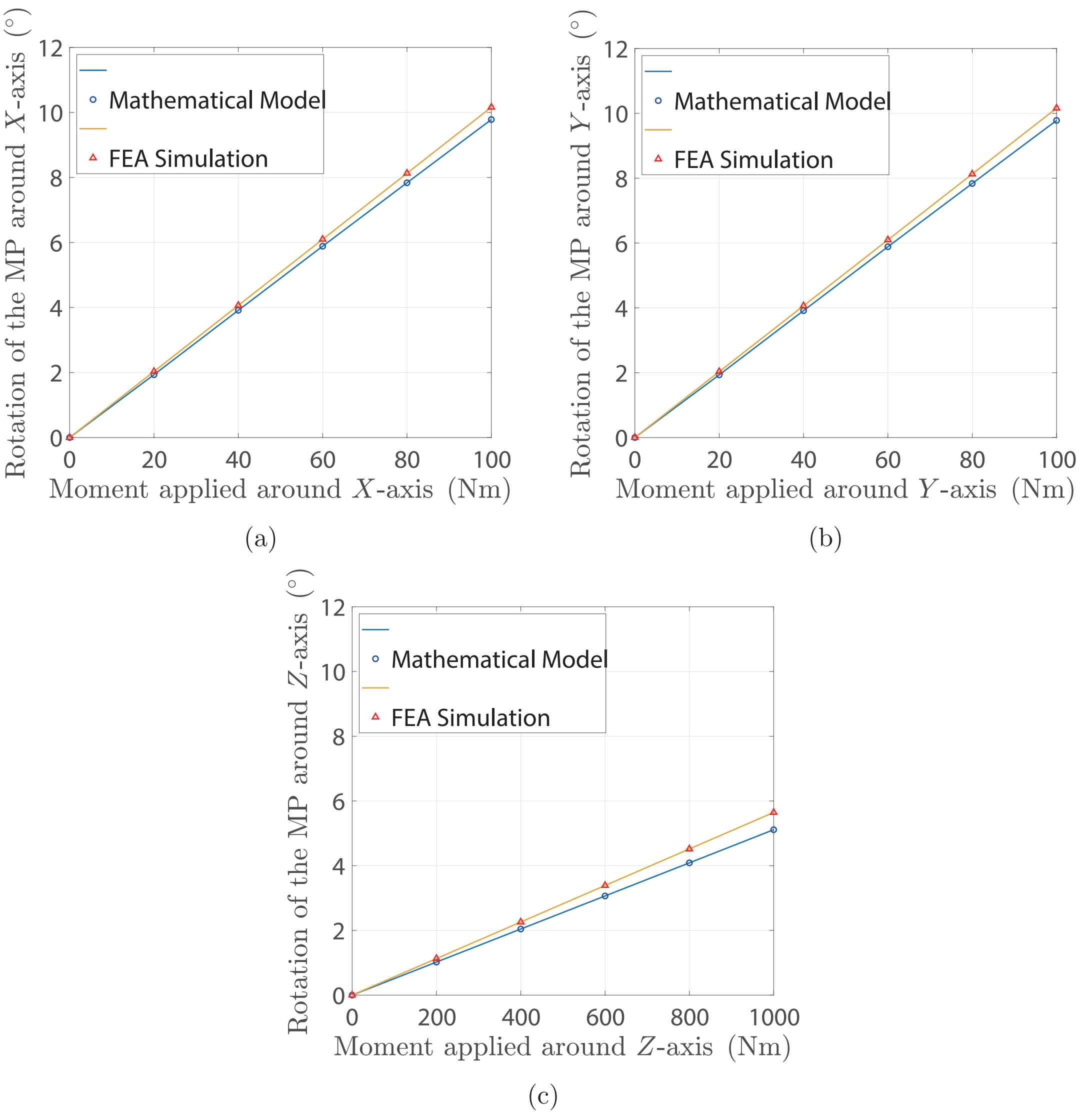

Fig. 3.10 Rotation of the MP under the moments around X, Y and Z axes

3.7 Summary

The elastostatic modelling and stiffness evaluation of a three-limb, full-mobility parallel robot, dubbed the SDelta, were studied in this chapter. The motor shafts, together with their corresponding couplings, are modelled as identical linearly elastic torsional springs, the light-weight limb-rods as identical linearly elastic beams. The numerical stiffness values of different flexible parts were calculated and compared. According to the

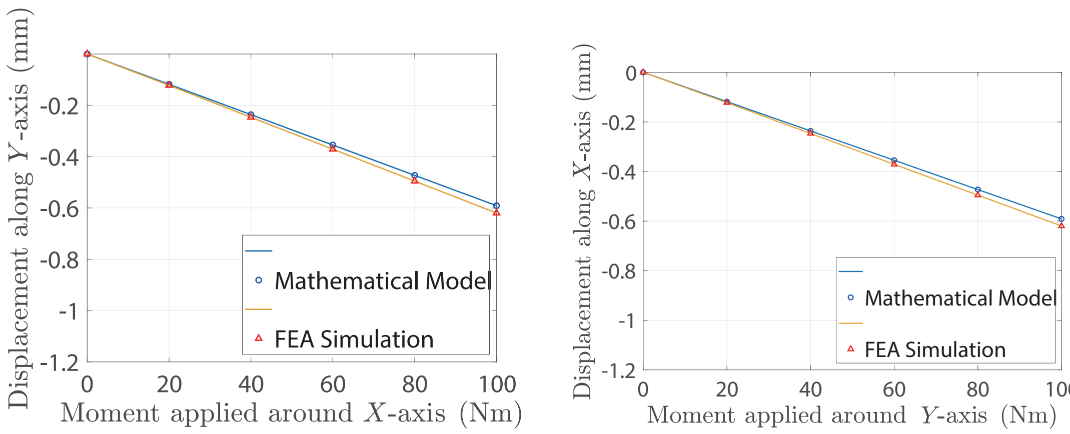

(a) (b)

Fig. 3.11 Translation of the MP c.o.m. under the moments around X and Y axes

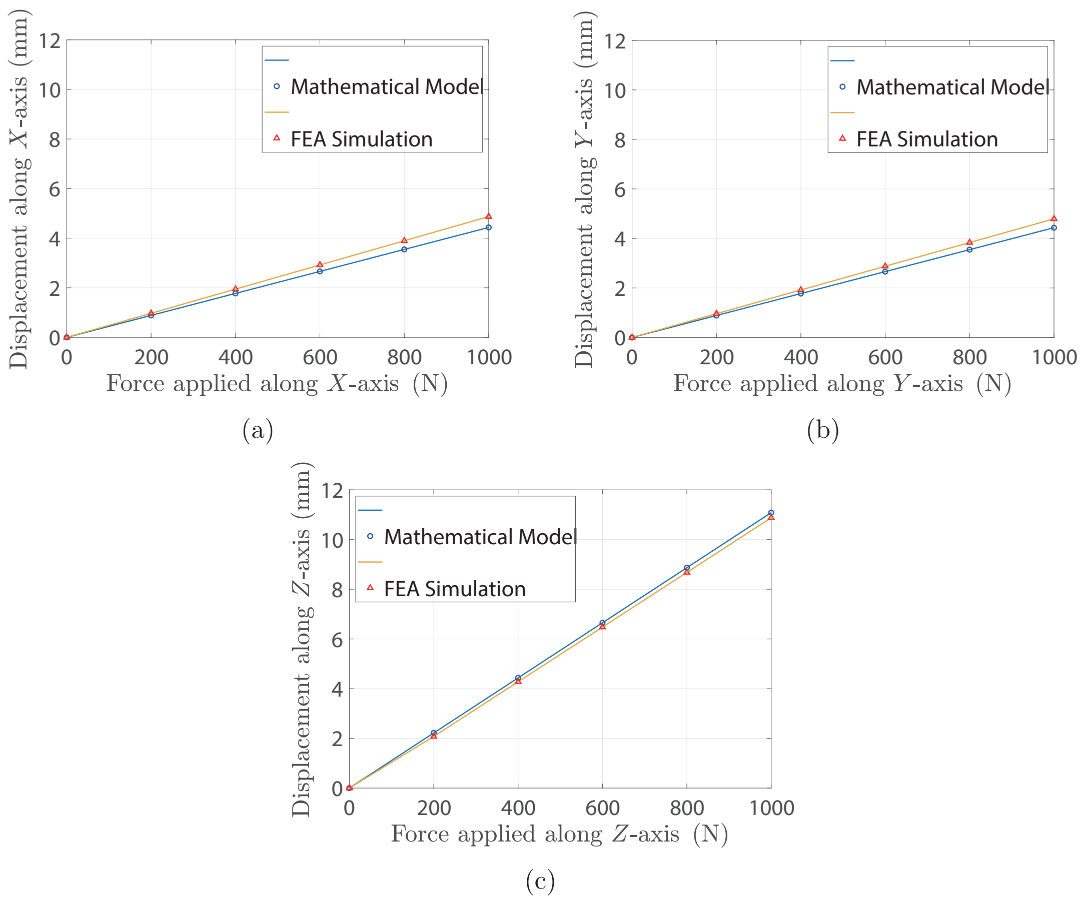

(a) (b) (c)

Fig. 3.12 Translation of the MP c.o.m. under the forces along X, Y and Z axes numerical results, the motor shaft, together with its coupling, is much stiffer than the limb-rod. Therefore, in some cases, the compliance of the C-drive can be neglected for simplicity. By means of the VJM, the 6×6 CSM of the robot is obtained. The CSM is posture-dependent and dimensionally inhomogeneous. Then, based on the modified eigenproblem of the CSM, three types of elastostatic performance indices were defined, associated with the eigenscrews, the wrench-compliant axes and the twist-compliant axes. These allow, respectively, the evaluation of the overall stiffness, the translational and the torsional stiffness of the PKM. The three alternative indices allow us to choose the most appropriate one for our purposes. The CSM and the stiffness indices drawn from the foregoing analysis were derived at a specific symmetric posture, for a prototype at the desktop scale. These results were then validated by FEA simulation. The philosophy adopted at the outset, for the Cartesian elstostatic modelling and evaluation of the SDelta robot, is applicable to other, similar six-dof multi-loop mechanical systems.

Chapter 4

Elastodynamics: Cartesian Frequency Matrix and Vibration Analysis

4.1 Overview

The elastodynamics behaviour of the *Cartesian mass-spring* system is governed by the model:

$$\mathbf{M}\delta\ddot{\mathbf{x}} + \mathbf{K}\delta\mathbf{x} = \mathbf{0} \tag{4.1}$$

where $\mathbf{K}$ is the 6×6 matrix representing the stiffness of the *Cartesian spring*, as introduced in Chapter 3. Moreover, $\mathbf{M}$ is the 6×6 inertia dyad of the rigid body mounted on the *Cartesian spring*. The system frequency *spectrum*, calculated from the elastodynamics model, determines the upper limit of the operation frequency. When the former lies below the latter, resonance is likely to occur. Therefore, vibration analysis is of the utmost importance when designing a mechanical system intended for high-frequency operations.

The natural frequencies and natural modes of the *Cartesian mass-spring system* of eq. (2.6) are calculated upon solving the *generalized eigen-problem*[1]:

$$\omega_i^2 \mathbf{M}\mathbf{h}_i = \mathbf{K}\mathbf{h}_i, \quad i = 1, \ldots, 6 \tag{4.2}$$

where $\{\omega_i\}_1^6$ includes the six natural frequencies, $\{\mathbf{h}_i\}_1^6$ the corresponding modal vectors of the system. In eq. (4.2), two matrices, the CMM and the CSM, are required in the analysis. Here comes the question: *can a single matrix, based on the CMM and the CSM, be defined to represent the system elastodynamics properties?*

To answer the above question, the natural frequency of the one-dof mass-spring system is recalled. The natural frequency is governed by eq. (2.19), $\omega = \sqrt{k/m}$. As a generalization of the concept of natural frequency in the mechanics of a particle, a 6×6 *Cartesian frequency matrix* (CFM) can also be attributed to the *Cartesian mass-spring system*. This chapter aims to define a *symmetric*, *positive-(semi)definite* and *analytic* CFM whose eigenvalues and eigenvectors provide the *natural frequencies* and the *natural modes* of the system under study.

4.2 Cartesian Frequency Matrix

4.2.1 Related Concepts

The concept of interest, *frequency matrix*, is not completely new. It has been extensibly discussed in the generalized space on elastodynamics of n-dof mechanical systems in various versions, under different names. The system usually includes n decoupled translational and rotational dimensions, which leads to simple diagonal forms of the system stiffness and mass matrices. Therefore, the corresponding frequency matrix will be diagonal and *dimensionally homogenous*. Different versions of the *generalized frequency matrix*

[1]The emphasized term refers to the presence of a square matrix (other than the identity matrix) on both sides of the model of eq. (2.9)

are recalled, then they are applied to the *Cartesian space*, which contains six *coupled* motions, namely, three translations and three rotations.

The best known pertinent concept is the *dynamic matrix*, defined as the product of the inverse of the mass matrix times the stiffness matrix, in this order [46, 47, 48, 49, 50]. The natural frequencies of the system are then calculated as the square roots of the eigenvalues of the dynamic matrix, while the natural modes of the system are obtained as the corresponding eigenvectors. However, when applying the concept of dynamic matrix to the *Cartesian mass-spring system*, *two stumbling blocks* occur.

First, the *Cartesian mass-spring system* is a "hybrid" elastodynamic system, involving both rotational and translational modes, the *Cartesian dynamic matrix* (CDM) then being *dimensionally inhomogeneous*, its physical meaning thus being elusive. Based on eqs. (6) and (7), the CDM can be partitioned into four 3×3 blocks with disparate units, namely,

$$\mathbf{D} \equiv \mathbf{M}^{-1}\mathbf{K} = \begin{bmatrix} \mathbf{D}_{11} & \mathbf{D}_{12} \\ \mathbf{D}_{21} & \mathbf{D}_{22} \end{bmatrix} \tag{4.3}$$

where the diagonal blocks, $\mathbf{D}_{11}$ and $\mathbf{D}_{22}$, bear units of frequency-squared: $\text{rad}^2\text{s}^{-2}$. However, $\mathbf{D}_{12}$ bears units of $\text{m}^{-1}\text{rad}^2\text{s}^{-2}$, while $\mathbf{D}_{21}$ bears units of $\text{m}\cdot\text{rad}^2\text{s}^{-2}$—the period in the foregoing units is intended to prevent confusion with *milliradians*.

The second stumbling block is the lack of *symmetry*. The mass matrix is *symmetric* and positive-definite, while the stiffness matrix is *symmetric* and at least positive semi-definite. Although the dynamic matrix preserves positive-definiteness, it loses the *symmetry* of its factors. "Symmetry" is an important property, since it guarantees real eigenvalues and mutually orthogonal eigenvectors. In the realm of Lagrangian mechanics, the numerical eigenvalues of the $n \times n$ dynamic matrix can be complex because of the unavoidable roundoff error during number-crunching. In these cases, the usual practice is to simply neglect the imaginary parts, while invoking roundoff error.

Therefore, when analyzing the elastodynamics of a mechanical system in *Cartesian space*, defining a dimensionally homogenous matrix that preserves the *symmetry* and positive-(semi)definiteness of the mass and stiffness matrices, respectively, is of paramount importance.

Related concepts were proposed by Inman [77] and Meirovitch [78] independently, as pertaining to generic n-dof linear mechanical systems. In the two cases as well, the matrix of interest is defined as a *congruent transformation* of the stiffness matrix, the transformation being given by the inverse of one of the factors of the *Cholesky decomposition* [79] of the mass matrix. In the *Cartesian mass-spring system*, the matrix of interest is defined as

$$\mathbf{\Omega}_L \equiv \mathbf{L}_M^{-1}\mathbf{K}\mathbf{L}_M^{-T} \ (\mathrm{rad}^2{\cdot}\mathrm{s}^{-2}) \tag{4.4}$$

where $\mathbf{L}_M$ is the lower-triangular Cholesky factor of the CMM. Matrix $\mathbf{\Omega}_L$ is *symmetric* and positive-(semi)definite. Moreover, this matrix is dimensionally homogeneous, bearing units of angular-frequency squared. However, given that the Cholesky factors have no physical meaning—they are numerical artifacts—the frequency matrix thus resulting is not an *analytic function* of the mass and stiffness matrices.

According to the above discussion, a *symmetric*, *positive-(semi)definite* and *analytic* frequency matrix based on the Cartesian mass-spring model is needed.

4.2.2 Definition of the Cartesian Frequency Matrix

The 6×6 *Cartesian frequency matrix* (CFM) is introduced formally in this subsection. Let $\sqrt{\mathbf{M}}$ represent the *unique* positive-definite square root of the CMM. Pre-multiplying eq. (2.6) by $\sqrt{\mathbf{M}}^{-1}$, the Cartesian elastodynamics model becomes

$$\sqrt{\mathbf{M}}\,\ddot{\mathbf{s}} + (\sqrt{\mathbf{M}})^{-1}\mathbf{K}(\sqrt{\mathbf{M}})^{-1}(\sqrt{\mathbf{M}}\,\mathbf{s}) = \mathbf{0} \tag{4.5}$$

with

$$\sqrt{\mathbf{M}} = \begin{bmatrix} \sqrt{\mathbf{I}} & \mathbf{O} \\ \mathbf{O} & \sqrt{m}\mathbf{1} \end{bmatrix} \tag{4.6}$$

where, again, $\sqrt{\mathbf{I}}$ denotes the *unique* positive-definite[2] square root of $\mathbf{I}$.

Upon the change of variable $\mathbf{y} = \sqrt{\mathbf{M}}\,\mathbf{s}$, eq. (4.5) becomes

$$\ddot{\mathbf{y}} + \mathbf{\Omega}^2\mathbf{y} = \mathbf{0} \tag{4.7}$$

with

$$\mathbf{\Omega}^2 \equiv (\sqrt{\mathbf{M}})^{-1}\mathbf{K}(\sqrt{\mathbf{M}})^{-1} \ (\mathrm{rad}^2{\cdot}\mathrm{s}^{-2}) \tag{4.8}$$

$\mathbf{\Omega}$ being the CFM. Thereafter, the eigen-decomposition of $\mathbf{\Omega}$ provides full information on the elastodynamics behaviour of the system. The square of this matrix is defined as a *congruent transformation* of the CSM via the inverse of the positive-definite square root[3] of the CMM.

Here, the CMM is assumed, plausibly, to be of full rank. Moreover, $\sqrt{\mathbf{M}}$ is a real-valued *analytic function* of $\mathbf{M}$. Based on the *Cayley-Hamilton Theorem* [62], $\sqrt{\mathbf{M}}$ can be expressed as a linear combination of the first *six* powers of $\mathbf{M}$, i.e.,

$$\sqrt{\mathbf{M}} = f(\mathbf{M}) = \sum_{i=0}^{5}\gamma_k\mathbf{M}^k, \quad \gamma_k \in \mathbb{R} \tag{4.9}$$

Notice that, in order to make the square-root matrix $\sqrt{\mathbf{M}}$ meaningful, the CMM must be block-decoupled, i.e., defined w.r.t. the system c.o.m., as explained presently. The

[2] Positive-definiteness, or semi-definiteness for that matter, are not really needed, but chosen so for uniqueness.

[3] In general, a $n\times n$ positive-(semi)definite matrix admits 2^n square roots, only one of which is positive-(semi)definite.

CMM referred to an arbitrary point A bears a general block-form:

$$\mathbf{M}_A = \begin{bmatrix} \mathbf{I}_A & m(\mathbf{C}-\mathbf{A}) \\ m(\mathbf{C}-\mathbf{A})^T & m\mathbf{1} \end{bmatrix} \tag{4.10}$$

where $\mathbf{I}_A$ denotes the 3×3 moment-of-inertia matrix of the body w.r.t. A. Moreover, $\mathbf{C}$ and $\mathbf{A}$ are the cross-product matrices[4] of the position vectors of the c.o.m. C and point A, respectively. Due to the non-zero off-diagonal blocks, the powers of $\mathbf{M}_A$ involve additions of blocks that carry different physical units, which renders the square root of $\mathbf{M}_A$ *meaningless*. To cope with this quandary, the CFM $\mathbf{\Omega}$ should be defined after shifting the frame origin to the system c.o.m., so as to render it block-diagonal [61].

4.2.3 Properties of the Cartesian Frequency Matrix

Based the above definition, the properties of the CFM are summarized below:

(i) The CFM is an *analytic function* of the CMM and the CSM.

(ii) The CFM is *dimensionally homogeneous*, bearing units of angular frequency, rad/s.

(iii) The CFM preserves the *symmetry* and positive-(semi)definiteness of the CSM.

Property (i) becomes advantageous in the optimization of a scalar function $f(\mathbf{\Omega})$ w.r.t. the entries of the matrix, since an analytic function of a matrix argument is amenable to *explicit differentiation*. Moreover, the analyticity of the CFM allows for the representation of the time-response of an elastodynamic system in the form of an analytic matrix function of time. Property (ii) indicates that the CFM is closely related to the frequency response of the system. Furthermore, property (iii), *symmetry*, makes the eigen-decomposition of

[4]The cross-product matrix $\mathbf{A}$ of the three-dimensional vector $\mathbf{a}$ is defined as $\mathbf{A} = \mathrm{CPM}(\mathbf{a}) = \partial(\mathbf{a} \times \mathbf{v})/\partial\mathbf{v}, \quad \forall \mathbf{v} \in \mathbb{R}^3$.

the CFM more reliable and accurate than the CDM in terms of numerical calculation, as shown in Section 4.4.

Table 4.1 Properties of three types of frequency matrices in Cartesian space

	D	Ω_L	Ω
Symmetry	✘	✓	✓
Dimensional-homogeneity	✘	✓	✓
Analyticity	✓	✘	✓

Properties of the foregoing three types of frequency matrices in the *Cartesian space* are summarized in Table 4.1. Apparently, the novel CFM, $\mathbf{\Omega}$, carries all three properties of Table 1. The above properties make the CFM a direct extension of the natural frequency in the single-dof case to the six-dof *Cartesian space*. Moreover, the CFM should be a convenient and useful engineering tool for the analysis of the elastodynamics of a mechanical system in *task space*.

4.3 Vibration Analysis: Natural Frequencies and Natural Modes

4.3.1 Eigenvalue Decomposition of the Cartesian Frequency Matrix

By virtue of the *symmetry* and positive-(semi)definiteness of the CFM, the matrix admits six real non-negative eigenvalues $\{\omega_i\}_1^6$ and a complete set of real, mutually-orthogonal eigenvectors $\{\mathbf{v}_i\}_1^6$, namely,

$$\mathbf{\Omega}\mathbf{v}_i = \omega_i \mathbf{v}_i, \quad i = 1, 2, \ldots, 6, \quad \mathbf{\Omega}\mathbf{V} = \mathbf{\Lambda}\mathbf{V} \tag{4.11}$$

with

$$\mathbf{V} = \begin{bmatrix} \mathbf{v}_1 & \mathbf{v}_2 & \cdots & \mathbf{v}_6 \end{bmatrix}, \quad \mathbf{V}^T\mathbf{V} = \mathbf{1}_6 \tag{4.12a}$$

and $\mathbf{1}_6$ denoting the 6×6 identity matrix, while

$$\mathbf{\Lambda} = \mathrm{diag}(\omega_1, \omega_2, \cdots, \omega_6) \tag{4.12b}$$

The eigenvectors $\mathbf{v}_i$ are, as usual, defined as non-dimensional unit vectors, while the eigenvalues ω_i bear units of angular frequency, rad/s.

In the six-dimensional *Cartesian space*, where both translation and rotation are involved, the frame-invariance of the eigenvalues and eigenvectors of the CFM should be proven, to guarantee the above eigenvalue decomposition meaningful.

Under a *Cartesian frame transformation* $\mathbf{S}$ defined in eq. (3.30), the SAD screw, the wrench, the CMM, and the CSM change accordingly:

$$\mathbf{s}' = \mathbf{S}^{-1}\mathbf{s} = \begin{bmatrix} \boldsymbol{\theta}' \\ \mathbf{u}' \end{bmatrix}, \quad \mathbf{w}' = \mathbf{\Gamma}\mathbf{S}^{-1}\mathbf{\Gamma}\mathbf{w} = \mathbf{S}^T\mathbf{w} \begin{bmatrix} \mathbf{n}' \\ \mathbf{f}' \end{bmatrix} \tag{4.13}$$

$$\mathbf{M}' = \mathbf{\Gamma}\mathbf{S}^{-1}\mathbf{\Gamma}\mathbf{M}\mathbf{S} = \mathbf{S}^T\mathbf{M}\mathbf{S} = \begin{bmatrix} \mathbf{M}'_{11} & \mathbf{M}'_{12} \\ (\mathbf{M}'_{12})^T & \mathbf{M}'_{22} \end{bmatrix} \tag{4.14a}$$

$$\mathbf{K}' = \mathbf{\Gamma}\mathbf{S}^{-1}\mathbf{\Gamma}\mathbf{K}\mathbf{S} = \mathbf{S}^T\mathbf{K}\mathbf{S} = \begin{bmatrix} \mathbf{K}'_{11} & \mathbf{K}'_{12} \\ (\mathbf{K}'_{12})^T & \mathbf{K}'_{22} \end{bmatrix} \tag{4.14b}$$

with

$$\mathbf{\Gamma} \equiv \begin{bmatrix} \mathbf{O} & \mathbf{1} \\ \mathbf{1} & \mathbf{O} \end{bmatrix}, \quad \mathbf{\Gamma}^{-1} = \mathbf{\Gamma} \tag{4.15}$$

$\mathbf{\Gamma}$ thus denoting a *swapping matrix*[5]. Moreover, $\mathbf{O}$ and $\mathbf{1}$ are the 3×3 zero and identity matrices, respectively. An *affine* transformation keeps the units of scalars, vectors

[5]This matrix *swaps* the two three-dimensional blocks in a screw, a *twist* or a wrench, hence the moniker. The swapping is needed to transfer screw arrays from *ray-coordinates* into *axis-coordinates*, and vice-versa, in order to lead to meaningful operations in the ensuing analysis.

and matrices, while preserving the *symmetry* and positive-definiteness[6] of the mass and stiffness matrices, their physical meaning thus being kept.

Based on eqs. (4.3) and (4.8), the square of the CFM is a *similarity transformation* of the CDM $\mathbf{D}$ via matrix $\sqrt{\mathbf{M}}$ defined in eq. (4.6), namely,

$$\mathbf{\Omega}^2 = \sqrt{\mathbf{M}}\mathbf{D}(\sqrt{\mathbf{M}})^{-1} \tag{4.16}$$

which shows that $\mathbf{\Omega}^2$ and $\mathbf{D}$ share the same set of eigenvalues, their corresponding eigenvectors being related via the linear transformation given by matrix $\sqrt{\mathbf{M}}$. Therefore, proving the frame-invariance of the eigenvalue decomposition of $\mathbf{\Omega}$ is equivalent to proving that of $\mathbf{D}$.

Under a change of frame represented by $\mathbf{S}$, the transformed matrix $\mathbf{D}'$ of $\mathbf{D}$ becomes

$$\begin{aligned} \mathbf{D}' &= (\mathbf{M}')^{-1}\mathbf{K}' = (\mathbf{S}^T\mathbf{M}\mathbf{S})^{-1}\mathbf{S}^T\mathbf{K}\mathbf{S} \\ &= \mathbf{S}^{-1}\mathbf{M}^{-1}\mathbf{K}\mathbf{S} = \mathbf{S}^{-1}\mathbf{D}\mathbf{S} \end{aligned} \tag{4.17}$$

which proves that $\mathbf{D}'$ is, indeed, *similar* to $\mathbf{D}$. Therefore, the *eigenvalue decomposition* of the CFM *is preserved under a change of Cartesian frame*. Therefore, the eigenvalues and eigenvectors of the CFM are *characteristic* concepts that can help engineers gain insight into the elastodynamic response of a mechanical system, especially at the design stage.

4.3.2 Caculation of Natural Frequencies and Natural Modes

The eigenvalue problem associated with $\mathbf{\Omega}$ now follows:

$$\mathbf{\Omega}^2\mathbf{v}_i \equiv \omega_i\mathbf{\Omega}\mathbf{v}_i = \omega_i^2\mathbf{v}_i \tag{4.18}$$

[6]Or semi-definiteness, as the case may be.

Substitution of eq. (4.8) into eq. (4.18) leads to

$$(\sqrt{\mathbf{M}})^{-1}\mathbf{K}(\sqrt{\mathbf{M}})^{-1}\mathbf{v}_i = \omega_i^2\mathbf{v}_i \tag{4.19}$$

Upon premultiplying both sides of eq. (4.19) by $\sqrt{\mathbf{M}}$, one obtains

$$\mathbf{K}(\sqrt{\mathbf{M}})^{-1}\mathbf{v}_i = \omega_i^2\mathbf{M}\left[(\sqrt{\mathbf{M}})^{-1}\mathbf{v}_i\right] \tag{4.20}$$

Further, under a change of variable[7]

$$\mathbf{h}_i = (\sqrt{\mathbf{M}})^{-1}\mathbf{v}_i \tag{4.21}$$

one obtains

$$\mathbf{K}\mathbf{h}_i = \omega_i^2\mathbf{M}\mathbf{h}_i \tag{4.22a}$$

i.e.,

$$\left(\omega_i^2\mathbf{M} - \mathbf{K}\right)\mathbf{h}_i = \mathbf{0} \in \mathbb{R}^6, \quad i = 1, 2, \ldots, 6 \tag{4.22b}$$

Equation (4.22b) indicates that the Cartesian-spring equation (2.6) can be fully decoupled via the *eigenvalue decomposition* of the CFM. The eigenvalues $\{\omega_i\}_1^6$ of the CFM are the *natural frequencies* of the system. Moreover, the ith natural mode associated with the ith natural frequency ω_i is $\mathbf{h}_i$. The natural modes $\{\mathbf{h}_i\}_1^6$ of the system are linear transformations of the eigenvectors $\mathbf{v}_i$ of the CFM, the transformation given by the square root of the CMM. Furthermore, the eigenvectors $\mathbf{v}_i$ are mutually orthogonal; therefore,

[7] The change of variable introduced in eq. (4.19) is *not a change of frame*, since the matrix $(\sqrt{\mathbf{M}})^{-1}$ does not represent an *affine* transformation.

the natural modes $\mathbf{h}_i$ of the system are mutually orthogonal w.r.t. the CMM $\mathbf{M}$, i.e.,

$$\mathbf{h}_i^T \mathbf{M} \mathbf{h}_j = \begin{cases} 1, & i = j \\ 0, & i \neq j \end{cases}, \quad i, j = 1, 2, \ldots, 6 \tag{4.23}$$

Furthermore, the modal vector $\mathbf{h}_i$ is *dimensionally inhomogeneous*. It can be partitioned, as vector $\mathbf{s}$ in eq. (2.5), into two three-dimensional vectors, each with its own units. The dimensionless eigenvector $\mathbf{v}_i$ of the frequency matrix $\mathbf{\Omega}$ and the system natural mode $\mathbf{h}_i$ are partitioned as

$$\begin{aligned} \mathbf{v}_i &= \begin{bmatrix} \mathbf{a}_i \\ \mathbf{b}_i \end{bmatrix}, \quad \|\mathbf{a}_i\|^2 + \|\mathbf{b}_i\|^2 = 1, \quad \mathbf{a}_i,\ \mathbf{b}_i \in \mathbb{R}^3 \\ \mathbf{h}_i &= (\sqrt{\mathbf{M}})^{-1} \mathbf{v}_i = \begin{bmatrix} \boldsymbol{\eta}_i \\ \boldsymbol{\zeta}_i \end{bmatrix}, \quad \boldsymbol{\eta}_i,\ \boldsymbol{\zeta}_i \in \mathbb{R}^3 \end{aligned} \tag{4.24}$$

Then, the relation between the eigenvectors of the frequency matrix and its corresponding natural modes follows:

$$\begin{aligned} \boldsymbol{\eta}_i &= \sqrt{\mathbf{I}^{-1}}\, \mathbf{a}_i \ \left(\mathrm{kg}^{-1/2} {\cdot} \mathrm{m}^{-1}\right) \\ \boldsymbol{\zeta}_i &= (1/\sqrt{m}) \mathbf{b}_i \ \left(\mathrm{kg}^{-1/2}\right) \end{aligned} \tag{4.25}$$

vector $\mathbf{h}_i$ thus being *dimensionally inhomogeneous*. The striking similarity between the two above expressions is to be highlighted: the counterpart of the matrix coefficient of $\boldsymbol{\eta}_i$ is the coefficient in parenthesis in the expression for $\boldsymbol{\zeta}_i$, $(1/\sqrt{m})\mathbf{1}$, with the identity matrix $\mathbf{1}$ obviated in the latter. The units of $\boldsymbol{\zeta}_i$ are those of $\boldsymbol{\eta}_i$ times units of length. Then, $\mathbf{h}_i$ can be normalized into a unit screw $\boldsymbol{\rho}_i$. The normalized screws $\boldsymbol{\rho}_i$ are the *modal screws*, or *eigenscrews*, of the system.

If $\mathbf{a}_i \neq \mathbf{0}$ and $\boldsymbol{\eta}_i \neq \mathbf{0}$, then the ith modal screw $\boldsymbol{\rho}_i$ can be expressed as

$$\boldsymbol{\rho}_i = \frac{1}{\|\boldsymbol{\eta}_i\|}\mathbf{h}_i = \begin{bmatrix} \mathbf{e}_i \\ \mathbf{p}_i \times \mathbf{e}_i + p_i \mathbf{e}_i \end{bmatrix}, \quad i = 1, 2, \ldots, 6 \tag{4.26}$$

with

$$\mathbf{e}_i = \frac{1}{\|\boldsymbol{\eta}_i\|}\boldsymbol{\eta}_i, \quad \mathbf{p}_i = \frac{\boldsymbol{\eta}_i \times \boldsymbol{\zeta}_i}{\|\boldsymbol{\eta}_i\|^2}, \quad p_i = \frac{\boldsymbol{\eta}_i^T \boldsymbol{\zeta}_i}{\|\boldsymbol{\eta}_i\|^2} \tag{4.27}$$

the unit vector $\mathbf{e}_i \in \mathbb{R}^3$ representing the direction of the axis of the eigenscrew, $\mathbf{p}_i \in \mathbb{R}^3$ the position vector $\mathbf{c}$ and $\mathbf{a}$ of the point of the screw axis that lies *closest to the origin*, and p_i the pitch of the screw. If $\mathbf{h}_i$ turns out to be a *zero-pitch screw*, i.e., if $p_i = 0$, then the screw array degenerates into a *pure rotation*, whose representation is known to degenerate, in turn, into the Plücker array [39] of a line, i.e., the vibration mode becomes a *pure rotation* about that line.

When $\mathbf{a}_i = \mathbf{0}$ and $\mathbf{b}_i \neq \mathbf{0}$, then $\boldsymbol{\eta}_i = \mathbf{0}$ and $\boldsymbol{\zeta}_i \neq \mathbf{0}$. Hence, the modal screw $\boldsymbol{\rho}_i$ becomes

$$\boldsymbol{\rho}_i = \begin{bmatrix} \mathbf{0} \\ \mathbf{n}_i \end{bmatrix}, \quad \mathbf{n}_i = \frac{1}{\|\boldsymbol{\zeta}_i\|}\boldsymbol{\zeta}_i \tag{4.28}$$

which represents a screw of *infinite pitch*. In line geometry [69], the foregoing six-dimensional array represents a *line at infinity*, which means that, in this case, the vibration mode becomes a *pure translation*.

Upon normalizing the modal vector $\mathbf{h}_i$, eq. (4.22b) becomes

$$\left(\omega_i^2 \mathbf{M} - \mathbf{K}\right) \boldsymbol{\rho}_i = \mathbf{0} \in \mathbb{R}^6, \quad i = 1, 2, \ldots, 6 \tag{4.29}$$

The unit *eigenscrew* $\boldsymbol{\rho}_i$ is the *modal screw* of the system, associated with the natural frequency ω_i. *A natural mode of the system is not necessarily associated with a pure* *rotation or a pure translation.* When $\boldsymbol{\eta}_i = \mathbf{0}$ and $\boldsymbol{\zeta}_i \neq \mathbf{0}$, the mode $\boldsymbol{\rho}_i$ in question is a *pure translation* along a direction parallel to $\mathbf{n}_i$. When $\boldsymbol{\eta}_i \neq \mathbf{0}$ and $p_i = 0$, the mode $\boldsymbol{\rho}_i$ represents a *pure rotation* whose axis is parallel to $\mathbf{e}_i$ and located by $\mathbf{p}_i$. When $\boldsymbol{\eta}_i \neq \mathbf{0}$ and $p_i \neq 0$, the mode $\boldsymbol{\rho}_i$ represents a combination of rotation and translation, both related by the pitch p_i.

Moreover, in most cases, the three rotations and the three translations of the system *cannot be decoupled. An arbitrary system doesn't necessarily entail three independent rotational modes and three independent translational modes.* In general, a natural mode represents a screw motion, particular cases being a *pure rotation* and a *pure translation*.

The natural frequency of the PKM determines the upper limit of the operation frequency under the corresponding natural mode. When the operation frequency lies above the system natural frequency, resonance is likely to occur. In order to further improve the PKM performance and expand the range of its operation frequency, the natural frequencies of the PKM should be prescribed as high as the conditions permit.

4.4 Case Study: Vibration Analysis of the SDelta Robot

The foregoing modelling and analysis methods are now applied to a three-limb, full-mobility PKM, the *SDelta* robot, depicted in Fig. 3.1. Using the VJM, the mechanical system with rigid and flexible links, is transformed into a multi-rigid-body system actuated by virtual joints, as depicted in Fig. 3.7 [8]. The expression of the CSM $\mathbf{K}$ of the *SDelta* is shown in eqs. (3.27–3.29).

Furthermore, a homogeneous stainless steel cube test-specimen is assumed to be attached to the MP. The c.o.m. of the test-specimen lies right above, i.e., on the *vertical* of, the c.o.m. of the MP triangle. The mass m_t and the side length a_t of the specimen are

[8] The figure is intended to convey information on the system *topology*, not on its *geometry*.

assumed to be

$$m_t = 3 \text{ (kg)}, \quad a_t = 72 \text{ (mm)} \tag{4.30}$$

Then, the elastodynamics behaviour of the *SDelta* is analyzed below at two distinct postures.

4.4.1 The "Symmetric" Posture

Three views of the "*symmetric*" posture of the *SDelta* robot are shown in Fig. 3.8. A detailed description of the "symmetric" posture and parameters of the prototype at this posture are shown in Section 3.5.1.

At the above "*symmetirc* posture", the CMM $\mathbf{M}_S$ of the system, referred to the MP c.o.m. S is, block-wise, given below:

$$\mathbf{M}_{11}^S = \begin{bmatrix} 0.0125 & 0 & 0 \\ 0 & 0.0125 & 0 \\ 0 & 0 & 0.0117 \end{bmatrix} (\text{kg}\cdot\text{m}^2) \tag{4.31a}$$

$$\mathbf{M}_{12}^S = \begin{bmatrix} 0 & -0.1267 & 0 \\ 0.1267 & 0 & 0 \\ 0 & 0 & 0 \end{bmatrix} (\text{kg}\cdot\text{m}) = (\mathbf{M}_{21}^S)^T \tag{4.31b}$$

$$\mathbf{M}_{22}^S = \begin{bmatrix} 4.4857 & 0 & 0 \\ 0 & 4.4857 & 0 \\ 0 & 0 & 4.4857 \end{bmatrix} (\text{kg}) \tag{4.31c}$$

The mass m of the system is 4.4857 kg. Vector $\boldsymbol{\delta}_m$, defined as directed from O to the system c.o.m. C, is, thus,

$$\boldsymbol{\delta}_m = \mathrm{vec}(\mathbf{M}_{12}^A/m) = \mathrm{vec}(\boldsymbol{\Delta}_m) = \begin{bmatrix} 0 \\ 0 \\ 28.3 \end{bmatrix} \text{ (mm)} \tag{4.32}$$

where vec(·) denotes the *axial vector*[9] of a 3×3 matrix. This means that the system c.o.m. C is located above the MP c.o.m. S on the Z-axis. Moreover, the distance between S and C is 28.3 mm.

Furthermore, the 3×3 blocks of the *SDelta* CSM w.r.t. the MP c.o.m. S at the "symmetric posture" has been calculated, as shown in eq. (3.56).

Upon shifting the reference point from the MP c.o.m. S to the system c.o.m. C, the CMM $\mathbf{M}$ at the system c.o.m. is obtained from the inertia dyad $\mathbf{I}$ and the mass m, namely[10],

$$\mathbf{I} = \begin{bmatrix} 0.0089 & 0 & 0 \\ 0 & 0.0089 & 0 \\ 0 & 0 & 0.0117 \end{bmatrix} \text{ (kg·m}^2\text{)}, \quad m = 4.4857 \text{ (kg)} \tag{4.33}$$

[9] The axial vector of a 3×3 matrix $\mathbf{A}$ is defined as the vector $\mathbf{a}$ with the property, $\mathbf{a}\times\mathbf{v} = (\mathbf{A}-\mathbf{A}^T)\mathbf{v}/2$, $\forall \mathbf{v} \in \mathbb{R}^3$

[10] Notice that $\mathbf{I}$ is *isotropic* in the X–Y plane, a result of both the *symmetric* design and the chosen posture.

In turn, the blocks of the CSM $\mathbf{K}$ at the system c.o.m. C are

$$\mathbf{K}_{11} = \begin{bmatrix} 0.2488 & 0 & 0 \\ 0 & 0.2488 & 0 \\ 0 & 0 & 1.2003 \end{bmatrix} \times 10^4 \text{ (N·m)} \tag{4.34a}$$

$$\mathbf{K}_{12} = \begin{bmatrix} 0 & 2.9570 & 0 \\ -2.9570 & 0 & 0 \\ 0 & 0 & 0 \end{bmatrix} \times 10^4 \text{ (N)} \; = \mathbf{K}_{21}^T \tag{4.34b}$$

$$\mathbf{K}_{22} = \begin{bmatrix} 4.8011 & 0 & 0 \\ 0 & 4.8011 & 0 \\ 0 & 0 & 1.0669 \end{bmatrix} \times 10^5 \text{ (N/m)} \tag{4.34c}$$

The Cartesian Frequency Matrix

Upon substitution of eqs. (4.33) and (4.34) into eq. (4.8), the CFM $\boldsymbol{\Omega}$ is calculated as

$$\boldsymbol{\Omega} = \begin{bmatrix} 0.4894 & 0 & 0 & 0 & 0.1966 & 0 \\ 0 & 0.4894 & 0 & -0.1966 & 0 & 0 \\ 0 & 0 & 1.0121 & 0 & 0 & 0 \\ 0 & -0.1966 & 0 & 0.2615 & 0 & 0 \\ 0.1966 & 0 & 0 & 0 & 0.2615 & 0 \\ 0 & 0 & 0 & 0 & 0 & 0.1542 \end{bmatrix} \times 10^3 \text{ (rad/s)} \tag{4.35}$$

The system natural frequencies, namely, the eigenvalues of $\boldsymbol{\Omega}$, are arrayed in vector $\boldsymbol{\lambda}$:

$$\begin{aligned} \boldsymbol{\lambda} &= [148.2,\ 148.2,\ 154.2,\ 602.7,\ 602.7,\ 1012.1]^T \text{ (rad/s)} \\ &= [23.6,\ 23.6,\ 24.5,\ 95.9,\ 95.9,\ 161.1]^T \text{ (Hz)} \end{aligned} \tag{4.36}$$

The system non-normalized natural modes, i.e., the linear transformation of the eigenvectors of $\mathbf{\Omega}$ via matrix $\sqrt{\mathbf{M}^{-1}}$, arrayed as the columns of matrix $\mathbf{H}$, are displayed below:

$$\mathbf{H} = \begin{bmatrix} 5.2791 & 0 & 0 & 9.1623 & 0 & 0 \\ 0 & 5.2791 & 0 & 0 & -9.1623 & 0 \\ 0 & 0 & 0 & 0 & 0 & 9.2382 \\ 0 & 0.2599 & 0 & 0 & 0.4946 & 0 \\ -0.2599 & 0 & 0 & 0.4946 & 0 & 0 \\ 0 & 0 & 0.4722 & 0 & 0 & 0 \end{bmatrix} \tag{4.37}$$

Orthogonality of the Natural Modes

The orthogonality of the natural modes w.r.t. both the CMM and the CSM is verified below with four decimals of precision:

$$\mathbf{H}^T\mathbf{M}\mathbf{H} = \begin{bmatrix} 1.0000 & 0 & 0 & -0.0000 & 0 & 0 \\ 0 & 1.0000 & 0 & 0 & 0.0000 & 0 \\ 0 & 0 & 1.0000 & 0 & 0 & 0 \\ -0.0000 & 0 & 0 & 1.0000 & 0 & 0 \\ 0 & 0.0000 & 0 & 0 & 1.0000 & 0 \\ 0 & 0 & 0 & 0 & 0 & 1.0000 \end{bmatrix} \tag{4.38a}$$

$$\mathbf{H}^T\mathbf{K_C}\mathbf{H} = \begin{bmatrix} 0.0220 & 0 & 0 & -0.0000 & 0 & 0 \\ 0 & 0.0220 & 0 & 0 & 0.0000 & 0 \\ 0 & 0 & 0.0238 & 0 & 0 & 0 \\ -0.0000 & 0 & 0 & 0.3633 & 0 & 0 \\ 0 & 0.0000 & 0 & 0 & 0.3633 & 0 \\ 0 & 0 & 0 & 0 & 0 & 1.0244 \end{bmatrix} \times 10^6 \tag{4.38b}$$

The orthogonality of the natural modes w.r.t. the CMM and CSM is verified, in turn, by means of the Frobenius norm[11] of the two matrices:

$$\|\mathbf{H}^T\mathbf{M}\mathbf{H} - \mathbf{1}_6\|_F = 4.5206 \times 10^{-15} \tag{4.39a}$$

$$\|\mathbf{H}^T\mathbf{K}_C\mathbf{H} - \mathbf{\Lambda}^2\|_F = 1.4592 \times 10^{-10}\ (\mathrm{rad/s})^2 \tag{4.39b}$$

with $\mathbf{\Lambda}$ defined in eq. (4.12b).

As per the above results, the CFM in eq. (4.35) bears a *symmetric* structure. *The symmetry of the CFM guarantees both real eigenvalues and the mutual orthogonality of the eigenvectors. The real natural frequencies and the orthogonality among the natural modes w.r.t. the CMM and the CSM are thus preserved in the numerical caculation.*

FEA Validation

The first six natural frequencies, obtained by means of ANSYS *Workbench*, a FEA software package, are illustrated in Fig. 4.1. A comparison of the natural frequencies found by the CEM and ANSYS is shown in Table 4.2. The differences are all smaller than

Table 4.2 Comparison of the natural frequencies (Hz), as found by the CEM and ANSYS

	CEM	FEA	Differences
1	23.6	21.4	9.3%
2	23.6	22.2	5.9%
3	24.5	23.9	2.4%
4	95.9	100.7	5.0%
5	95.9	104.3	8.8%
6	161.1	175.3	8.8%

10%, which shows that our CFM analysis is reasonably accurate. The numerical results

[11] The Frobenius norm of a matrix is nothing but the rms value of its elements.

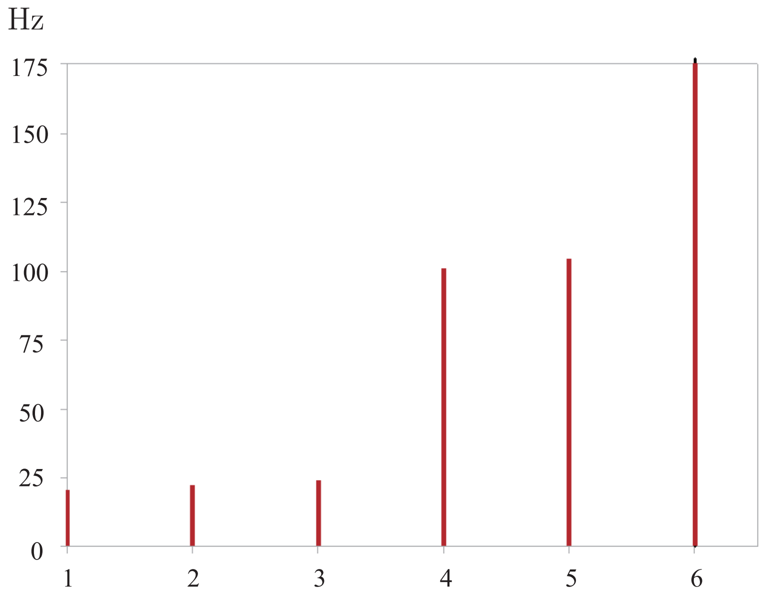

Fig. 4.1 The first six natural frequencies found under FEA simulation

calculated from the CFM are thus deemed fairly reliable.

Interpretation of the Natural Modes

The six natural frequencies of the system are arrayed in vector $\mathbf{w}_f$[12] :

$$\mathbf{w}_f = \begin{bmatrix} 148.2 \\ 148.2 \\ 154.2 \\ 602.7 \\ 602.7 \\ 1012.1 \end{bmatrix} \text{(rad/s)} = \begin{bmatrix} 23.6 \\ 23.6 \\ 24.5 \\ 95.9 \\ 95.9 \\ 161.1 \end{bmatrix} \text{(Hz)} \tag{4.40}$$

[12]Notice that the system at this posture shows a *partial isotropy* of the mass and stiffness matrices: it entails two pairs of identical natural frequencies.

Upon normalization of $\mathbf{H}$, the unit natural modes, i.e., the eigenscrews (or modal screws) of the system, arrayed as the columns of matrix $\mathbf{E}_s$[13], are displayed below:

$$\mathbf{E}_s = \begin{bmatrix} 1.0000 & 0 & 0 & 1.0000 & 0 & 0 \\ 0 & 1.0000 & 0 & 0 & -1.0000 & 0 \\ 0 & 0 & 0 & 0 & 0 & 1.0000 \\ 0 & 0.0492 & 0 & 0 & 0.0540 & 0 \\ -0.0492 & 0 & 0 & 0.0540 & 0 & 0 \\ 0 & 0 & 1.0000 & 0 & 0 & 0 \end{bmatrix} \tag{4.41}$$

The third eigenscrew is a line at infinity, of axis pointing in the Z-direction, which represents a *pure translation* along the Z-axis. The position vectors and pitches of the eigenscrews are obtained from matrix $\mathbf{E}_s$ as

$$\begin{aligned} &\mathbf{p}_1 = [0,\ 0,\ -0.0492]^T \ \text{(m)}, && p_1 = 0 \\ &\mathbf{p}_2 = [0,\ 0,\ -0.0492]^T \ \text{(m)}, && p_2 = 0 \\ &\mathbf{p}_3 \ \text{undefined}, && p_3 \to \infty \\ &\mathbf{p}_4 = [0,\ 0,\ 0.0540]^T \ \text{(m)}, && p_4 = 0 \\ &\mathbf{p}_5 = [0,\ 0,\ 0.0540]^T \ \text{(m)}, && p_5 = 0 \\ &\mathbf{p}_6 = [0,\ 0,\ 0]^T \ \text{(m)}, && p_6 = 0 \end{aligned} \tag{4.42}$$

The physical meaning of the eigenvalue decomposition of the system is now described. The first natural frequency of the system, $f_1 = 23.6$ Hz, is associated with a *pure rotation* around an axis parallel to the X-direction and passing through P_1, whose relative coordinates w.r.t. C are $[0,\ 0,\ -0.0492]^T$ m. The second natural frequency, identical to the first one, $f_2 = f_1$, is associated with a *pure rotation* around an axis parallel to the Y-direction and passing through P_1, whose relative coordinates w.r.t. C are $[0,\ 0,\ -0.0492]^T$ (m).

[13]The first three rows are dimensionless, the last three bearing units of length, m in our case.

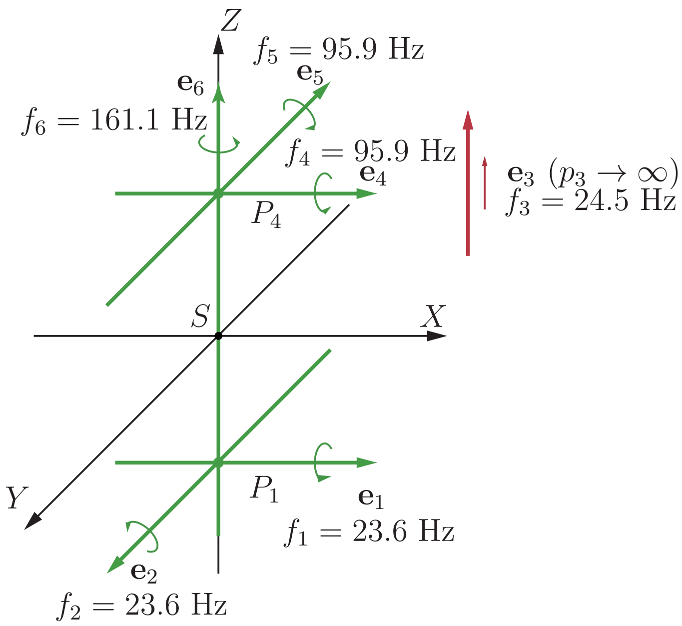

Fig. 4.2 Eigenscrews of the *SDelta* at the symmetric posture

The third natural frequency of the system, $f_3 = 24.5$ Hz, represents a *pure translation* parallel to the Z-axis. The fourth natural frequency, $f_4 = 95.9$ Hz, is associated with a *pure rotation* around an axis parallel to the X-direction and passing through P_4, whose relative coordinates w.r.t. C are $[0,\ 0,\ 0.0540]^T$ m. The fifth natural frequency, identical to the fourth one, $f_5 = f_4$, is associated with a *pure rotation* around an axis parallel to the Y-direction and passing through P_4, whose relative coordinates w.r.t. C are $[0,\ 0,\ 0.0540]^T$ m. The sixth natural frequency of the system, $f_6 = 161.1$ Hz, is associated with a *pure rotation* around an axis parallel to the Z-direction and passing through C.

The numerical results also show that the first natural frequency of the *SDelta* at the *symmetric* posture is 23.6 Hz, which means that the *SDelta* is safe to provide vibration for a 3 kg payload at frequencies below 23.6 Hz at its *symmetric* posture.

The "*symmetric*" posture thus has five natural modes associated with a *pure rotation* and one natural mode associated with a *pure translation*. The distribution of the eigenscrews in the *Cartesian space* is shown in Fig. 4.2.

4.4.2 An Arbitrary Posture

The "*symmetric*" posture was selected as the reference posture. Now, an arbitrary posture is defined by the rotation matrix $\mathbf{Q}$ representing an orientation of the MP from the reference attitude, and the position vector $\mathbf{c}$ of the MP c.o.m. Assuming that the posture of interest is attained by rotating the MP around the Z axis through 10°, around the X axis through 5°, and around the Y axis through 8°, the rotation matrix of the MP pose thus resulting is

$$\mathbf{Q} = \mathbf{R}_z(10^\circ)\mathbf{R}_x(5^\circ)\mathbf{R}_y(8^\circ) = \begin{bmatrix} 0.9731 & -0.1730 & 0.1520 \\ 0.1839 & 0.9811 & -0.0608 \\ -0.1386 & 0.0872 & 0.9865 \end{bmatrix} \tag{4.43}$$

with the MP c.o.m. S, of position vector $\mathbf{a}$, given below:

$$\mathbf{a} = [5,\ 3,\ 155]^T \text{ (mm)} \tag{4.44}$$

Three views of this posture are shown in Fig. 4.3.

Upon following a procedure similar to that in Subsection 4.4.1, the relative coordinates of the c.o.m. C of the system w.r.t. the MP c.o.m. S are derived. They are given by $[0.0062,\ -0.0025,\ 0.0402]^T$ (m).

The system moment-of-inertia matrix $\mathbf{I}$ w.r.t. its c.o.m. is

$$\mathbf{I} = \begin{bmatrix} 0.9002 & -0.0031 & 0.0618 \\ -0.0031 & 0.8959 & -0.0347 \\ 0.0618 & -0.0347 & 1.1643 \end{bmatrix} \times 10^{-2} \text{ (kg·m}^2\text{)} \tag{4.45}$$

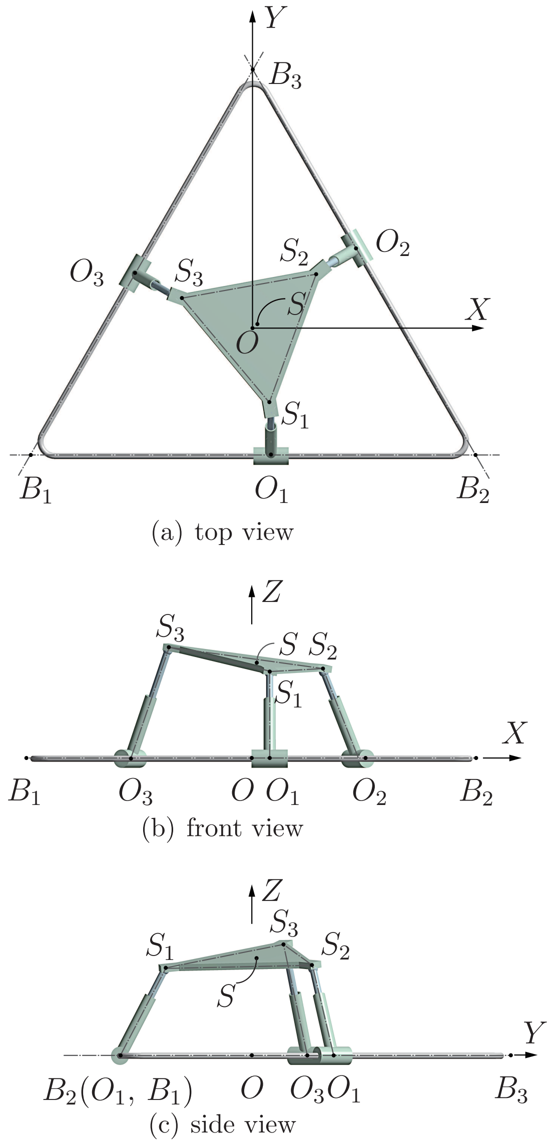

Fig. 4.3 Three views of the symmetric posture

the total mass of the system being, as before,

$$m = 4.4857 \text{ (kg)} \tag{4.46}$$

In turn, the blocks of the CSM $\mathbf{K}$ at the c.o.m. of the system are

$$\mathbf{K}_{11} = \begin{bmatrix} 0.2943 & -0.0356 & 0.0714 \\ -0.0356 & 0.2205 & -0.0412 \\ 0.0714 & -0.0412 & 1.1843 \end{bmatrix} \times 10^4 \text{ (N·m)} \tag{4.47a}$$

$$\mathbf{K}_{12} = \begin{bmatrix} 0.0745 & 2.9135 & -0.2830 \\ -2.8903 & 0.1171 & -0.2439 \\ -0.1007 & -0.1968 & -0.1916 \end{bmatrix} \times 10^4 \text{ (N)} \ = \mathbf{K}_{21}^T \tag{4.47b}$$

$$\mathbf{K}_{22} = \begin{bmatrix} 4.8571 & -0.0199 & 0.0333 \\ -0.0199 & 4.7564 & -0.0736 \\ 0.0333 & -0.0736 & 1.0557 \end{bmatrix} \times 10^5 \text{ (N/m)} \tag{4.47c}$$

Then, the CFM is calculated as

$$\mathbf{\Omega} = \begin{bmatrix} 0.5365 & -0.0448 & 0.0187 & -0.0101 & 0.1829 & -0.0243 \\ -0.0448 & 0.4455 & -0.0121 & -0.2080 & 0.0233 & -0.0279 \\ 0.0187 & -0.0121 & 1.0075 & -0.0072 & -0.0123 & -0.0070 \\ -0.0101 & -0.2080 & -0.0072 & 0.2540 & 0.0120 & -0.0136 \\ 0.1829 & 0.0233 & -0.0123 & 0.0120 & 0.2677 & 0.0085 \\ -0.0243 & -0.0279 & -0.0070 & -0.0136 & 0.0085 & 0.1479 \end{bmatrix} \times 10^3 \text{ (rad/s)} \tag{4.48}$$

The six natural frequencies of the robot, given by the eigenvalues of $\mathbf{\Omega}$, are arrayed in vector $\mathbf{w}_f$:

$$\mathbf{w}_f = \begin{bmatrix} 85.0 \\ 163.4 \\ 191.1 \\ 572.4 \\ 638.5 \\ 1008.7 \end{bmatrix} \text{(rad/s)} = \begin{bmatrix} 13.5 \\ 26.0 \\ 30.4 \\ 91.1 \\ 101.6 \\ 160.5 \end{bmatrix} \text{(Hz)} \tag{4.49}$$

After both a change of variable and the normalization introduced in Section 4.3.2, the corresponding modal screws, i.e., the eigenscrews of the system, arrayed as the columns of matrix $\mathbf{E}_s$, are displayed below:

$$\mathbf{E}_s = \begin{bmatrix} -0.4438 & -0.0461 & 0.9222 & 0.3509 & -0.9330 & 0.0125 \\ -0.8960 & -0.9989 & -0.3761 & 0.9363 & 0.3535 & -0.0083 \\ -0.0109 & -0.0111 & -0.0900 & 0.0112 & 0.0679 & 0.9999 \\ -0.0310 & -0.0523 & -0.0258 & -0.0534 & -0.0181 & -0.0022 \\ 0.0182 & 0.0086 & -0.0599 & 0.0212 & -0.0462 & -0.0041 \\ -0.0463 & 0.1544 & -0.0168 & 0.0020 & 0.0004 & -0.0004 \end{bmatrix} \tag{4.50}$$

The position vectors and pitches of the eigenscrews are, in turn,

$$\begin{aligned} \mathbf{p}_1 &= [0.0417,\ -0.0202,\ -0.0359]^T \text{ (m)}, & p_1 &= -0.0021\,\text{(m)} \\ \mathbf{p}_2 &= [-0.1541,\ 0.0077,\ -0.0527]^T \text{ (m)}, & p_2 &= -0.0079\,\text{(m)} \\ \mathbf{p}_3 &= [0.0009,\ 0.0178,\ -0.0649]^T \text{ (m)}, & p_3 &= 0.0002\,\text{(m)} \\ \mathbf{p}_3 &= [0.0017,\ -0.0013,\ 0.0574]^T \text{ (m)}, & p_4 &= 0.0011\,\text{(m)} \\ \mathbf{p}_5 &= [0.0033,\ -0.0009,\ 0.0495]^T \text{ (m)}, & p_5 &= 0.0006\,\text{(m)} \\ \mathbf{p}_6 &= [0.0041,\ -0.0022,\ -0.0001]^T \text{ (m)}, & p_6 &= -0.0004\,\text{(m)} \end{aligned} \tag{4.51}$$

Apparently, all the natural modes are associated with non-zero-pitch eigenscrews, and hence, represents motions involving, concurrently, rotations and translations. For example, the first natural frequency of the system, $f_1 = 13.5$ Hz, is associated with a screw motion of screw axis $\mathcal{L}_1$ parallel to $\mathbf{e}_1 = [-0.4438, -0.8960, , -0.0109]^T$ and passing through P_1 with relative coordinates w.r.t. C given by $[0.0417, -0.0202, -0.0359]^T$ m, and pitch $p_1 = -0.0021$ m. This screw motion represents a combination of a translation along $\mathbf{e}_1$ and a rotation around the axis $\mathcal{L}_1$. Moreover, the ratio of the velocity of the translation to the angular velocity of the rotation is given by the pitch p_1. The above results also show that *a natural mode is not necessarily associated with a pure rotation or a pure translation.*

4.5 Summary

A mechanical system bearing the morphology of a PKM, with compliant, light-weight links, can be modelled as a rigid body mounted on a six-dof *Cartesian spring*. The model, then, leads to a *Cartesian mass-spring system*. The simplified Cartesian model admits a 6×6 CFM, defined as the positive-(semi)definite square root of the *congruent transformation* of the CSM via the inverse of the positive-definite square root of the CMM. Therefore, the CFM is dimensionally homogeneous, symmetric and positive-(semi)definite. Moreover, the decoupling conditions of the CSM and the CMM are indenpendent; therefore, **the CSM and the CMM cannot be block-diagonalized concurrently, in general**. Consequently, *a natural mode of a Cartesian mass-spring system, in general, is a screw motion involving both a rotation about and a translation in a direction parallel to the same axis.* Upon the eigenvalue decomposition of the CFM, the elastodynamics model of the system is fully decoupled. The six non-negative eigenvalues of the CFM are the natural frequencies of the given system. Moreover, the natural modes of the system are obtained from a linear transformation of the eigenvectors of the CFM via the inverse of the positive-definite square root of the CMM. The six natural modes can be normalized into corresponding six unit screws, i.e., the eigenscrews of the system, which shows that *a natural mode is not necessarily associated with a pure rotation or a pure translation*. That is, in general, *a natural mode involves both rotation about a distinct axis and translation in a direction parallel to the same axis*. Numerical examples obtained at two postures of the SDelta are included, to better understand the concept of CFM and the physical meaning of the natural modes. Applications envisioned include the design of multibody systems with flexible elements that are used for shaking operations, for example. Such applications occur in a few industrial operations, e.g., in the mixing of liquids, and in finding experimentally the inertia matrix of heavy machinery, like land vehicles.

Chapter 5

Closing Remarks and Recommendations

A novel class of three-limb, full-mobility PKMs were proposed as a promising alternative to the traditional six-limb Stewart-Gough platforms. The reduction of the number of limbs from six to three is realized by virtue of a two-dof cylindrical actuator, the C-drive. This simpler architecture, with fewer moving components, extends its application domain for generating HFSA motions. For such applications, the inherent flexibility of the compliant links is taken into account. In this thesis, the Cartesian elastodynamics modelling of PKMs with flexible links is studied. The PKM is simplified into a six-dof Cartesian mass-spring model; then, a concise lump-parameter linear elastodynamics model is established to evaluate the system stiffness and vibration characteristics in a swift, effective way. These characteristics are deemed applicable to the optimum design and real-time control of PKMs for HFSA applications.

5.1 Conclusions

A PKM with compliant, light-weight links, is modelled as a rigid body mounted on a six-dof Cartesian spring, which leads to a *Cartesian mass-spring model*. In this model, the system stiffness is represented by means of a 6×6 CSM of the Cartesian spring, the system inertia by what von Mises termed the *inertia dyad*, i.e., the 6×6 CMM of the rigid MP.

The key to elstostatics is the CSM. Each flexible link is modelled as a rigid link with a virtual joint. By means of the VJM and screw theory, the CSM, representing the robot stiffness, is formulated. During the derivation, a means to compare two different kinds of stiffness, namely, the torsional stiffness and the translational stiffness of different links, is proposed. The CSM is, of course, *posture-dependent and dimensionally inhomogeneous*. Based on the modified eigenproblem of the CSM, three elastostatic performance indices are defined to evaluate the overall stiffness, the translational and the torsional stiffness of the PKM. In terms of elasodynamics, a novel concept, the CFM, is proposed. The 6×6 CFM is defined as the positive-(semi)definite square root of the *congruent transformation of the Cartesian stiffness matrix via the inverse of the positive-definite square root of the Cartesian mass matrix*. The CFM is *dimensionally homogeneous*, *symmetric* and *positive-(semi)definite*. Upon the eigenvalue decomposition of the CFM, the Cartesian elastodynamics model is fully decoupled. The system natural frequencies are the six non-negative eigenvalues of the CFM, while the system natural modes are a linear transformation of the eigenvectors of CFM. In general, a natural mode involves both rotation about a distinct axis and translation in a direction parallel to the same axis.

The foregoing modelling methods were applied and validated on a desktop-scale prototype of the *SDelta* robot. In terms of stiffness analysis, the CSM and the stiffness indices are derived at a specific symmetric posture under various conditions. As per the numerical results, the motor shaft, together with its coupling, is much stiffer than the limb rod.

Therefore, in some cases, the compliance of the C-drive can be neglected for simplicity. In terms of vibration analysis, numerical examples at two postures of the SDelta are obtained to better understand the concept of CFM and the physical meaning of the natural modes. The philosophy adopted at the outset, for the formulation of the elastodynamics model of the SDelta Robot, is deemed to be applicable to other, similar six-dof parallel robots.

The Cartesian mass-spring model is a practical simplification of the n-dof generalized elastodynamics model for some flexible mechanical systems, such as PKMs with flexible links intended for HFSA operations. Due to its concise expression and intuitive significance, the *Cartesian mass-spring model* provides engineers, swiftly and effectively, insight into the elastic properties of the PKM under design. This model is thus deemed valuable in: the stiffness and vibration evaluation of the system; the preliminary stages of design; and, further, the design of task-space real-time feedback control schemes applicable to flexible mechanical systems.

5.2 Recommendations for Further Research

Finally, some research directions are recommended for further work:

- This thesis focuses on the Cartesian elstodynamics modelling of PKMs intended for HFSA applications. The optimum design of these systems based on the proposed elastodynamic and elastodynamics performance indices, is to be under taken.

- In order to provide a pertinent representation of the real system, the damping term needs to be considered in the Cartesian elastodynamics of the PKMs. The Cartesian frequency matrix defined based on the Cartesian mass matrix, stiffness matrix and damping matrix is to be studied in further research.

- The numerical calculation and FEA simulation on the desktop-scale SDelta robot shows that it is stiff and capable of producing high-frequency (<23.6 Hz) motions. A prototype of the SDelta is to be built. Experiments should be conducted on the prototype to further validate its elastodynamic response.

- Cartesian real-time feedback control of the PKM considering the deformation of the flexible links should be further investigated.

- Applications of the PKM with flexible links intended for tasks such as rigid-body *inertia-parameter identification* under HFSA motions, should be conducted.

Bibliography

[1] Merlet, J. P., 2006. *Parallel Robots (Second Edition)*. Springer, Dordrecht, The Netherlands.

[2] Stewart, D., 1965. "A platform with six degrees of freedom". *Proceedings of the Institution of Mechanical Engineers,* **180**(1), pp. 371–386.

[3] Fichter, E. F., 1986. "A stewart platform based manipulator: General theory and practical construction". *The International Journal of Robotics Research,* **5**(2), p-p. 157–182.

[4] Boër, C. R., Molinari-Tosatti, L., and Smith, K. S., 2012. *Parallel Kinematic Machines: Theoretical Aspects and Industrial Requirements*. Springer, London.

[5] Taghirad, H. D., 2013. *Parallel Robots: Mechanics and Control*. CRC Press, Boca Raton.

[6] Podhorodeski, R., and Pittens, K., 1994. "A class of parallel manipulators based on kinematically simple branches". *Transactions-American Society of Mechanical Engineers Journal of Mechanical Design,* **116**, pp. 908–908.

[7] Yang, G. L., Chen, I. M., Chen, W. H., and Lin, W. "Kinematic design of a six-dof parallel-kinematics machine with decoupled-motion architecture". *IEEE Transactions on Robotics and Automation,* **20**(5), pp. 876–884.

[8] Li, W., and Angeles, J. "A novel three-loop parallel robot with full mobility: Kinematics, singularity, workspace, and dexterity analysis". *Journal of Mechanisms and Robotics,* **9**(5), p. 051003.

[9] Karimi Eskandary, P., and Angeles, J., 2018. "The translating Π-joint: Design and applications". *Mechanism and Machine Theory,* **122**, pp. 361–370.

[10] Monsarrat, B., and Gosselin, C. M. "Workspace analysis and optimal design of a 3-leg 6-dof parallel platform mechanism". *IEEE Transactions on Robotics and Automation,* **19**(6), pp. 954–966.

[11] Azulay, H., Mahmoodi, M., Zhao, R., Mills, J. K., and Benhabib, B. "Comparative analysis of a new 3 x pprs parallel kinematic mechanism". *Robotics and Computer-Integrated Manufacturing,* **30**(4), pp. 369–378.

[12] Fu, J. X., Gao, F., Pan, Y., and Du, H. "Forward kinematics solutions of a special six-degree-of-freedom parallel manipulator with three limbs". *Advances in Mechanical Engineering,* **7**(5), p. 1687814015582118.

[13] Chen, C., Gayral, T., Caro, S., Chablat, D., Moroz, G., and Abeywardena, S. "A six degree of freedom epicyclic-parallel manipulator". *Journal of Mechanisms and Robotics-Transactions of the ASME,* **4**(4), p. 041011.

[14] Yoon, J. W., Ryu, J., and Hwang, Y. K. "Optimum design of 6-dof parallel manipulator with translational/rotational workspaces for haptic device application". *Journal of Mechanical Science and Technology,* **24**(5), pp. 1151–1162.

[15] Schedlinski, C., and Link, M., 2001. "A survey of current inertia parameter identification methods". *Mechanical systems and signal processing,* **15**(1), pp. 189–211.

[16] Li, W., and Angeles, J., 2018. "The design of a 3-$\underline{\text{C}}$PS parallel robot for maximum dexterity". *Mechanism and Machine Theory,* **122**, pp. 279–291.

[17] Lončarić, J., 1987. "Normal forms of stiffness and compliance matrices". *IEEE Journal of Robotics and Automation,* **3**(6), pp. 567–572.

[18] von Mises, R., 1924. "Motorrechnung, ein neues Hilfsmittel der Mechanik". *ZAMM-Journal of Applied Mathematics and Mechanics/Zeitschrift für Angewandte Mathematik und Mechanik,* **4**(2), pp. 155–181.

[19] Patterson, T., and Lipkin, H., 1993. "Structure of robot compliance". *ASME Journal of Mechanical Design,* **115**(3), pp. 576–580.

[20] Ding, X., and Selig, J. M., 2004. "On the compliance of coiled springs". *International Journal of Mechanical Sciences,* **46**(5), pp. 703–727.

[21] Hong, M. B., and Choi, Y. J., 2009. "Screw system approach to physical realization of stiffness matrix with arbitrary rank". *ASME Journal of Mechanisms and Robotics,* **1**(2).

[22] Lian, B., Sun, T., Song, Y., Jin, Y., and Price, M., 2015. "Stiffness analysis and experiment of a novel 5-dof parallel kinematic machine considering gravitational effects". *International Journal of Machine Tools and Manufacture,* **95**, pp. 82–96.

[23] Liu, H., Huang, T., Chetwynd, D. G., and Kecskeméthy, A., 2017. "Stiffness modeling of parallel mechanisms at limb and joint/link levels". *IEEE Transactions on Robotics,* **33**(3), pp. 734–741.

[24] Dong, C., Liu, H., Huang, T., and Chetwynd, D. G., 2019. "A Screw Theory-Based Semi-Analytical Approach for Elastodynamics of the Tricept Robot". *ASME Journal of Mechanisms and Robotics,* **11**(3), 04.

[25] Roth, B., 1984. "Screws, motors, and wrenches that cannot be bought in a hardware store". In The First International Symposium of Robotics Research, pp. 679–693.

[26] Gonçalves, R. S., and Carvalho, J. C. M., 2009. "Stiffness analysis of parallel manipulator using matrix structural analysis". In *Proceedings of EUCOMES 08*. Springer, pp. 255–262.

[27] Fasse, E. D., 2001. "A finite-element-based method to determine the spatial stiffness properties of a notch hinge". *Journal of Mechanical Design,* **123**, pp. 141–147.

[28] Corradini, C., Fauroux, J.-C., Krut, S., et al., 2003. "Evaluation of a 4-degree of freedom parallel manipulator stiffness". In Proceedings of the 11th World Congress in Mechanisms and Machine Science, Tianjin, China, pp. 18–21.

[29] Deblaise, D., Hernot, X., and Maurine, P., 2006. "A systematic analytical method for pkm stiffness matrix calculation". In Proceedings. IEEE International Conference on Robotics and Automation, IEEE, pp. 4213–4219.

[30] Caro, S., Chablat, D., and Chen, C., 2012. "Elastostatic modeling and shape optimization of a 6-dof haptic interface device". In ASME 2012 the 11th Biennial Conference on Engineering Systems Design and Analysis, American Society of Mechanical Engineers, pp. 265–274.

[31] Gosselin, C., 1990. "Stiffness mapping for parallel manipulators". *IEEE Transactions on Robotics and Automation,* **6**(3), pp. 377–382.

[32] Pashkevich, A., Chablat, D., and Wenger, P., 2009. "Stiffness analysis of overconstrained parallel manipulators". *Mechanism and Machine Theory,* **44**, pp. 966–982.

[33] Majou, F., Gosselin, C., Wenger, P., and Chablat, D., 2007. "Parametric stiffness analysis of the orthoglide". *Mechanism and Machine Theory,* **42**, pp. 296–311.

[34] Pashkevich, A., Chablat, D., and Wenger, P., 2008. "Stiffness analysis of multi-chain parallel robotic systems". *IFAC Proceedings Volumes,* **41**, pp. 127–132.

[35] Kefer, M., Zhang, J., and Xie, H., 2014. "A versatile, non-linear and elasto-static stiffness model of articulated industrial robots". In Proceedings. IEEE International Conference on Automation Science and Engineering, IEEE, pp. 208–214.

[36] Taghvaeipour, A., Angeles, J., and Lessard, L., 2012. "On the elastostatic analysis of mechanical systems". *Mechanism and Machine Theory,* **58**, pp. 202–216.

[37] Taghvaeipour, A., Angeles, J., and Lessard, L., 2014. "Optimum structural design of a two-limb schönflies motion generator". *Mechanism and Machine Theory,* **80**, pp. 125–141.

[38] Ball, R. S., 1876. "The theory of screws: A study in the dynamics of a rigid body". *Mathematische Annalen,* **9**(4), pp. 541–553.

[39] Selig, J. M., 2013. *Geometrical Methods in Robotics*. Springer, New York.

[40] Bhattacharya, S., Hatwal, H., and Ghosh, A. "On the optimum design of Stewart platform type parallel manipulators". *Robotica,* **13**, pp. 133–140.

[41] Xu, Q. S., and Li, Y. M., 2006. "GA-based architecture optimization of a 3-PUU parallel manipulator for stiffness performance". In WCICA 2006: Sixth World Congress on Intelligent Control and Automation, Vols 1-12, Conference Proceedings, pp. 153–153.

[42] Griffis, M., and Duffy, J., 1991. "Kinestatic Control: A Novel Theory for Simultaneously Regulating Force and Displacement". *Journal of Mechanical Design,* **113**(4), 12, pp. 508–515.

[43] Chen, G., Wang, H., Lin, Z., and Lai, X., 2015. "The principal axes decomposition of spatial stiffness matrices". *IEEE Transactions on Robotics,* **31**(1), pp. 191–207.

[44] Li, H., Yang, Z., and Huang, T., 2009. "Dynamics and elasto-dynamics optimization of a 2-dof planar parallel pick-and-place robot with flexible links". *Structural and multidisciplinary optimization,* **38**, pp. 195–204.

[45] Siciliano, B., and Khatib, O., 2016. *Springer handbook of robotics*. Springer.

[46] Meirovitch, L., 1986. *Elements of Vibration Analysis (Second Edition)*. McGraw-Hill, New York.

[47] Madhujit, M., 1986. *Vibrations, Dynamics and Structural Systems (Second Edition)*. A.A. Balkema Publishers, The Netherlands.

[48] De Silva, C. W., 2006. *Vibration: Fundamentals and Practice*. CRC Press, Boca Raton.

[49] Wittbrodt, E., Adamiec-Wójcik, I., and Wojciech, S., 2007. *Dynamics of Flexible Multibody Systems: Rigid Finite Element Method*. Springer, Berlin.

[50] Briot, S., and Khalil, W., 2015. *Dynamics of Parallel Robots: From Rigid Bodies to Flexible Elements*. Springer, Cham, Switzerland.

[51] Krefft, M., and Hesselbach, J., 2005. "Elastodynamic optimization of parallel kinematics". In Proceedings. IEEE International Conference on Automation Science and Engineering, IEEE, pp. 357–362.

[52] Lewis, F. L., Abdallah, C. T., and Dawson, D. M., 1993. *Control of robot manipulators*. Macmillan New York.

[53] Ma, O., and Angeles, J., 1993. "Optimum design of manipulators under dynamic isotropy conditions". In Proceedings. IEEE International Conference on Robotics and Automation, IEEE, pp. 470–475.

[54] Codourey, A., 1998. "Dynamic modeling of parallel robots for computed-torque control implementation". *The International Journal of Robotics Research,* **17**, pp. 1325–1336.

[55] Taghvaeipour, A., Angeles, J., and Lessard, L., 2015. "Elastodynamics of a two-limb schönflies motion generator". *Proceedings of the Institution of Mechanical Engineers, Part C: Journal of Mechanical Engineering Science,* **229**, pp. 751–764.

[56] Angeles, J., 2011. *Dynamic Response of Linear Mechanical Systems: Modeling, Analysis and Simulation*. Springer, New York.

[57] Sun, T., Liang, D., and Song, Y., 2017. "Singular-perturbation-based nonlinear hybrid control of redundant parallel robot". *IEEE Transactions on Industrial Electronics,* **65**(4), pp. 3326–3336.

[58] Sun, T., Lian, B., Song, Y., and Feng, L., 2019. "Elastodynamic optimization of a 5-dof parallel kinematic machine considering parameter uncertainty". *IEEE/ASME Transactions on Mechatronics,* **24**(1), pp. 315–325.

[59] Wu, Y., and Carricato, M., 2020. "Persistent manifolds of the special euclidean group se (3): a review". *Computer Aided Geometric Design,* **79**, p. 101872.

[60] Sun, T., Yang, S., and Lian, B., 2020. *Finite and instantaneous screw theory in robotic mechanism*. Springer Nature.

[61] Angeles, J., 2014. *Fundamentals of Robotic Mechanical Systems: Theory, Methods, Algorithms (Fourth Edition)*. Springer, New York.

[62] Hunt, K. H., 1978. *Kinematic Geometry of Mechanisms*, Vol. 7. Oxford University Press, New York.

[63] Björck, Å., 2015. *Numerical Methods in Matrix Computations*, Vol. 59. Springer, New York.

[64] Harada, T., Friedlaender, T., and Angeles, J., 2014. "The development of an innovative two-dof cylindrical drive: Design, analysis and preliminary tests". In Proceedings. IEEE International Conference on Robotics and Automation, pp. 6338–6344.

[65] Craig Jr, R. R., and Taleff, E. M., 2020. *Mechanics of Materials*. John Wiley & Sons.

[66] Angeles, J., 2010. "On the nature of the Cartesian stiffness matrix". *Ingeniería Mecánica, Tecnología y Desarrollo,* **3**(5), pp. 163–170.

[67] Salisbury, J. K., and Craig, J. J., 1982. "Articulated hands: Force control and kinematic issues". *The International Journal of Robotics Research,* **1**(1), pp. 4–17.

[68] Görgülü, İ., Carbone, G., and Dede, M. C., 2020. "Time efficient stiffness model computation for a parallel haptic mechanism via the virtual joint method". *Mechanism and Machine Theory,* **143**, p. 103614.

[69] Pottmann, H., and Wallner, J., 2001. *Computational Line Geometry*. Springer, Berlin-Heidelberg-New York.

[70] Bråting, K., and Kilhamn, C., 2021. "Exploring the intersection of algebraic and computational thinking". *Mathematical Thinking and Learning,* **23**(2), pp. 170–185.

[71] Schneider, P., and Eberly, D. H., 2002. *Geometric Tools for Computer Graphics*. Elsevier, San Francisco.

[72] Ma, J., Lv, Q., Yan, H., Ye, T., Shen, Y., and Sun, H., 2022. "Color-saliency-aware correlation filters with approximate affine transform for visual tracking". *The Visual Computer*, pp. 1–22.

[73] Huang, S., and Schimmels, J. M., 2000. "The eigenscrew decomposition of spatial stiffness matrices". *IEEE Transactions on Robotics and Automation,* **16**(2), pp. 146–156.

[74] Schimmels, J. M., and Huang, S., 2000. Spatial parallel compliant mechanism, Feb. 8. US Patent 6,021,579.

[75] Yaskawa. *Sigma-II Series SGMH/SGDM Users Manual: Servo Selection and Data Sheets*. Manual NO SIE-S800-31 1D.

[76] Ning, J., Fang, M., Ran, W., Chen, C., and Li, Y., 2020. "Rapid multi-sensor feature fusion based on non-stationary kernel jade for the small-amplitude hunting monitoring of high-speed trains". *Sensors,* **20**(12), p. 3457.

[77] Inman, D. J., and Singh, R. C., 1994. *Engineering Vibration*, Vol. 3. Prentice-Hall, Upper Saddle.

[78] Meirovitch, L., 2010. *Fundamentals of Vibrations*. Waveland Press, Long Grove, Illinois.

[79] Golub, G. H., and Van Loan, C. F., 2012. *Matrix Computations*, Vol. 3. The Johns Hopkins University Press, Baltimore.